DESIGN AND ANALYSIS OF RECONFIGURABLE PHOTONIC CRYSTALS AND WHISPERING GALLERY MODE RESONATORS BASED ON OPTICAL FORCE

by

Nusrat Jahan

A thesis submitted in partial fulfillment of the requirements

of

the degree of Master of Science in Electrical and Electronic Engineering

Department of Electrical and Electronic Engineering

Bangladesh University of Engineering and Technology (BUET)

Dhaka-1000, Bangladesh

August 6, 2019

DECLARATION

It is hereby declared that this thesis or any part of it has not been submitted elsewhere for the award of any degree or diploma.
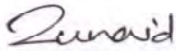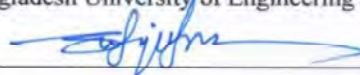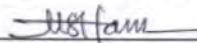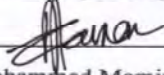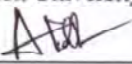
Signature of the student

(Nusrat Jahan)

APPROVAL CERTIFICATE

The thesis titled "DESIGN AND ANALYSIS OF RECONFIGURABLE PHOTONIC CRYSTALS AND WHISPERING GALLERY MODE RESONATORS BASED ON OPTICAL FORCE" submitted by Nusrat Jahan, Student ID: 0417062280, Session: April 2017 has been accepted as satisfactory in partial fulfillment of the requirement for the degree of Master of Science in Electrical and Electronic Engineering on August 6, 2019.

BOARD OF EXAMINERS

1. _____   Chairman
                                                                    (Supervisor)

Dr. Md. Zunaid Baten
Assistant Professor
Department of Electrical and Electronic Engineering
Bangladesh University of Engineering and Technology, Dhaka - 1000, Bangladesh.

2. _____   Member

Dr. Md. Shafiqul Islam   (Ex-Officio)
Professor & Head
Department of Electrical and Electronic Engineering
Bangladesh University of Engineering and Technology, Dhaka - 1000, Bangladesh

3. _____   Member

Dr. Md. Shah Alam
Professor
Department of Electrical and Electronic Engineering
Bangladesh University of Engineering and Technology, Dhaka - 1000, Bangladesh

4. _____   Member

Dr. Sharif Mohammad Mominuzzaman
Professor
Department of Electrical and Electronic Engineering
Bangladesh University of Engineering and Technology, Dhaka - 1000, Bangladesh

5. _____   Member

Dr. Mohammed Abdul Basith   (External)
Professor
Department of Physics,
Bangladesh University of Engineering and Technology, Dhaka - 1000, Bangladesh

ii

ACKNOWLEDGEMENT

ABSTRACT

Photonic crystals (PCs) and whispering gallery mode (WGM) resonators are two of the most versatile photonic structures in the field of photonics and cavity quantum electrodynamics. A long standing challenge in the design of these structures has been their dynamic tunability, which is the capability of varying their resonant characteristics without going through the fabrication process. In this work the prospect of dynamic tunability of polystyrene (PS) microparticle based PCs and WGM resonators is studied by spatially reconfiguring these structures employing optical force. The behavior of optical force exerted by monochromatic illumination via dual counter-propagating Gaussian beams is analyzed using Maxwell Stress Tensor and Finite Difference Time Domain (FDTD) analysis techniques. Both one dimensional (1D) and two dimensional (2D) water submerged periodic PS microsphere arrays are found to exhibit spatial re-orientation in the presence of optical force. Detailed analysis shows that such optical force induced reconfiguration can be controlled by varying the illumination intensity, incident wavelength, and also the surrounding medium of the PS microparticles. For illumination with 980 nm wavelength, 1D array results in an inhomogeneous stable spacing of microspheres whereas periodically reconfigured arrays can be attained by illuminating in direct correlation with the resonant wavelength of the structure. Changing illumination intensity enahnces the magnitude of optical force acting on the particles, though it does not alter their stable locations. On the other hand, variation of refractive index of the background medium alters the stable interparticle separation of particles. Band structures and transmission characteristics of the PS array are observed to evolve in accordance with the spatial reconfiguration. A complete bandgap with nearly 100% reflection is attained for the 1D array whereas nearly 94% reflectivity is obtained for the 2D array. Besides photonic crystals, WGM resonators comprising of polystyrene (PS) microspheres are also analyzed and their Q factors are compared with those of single solid monospherical WGM resonators. The highest Q-factor of 91224 is obtained for a water submerged 20μm monosphere WGM micro resonator whereas for multiple microsphere based circularly symmetric structures no WGM is observed. By changing the surrounding medium, an exponential rise in Q factor is achieved which peaks for air with a WGM mode having Q factor of 408. For water suspended hexagonal configurations of the microspheres, the WGM mode disappears in the presence of optical force, thereby resulting transition from a highly reflective to a nearly transparent medium. Based on such optical force mediated reconfiguration, conveniently tunable photonic crystals and whispering gallery mode resonators can be designed and implemented for novel sensing, detection and lasing applications.

Table of Contents

CHAPTER 3

MODEL AND GEOMETRY DESCRIPTION   **29**

CHAPTER 4

RESULTS AND DISCUSSION   **39**

CHAPTER 5

SUMMARY, CONCLUSION AND SUGGESTIONS FOR FUTURE WORKS   106

LIST OF REFERENCES   110

List of Figures

of the charge element dq in volume element dV and varies throughout the continuum.

CHAPTER 1

INTRODUCTION

1.1   Preface

Photonic crystals (PC) and whispering gallery mode (WGM) resonators have been topics of intense interest in the field of photonics and cavity quantum electrodynamics (QED). The pioneering work of Yablonovitch and John gifted us the key to open the gateway to PC, an optically engineered material that provides the liberty to affect the properties of photons in much the same way that ordinary semiconductor crystals affect the properties of electrons [1]. WGM resonator, another integral part of today's optical resonant systems, is a derivative of Lord Rayleigh's work on sound waves [2]. Light within an optical cavity if confined by continuous total internal reflection near the cavity perimeter engenders the resonant modes called WGMs. Through the unique combination of strong temporal and spatial confinement of light, PCs and WGMs have evolved as systems of interest for a number of fundamental research on light-matter interaction.

PCs possess specific topology with high-index-contrast materials with a periodicity on the order of optical wavelength. Its most significant feature is its band gap for which electromagnetic waves can experience a forbidden range of frequencies within the plane of periodicity. The other popular feature, WGM occurs in a smooth concave structure provided that its refractive index is higher than that of the surrounding medium. Microsphere, microdisk and microtoroid WGMs are prominent for the fundamental research and corresponding applications due to both the high quality factor (high-Q) and the small mode volume (V) [3]. The fascinating features of rotationally symmetric WGMs along with the inherently periodic PCs, have resulted in a surge in the world of research to explore multiple applications emerging from the strong interaction between light and matter in these optical systems.

As fundamental components of optical devices, like optical cavities or waveguides, photonic crystals have already claimed a superior position in terms of localization, tunability and efficiency. Like PCs, WGM resonances are also highly sensitive to morphological changes (such as the size, shape, or refractive index), as a result both of these structures have gained popularity in sensing technologies [4]-[6]. Apart from experiments on cavity QEDs, the research community found the WGM microresonators useful to probe the sphere environment, like temperature, pressure or chemical composition [7]. Applications of the high quality factor resonant modes of these periodic or rotationally symmetric structures also include ultra-low threshold lasing [8]-[10], quantum information

processing [11]-[12], probing [13], imaging [14]-[15], energy harvesting [16] and filtering [17]. Despite numerous applications, a long standing challenge in the design of PCS and WGM resonators, has been their dynamic tunability. Dynamic tunability provides them with the ability to reversibly change and recover their resonant characteristics by means of external stimuli. For optical communication, information processing reconfigurable PCs and WGMs are quite fascinating as they offer different tuning techniques of their optical characteristics [18]. Photonic materials with tuneable and switchable optical properties can potentially benefit applications in sensing, high-density optical memory, beam-steering, adaptive optics and light modulation [19]. There have been various methods proposed to modulate the parameters of basic PC structures or WGM resonators to obtain dynamic or static changes in the optical characteristics. Reconfiguration of photonic crystals have been realized employing different techniques like plasma control [20], opto-mechanical actuation [21], contact pressure [22], temperature [23], and nano-fluidic tuning [18]. However, an elegant approach yet to be investigated as far as reconfiguration of microparticle based PC and WGM resonator is concerned, is optical force induced tunability.

Ashkin et al.'s stimulating introduction to the world of optical trapping has incited the theoretical and empirical demonstrations of optical forces. Although it has already been employed to experimentally realize optical tweezers [24], optical force microscopy [25] [26], and optical force sensors [27], there is a lack of research regarding comprehensive understanding of the prospect of reorganizing polymer microparticle based photonic structures in a tunable optical force bound environment. Polymer composites have gained much importance in the field of optoelectronics due to their unique optical properties [20]. Also, due to their low cost, free standing nature, flexibility and relatively simple processing method, colloidal polystyrene(PS) microparticles have become one of the most suitable candidates for fabrication of photonic crystals or relevant photonic devices [28] [29]. However, the case of optical force tuning employing counter propagating dual Gaussian beam illumination for obtaining reconfigurable PC and WGM resonators still requires particular attention because of the versatility and ease of practical implementation of this particular technique.

1.2   Literature Review

In order to realize innovative electromagnetic properties unattainable in naturally existing materials, there has been a truly amazing amount of innovation regarding PCs over the last 30 years. The Study of periodic structures is much older than that and dates back to 1887 with Lord Rayleigh [30] whereas the term "Photonic Crystal" came into use in 1987 through Yablonovitch [31] and John [32]. Eli Yablonovitch [1986] demonstrated how spontaneous emission can be rigorously inhibited in solid state

periodic dielectric structures through the formation of band gap [31]. To encourage research mostly on semiconductor lasers, he exhibited the significance of the forbidden gap in the electromagnetic dispersion relation of lossless, modulated dielectric structures. Sajeev John, on the other hand, discussed that predictable strong Anderson localization of photons is possible in a certain disordered dielectric microstructure [32]. Their pioneering works have stimulated impressive progress of dielectric PCs for modification of light emission for desired application like lasers, sensors, optical telecommunications, and display devices.

Microsphere based WGM resonators consisting of highly transparent dielectric media possess various promising properties. A lot of laboratory-fabricated solid-state microspheres stemmed from the investigation of P W Barber and R K Chang on the morphology dependent WGMs in microspheres [33]. L. Collot et al recorded Q-factor exceeding 2×10^9 for coupling Mie resonance of a fused silica microsphere into glass prism back in 1993 [34]. In 2019, Yumeki Kobayashi et al proposed a novel diameter measurement technique of microspheres based on WGM resonant wavelength and corresponding radial mode number which is also based on a single micrpshere [35]. However, rotationally symmetric structures consisting multiple microspheres have not been studied that much to realize WGM resonators.

Strong confinement of light in High Q PC cavities have found applications in many areas of physics and engineering. Yoshihiro et al. designed high-Q nanocavity comprising 2D PC slab with air holes and missing rods [36]. In most cases, PC microresonators with sufficiently high Q factor are realized by introducing defects at the center of the PC slab, removing microparticles or changing the inner radius near the middle of the periodic structure [37]. But examples of high Q PC cavity using micropsheres is not significantly high, which is also true for WGM resonators.

Different design principles have been proposed and experimented to guide light through WGMs or in PCs using both plasmonic or dielectric materials [38][39]. Another practical approach is to exploit self-assembled colloidal polymer micropartilces, a promising candidate for the fabrication of photonic structures. Organic and Polymeric microstructures with superior photoelectric properties are exploited in various optoelectronic devices, for example, organic light-emitting diodes, field-effect transistors (FETs), solid-state lasers, optical logic gates etc [7]. Their weak bonding leads to various self-assembled morphologies. In contrast to inorganic microresonators, the facile, flexible and low cost self-assembly method of fabrication inspired Yi Chen Tao et al. to investigate active WGM resonators in self-assembled (E)-3-(4-(dip-tolylamino) phenyl)-1-(4-fluoro-2-hydroxyphenyl)prop-2-en-1-one (DTPHP) microspheres of different diameters. For a DTPHP particle (refractive index, $n_p=2.6$) with a diameter of 1.7μm in air, a Q factor around 90 was obtained [7]. This self-assembly of micro particles

may contribute to obtain tunable PC and WGMs and so the demand of optical force based reorganization of such self assembled optical structures is on the rise.

Optical trapping and manipulation of microparticles is a useful experimental tool but this tool has not yet been realized extensively for reconfiguring PCs and WGMs. In 1970 Arthur Ashkin proved that freely suspended dielctric microparticles can be accelerated and trapped using radiation pressure or scattering optical force [40]. More than 30 years after the pioneering work by Ashkin on the trapping of particles with light, optical manipulation has developed into an innovative and noninvasive technology for dynamic reconfiguration of micrometer-sized transparent particles. To exploit the mechanical forces exerted by laser light in 2003 Wolfgang Singer et al presented their experimental work with a theoretical model for a chain of PS microbeads confined in a counter propagating single mode fiber trap [41]. Although their model supports their size dependent self-organization of particles influenced by 1.064μm laser light, this model is not a universal one. Using similar beam fiber trap Metzger et al observed bistable equilibrium positions of optically bound 3μm silica microspheres in 1D (2006) [42]. Marc Guillon et al. reported on the experimental and theoretical studies of strong binding between two and three oil microdroplets (from 1 to 2.5μm in diameter and n_p=1.48) in air along the direction of the beam axis in a dual coherent circularly polarized laser beam system (2006). They claimed the high optical contrast between air and the oil droplets as the reason of stable trapping. They experimented on the displacement of the oil microdropltes exploiting their binding force and observed how they reach a potential minimum in presence of light force [43]. M. Kawano et al reported non-equilibrium spacing of PS microparticles illuminated by 980 nm light through dual Gaussian beam fiber-optic trap [44]. They utilized Maxwell Stress Tensor based Generalized Multipole Technique to analyze the experimental equilibrium positions of microspheres within the fiber trap. The self-assembly of polymer microparticles can lead to structures of different geometries and so was observed in C. Renaut et al's experimental work on 1μm PS microparticles optically bound by the evanescent field of a PC nanocavity. In their experiment on 1 to 7 self-assembled micro beads, they obtained multiple stable configurations with different shapes like straight line, triangle, square etc [45]. All these works were mainly carried out for a small number of particles and optical force induced reconfiguration of microsphere based PC and WGM structures is not yet well defined.

1.3   Motivation of the Work

Important information about PCs and WGMs lie in their periodicity. Although a good number of designs of PCs and WGM resonators have been modeled and experimented so far, incorporation of

optical force to reconfigure their periodicity has not been investigated that much. Liyong Cui et al proposed a method to reconfigure 1D array of dielectric slabs using light scattering induced optical binding. To construct a large scale optically bound structure they theoretically described that a stable 1D PC is obtained if illuminated by a certain frequency that points to its lower band edge [46]. But for 2D or rotationally symmetric structure and most importantly microsphere based periodic structures we do not find any rigorous study where optical force induced reconfiguration method is experimented. As exertion of optical force can cause PS particles to self-assemble in a kinetic equilibrium state- this concept is used this to analyze reconfigurable PC and WGM resonators consisting of PS microspheres.

Due to the difficulty of fabrication of PC based on real materials, and the inflexibility of solid PC structures to reconfiguration for modulating the optical properties, microsphere based PC seems a good choice. In 1998, Ryoko Shimada et al formed stable 2D self-assembled square and hexagonal close-packed PC using colloidal PS microparticles. They attributed the attractive surface tension between the colloidal particles to their self-assembly into ordered structures [47]. Self-assembly of commercially available colloidal solution on solid substrate is a convenient method for fabricating PS PC or WGM resonators. In 2003, Xiaoyong Hu et al demonstrated a continuously tunable photonic crystal with several picoseconds response time, made of 220nm PS spheres fabricated through this self-assembly formation method [48]. Jeong Rok Oh et al. exploited this method to form PS Photonic crystal multilayer from monolayer self-assmebled PS mciroparticles on air-water interface [49]. A. Yadav et al exploited the same method for forming and characterizing 3D dye-doped PS colloids with two different diameters in nano-level [50].

The diversified application of PS microparticle both as in PCs and WGMs motivates us to look more into the photo induced impact on their self-assembled structure. 2D and 3D PCs based on Polymer colloids like polystyrene were explored for visual detection of chemical compounds and gas analytes [51-52]. Ye Liu et al. obtained a response time of 10fsec for all optical switching from a 3D monodispersed PS PC [53]. The large 3rd order nonlinear susceptibility and extremely fast response time of organic polymer PS contributed to the ultrafast optical switching application realized by the shift in the photonic band gap under external laser pumping. Not only in PC, PS WGM microresonator was utilized as a refractive index sensor by Julie Lutti et al where they obtained a Q factor of 0.9×10^6 for a 44μm PS microparticle in water [54]. To contribute to the study of biochemical sensor based on optical fiber integrated micro resonators, Kyriaki Kosma et al experimented on a 10.43μm PS microparticle and reported a Q factor 2.2×10^3 for such a WGM microresonator embedded within a microstructured optical fiber (MOF) [55]. In the same year 2013, Alexandre Francois et al published

their experimental work on WGM sensor consisting MOF integrated dye doped 15μm PS microspheres and demonstrated an enhanced radiation efficiency with an effective Q factor of around 7700 [56]. But all these WGM models are based on mainly single microspheres. Although the self-assembled PS structures are investigated for PCs, they have not been explored for formation of WGM microresonators. Intrigued by the extensive research on PS periodic and circularly symmetric structures both in theoretical and experimental domain, the focus is set on the PS microsphere based PC and WGM resonator configurations and also their reorganization using optical force.

Conventional solid state PC and WGM resonators do not leave us with the liberty to tune their optical characteristics. Once fabricated the rigid behavior of these optical structures become difficult to tune them to incorporate new phenomenon. In fact, the requirement to change any characteristics dependent on their spatial profile or periodicity necessitates fabrication of a whole new structure. To avoid such difficulty and to bring insight into photo induced force tunable PC and WGMs consisting self-assembled PS microspheres, this research is carried out.

1.4   Objectives of the Work

Since in literature evidence of optical force tuned reconfiguration process of periodic and rotationally symmetric structures is quite insufficient, the aim of this research is to shed some line on this topic through this thesis. Inspired by the fascinating concept of optically bound PC and WGMs that can influence light propagation and its interaction with matter and can also change their shape and consequently optical properties, the target of this thesis is set to develop a comprehensive understanding of the resonance behaviors of PS microparticle-based PCs and WGM resonator under the effect of optical force. To make good use of optical binding- a versatile tool for optical trapping and manipulation, an easy, flexible and noninvasive optical reconfiguration method of microsphere based PCs and WGM resonators is proposed. So the prime objectives of this thesis are:

i.   To analyze the behavior of optical forces acting on systems of periodic and rotationally symmetric dielectric microparticles in a counter propagating dual Gaussian beam system of monochromatic illumination

ii.   To compute and compare resonant characteristics of the reconfigured PCs and WGM resonators upon application of optical force

iii.   To investigate the change in reconfiguration process for incident light of different intensities and wavelengths, and also for different background media

iv. To optimize design of the photonic crystal and whispering gallery mode resonator in order to achieve high sensitivity with respect to applied optical force

1.5   Outline of the Thesis

Chapter 2 begins with Maxwell Equations for microscopic objects. Then it discusses basic concepts of optical force and also its different categories like Gradient, Scattering and Binding forces with some mathematical formulation. Then the theoretic model of PC and WGM resonators are discussed respectively. The important characteristic features of these two structures are presented along with their different possible geometries.

Chapter 3 describes the widely used method for computing Optical force, Maxwell Stress Tensor. Then it provides brief description of Finite Difference Time Domain (FDTD) method and formulation of Maxwell Equations using FDTD. In the next section of this chapter the geometries used for this thesis are presented along with the configuration of light source.

Chapter 4 presents the detailed discussion on the results obtained from the application of dual Gaussian beam induced optical force on periodic PS PC and WGM micro resonators. It describes the optically bound reconfiguration process of periodic PS arrays and circularly symmetric hexagonal lattice structures described in Chapter 3. In the first section the effect of optical force on 1D periodic PS arrays are presented. The effect of variation of illumination intensity, background medium and the illumination wavelength on the reconfiguration process are discussed in this section. The resonant characteristics of 1D PS PC before and after dual beam illumination are presented in terms of their band structure and transmittance curves. The second section focuses on the optical force tuned 2D square lattice periodic structures and the results of WGM PS micro resonators are accumulated in the last section. The stable reconfigurations for all three cases are illustrated and the possible manipulation of such reconfiguration method is discussed at length.

Chapter 5 draws conclusion of this work. This chapter summarizes the findings of the study and their impacts on future experiments. It also puts forward suggestions regarding future scopes of the works carried out in this thesis.

CHAPTER 2

THEORETICAL BACKGROUND

In order to study light-matter interaction in inherently periodic photonic crystal (PC) and rotationally symmetric whispering gallery mode (WGM) resonator in presence of optical force, this chapter begins with Maxwell Equations in Section 2.1. Section 2.2 describes the basic idea of optical force and also the mathematical formulation to define photon induced force. In Sections 2.3 and 2.4, some generalized idea about PC and WGM resonator is presented.

2.1   The Maxwell Equations

To deal with any electromagnetic problems including PC and WGM resonator it is mandatory to look at the four macroscopic Maxwell Equations.

For time harmonic electric field, **E**, a vector field, and the magnetic flux density, **B**, a pseudovector field, and for a given total electric charge density (total charge per unit volume), ρ, and total electric current density (total current per unit area), J, the Maxwell equations can be expressed as:

Gauss's Law $\qquad\qquad\qquad\qquad \nabla . \mathbf{E} = \dfrac{\rho}{\varepsilon_0} \qquad\qquad$ (2.1)

Gauss's Law for Magnetism $\qquad\qquad \nabla . \mathbf{B} = \mathbf{0} \qquad\qquad$ (2.2)

Maxwell–Faraday equation $\qquad\qquad \nabla \times \mathbf{E} = -\dfrac{\partial \mathbf{B}}{\partial t} \qquad\qquad$ (2.3)

Ampere's Circuital Law $\qquad\qquad \nabla \times \mathbf{B} = \mu_0 \mathbf{J} + \ \varepsilon_0 \mu_0 \dfrac{\partial \mathbf{E}}{\partial t} \qquad$ (2.4)

These four equations regulate the master equation to describe photonic structures like PC and also the Helmholtz equation on which the WGMs are based on. Moreover, Maxwell Stress Tensor, the inevitable part to study optical force- directly depends on the equations above.

2.2   Optical Force

Light carries energy and both linear and angular momenta that can be transferred to atoms, molecules and particles. This light-matter interaction gives rise to optically induced forces that have had a deep-seated impact in the past four decades.

Optical forces on small particles are usually expressed as the sum of two terms: the dipole or gradient force and the radiation pressure or scattering force and these two arise directly from the incident field [57]. The induced dipole is drawn by field intensity gradients which compete with radiation pressure due to momentum transferred from the photons in the beam. For nanoscale particles, the origin of these forces are attributed to the polarizability of a specimen [58]. Upon illumination by light, charges respond to the local electric field and develop electric (magnetic) dipole moment in response to the light electric (magnetic) field [58][59].

2.2.1   Gradient Force

The optomechanical interaction required for particle trapping and manipulation, as well as for near-field optical imaging in scanning probe microscopy is basically provided by optical gradient force. It can be interpreted in a number of ways. For small objects (nanoscale) the interaction of an induced dipole with the field gradient of the focused electromagnetic field is termed to be the gradient force. For large particles with diameter significantly exceeding the illumination wavelength, the refraction of light by the particle exerts a force upon the object pulling it to the location of the maximal field intensity provided that the refractive index of the particles is higher than their surroundings [57].

2.2.2   Scattering Force

The classical Maxwell theory showed in 1873 that the radiation field can exert "light pressure" on illuminated objects and scattering from an object can change its momentum [60]. To maintain this law followed by Newton's third law of motion, any change in the total momentum of the electromagnetic waves or photons must involve an equal and opposite change in the momentum of the matter it interacts with. And Scattering forces arise mainly due to this effect. Particles confined in a beam are pushed in the direction of the light propagation, e.g., in a single beam gradient trap, termed "optical tweezers," the equilibrium position of the particles are affected by the presence of scattering as it displaces the particles toward the direction of propagation and slightly beyond the beam focus. The very first observation of optical momentum transfer to small particles was performed in 1970 by Ashkin [40]. In another highly popular trapping geometry, that of a dual beam counter propagating (CP) trap, the scattering force plays the key role in keeping the particle equilibrium position between the two incident beams. The optical lattice formed by the presence of this force confines microspheres in the maxima of light interference patterns and push them, against the top surface of the sample cell [57]. Scattering forces are also well known as radiation pressure forces.

2.2.3 Binding Force

Gradient and scattering forces emerge directly from the incident field while the binding forces depend on the modification of the incident field in the presence of multiple simultaneously illuminated objects. The light scattered from these objects consequently create a light redistribution and contribute to organizing themselves into specific static or dynamic configurations [85].

From historical perspective, optical binding generally refers to stable spatial reconfiguration of microparticles following light illumination which arise due to the light momentum redistribution in the incident beam by the objects together with the light scattered from one object toward the others [86]. The stable positions of these microparticles are somewhat well-defined and these configurations are influenced by the interplay of the scattered photons, the physical attributes of the particles and the surrounding medium, and most importantly the illuminating light field.

Unlike electrostatic interactions, the interparticle forces produced by light scattering are not conservative and have a varying dependence upon the interparticle separation. The spatial shaping of the incident beam is not necessarily the prime criterion for optical binding rather a homogeneous beam like a plane wave can even create stable configuration between objects (at least along the beam propagation axis). Therefore, self-arranged configurations of colloids with micrometer-scale inter particle distances may be obtained even by plane-wave illumination of the sample and it has been experimentally proved that redistributed light momentum can greatly impact the stable positions of other adjacent colloidal objects [87].

The pioneering experiments of optical binding has subdivided it into two classes: transverse (lateral) binding and longitudinal binding. For the transverse binding, the incident light field propagates orthogonally to the direction of the binding process while for longitudinal optical binding, the light field propagates in the direction of organization of the particle chains [88].

2.2.4 Mathematical Formulation:

The total force exerted on spherical particle placed within an electromagnetic field can be expressed in the following form[59][62]:

$$\mathbf{F} = \mathbf{F_e} + \mathbf{F_m} + \mathbf{F_{em}} \tag{2.5}$$

The first two terms, $\mathbf{F_e}$ and $\mathbf{F_m}$ express the electric and magnetic dipolar forces and the third one is the result of electric-magnetic dipolar interaction. Apart from the first two terms, the force component due to the electric-magnetic dipolar interaction, $\mathbf{F_{em}}$ contributes to both the radiation pressure, or scattering force, and to the gradient force [59].

2.2.4.1 Dipole Approximation:

For the subwavelength radius of a sphere ($a \ll \lambda$) the total force due to an external electromagnetic field is usually split into two parts. According to **the dipole approximation** [62] the optically induced force experienced by such small particles can be expressed as [63]:

$$F = (\mathbf{p}.\nabla)E + \frac{1}{c}\,\dot{\mathbf{p}} \times \mathbf{B} \tag{2.6}$$

Here the first part is the gradient force $(\mathbf{p}.\nabla)E$, which is essentially due to interaction of the particle-induced dipole moment $\mathbf{p}$ with the electric field $\mathbf{E}$ and the second part is termed as the scattering and absorbing forces $1/c\ \dot{\mathbf{p}}\mathrm{x}\mathbf{B}$.

The time averaged total force exerted by an arbitrary time-harmonic electromagnetic field on a small particle can be expressed as [57][62][64][65] :

$$\langle \mathbf{F} \rangle = \frac{1}{2}\mathrm{Re}\left\{\sum_i \alpha_i^* E_i^*(r)\nabla E_i(r)\right\} \tag{2.7}$$

where $i = x, y, z$ in Cartesian coordinate; $\nabla E\ (r)$ is the gradient of the optical electric field, influenced by the polarization of the particle. The polarizability of the small particle α, including the radiation wavenumber, $k = \omega c/n$ in the medium with the refraction index $n = \sqrt{\mu\varepsilon}$, is described as

$$\alpha = \frac{\alpha_0}{1 - \frac{2}{3}ik^3\alpha_0} \tag{2.8}$$

and α_0 is the particle polarizability that satisfies the Clausius–Mossotti equation:

$$\alpha_0 = 4\pi\varepsilon_0\varepsilon_m\left(\frac{\varepsilon_p - \varepsilon_m}{\varepsilon_p + 2\varepsilon_m}\right)a^3 \tag{2.9}$$

where a is the particle radius and ε_p is the relative permittivity of the particle and ε_m is the relative permittivity of the medium.

According to the dipole approximation, it is customary to express the gradient force acting on a subwavelength sphere as [62]:

$$F_{grad} = (1/2)\,\alpha_0 \nabla E^2 \tag{2.10}$$

The gradient component of the total force is proportional to the dispersive part (real part) of the complex polarizability.
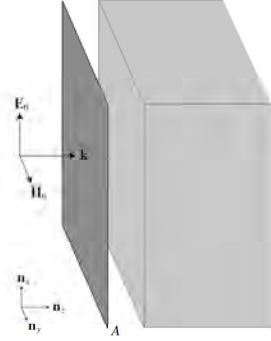
Figure 2-1: Configuration used to derive the radiation pressure. A is a planar surface parallel to the interface. [60]

The radiation pressure P can be computed by integrating Maxwell's stress tensor on an infinite planar surface "A" parallel to the interface [Figure 2.1]:

$$P \, \mathbf{n}_z = \frac{1}{A} \int_A \langle \overleftrightarrow{T} \, (r,t) \rangle \, . \, \mathbf{n}_z da \tag{2.11}$$

For small spheres, the radiation pressure forces can also be approximated through the absorbing (C_{abs}) and scattering (C_{scat}) cross sections as: [62]

$$F_{scat} \quad = \frac{|E|^2}{8\pi} \, (\, C_{abs} + C_{scat}) \mathbf{k}/|\mathbf{k}| \tag{2.12}$$

The terms of these cross sections can be calculated using the method mentioned in reference 66 and **k** is the wave number.

2.2.4.2   Maxwell Stress Tensor:

The time averaged force $\langle \mathbf{F} \rangle$ on the illuminated object can be calculated by integrating the Maxwell stress tensor [67] which is derived from Lorentz force law combined with Maxwell's equations.

$$\langle \mathbf{F} \rangle \quad = \frac{1}{2} \left\{ \int_S < \overleftrightarrow{T} >. \mathbf{n} dS \right\} \tag{2.13}$$

with surface S and surface normal **n**. The components of the Maxwell stress tensor $\overleftrightarrow{T}$ have the following form:

$$T_{ij} = \epsilon_0 \left(E_i E_j - \frac{1}{2} |E|^2 \delta_{ij} \right) + \frac{1}{\mu_0} (B_i B_j - \frac{1}{2} |B|^2 \delta_{ij}) \tag{2.14}$$

where E_i is the ith component of the electric field, B_i is the ith component of the magnetic flux field [58].

For micron sized particles, i.e. for particles way beyond the Rayleigh condition (ka>>1) the optical force arising from the transfer of photon momentum to the microparticle, can be computed using Maxwell Stress Tensor as computed by equation (2.13). More about Maxwell Stress Tensor are described in a later section.

2.3   Photonic Crystal

A solid state crystal is a periodic arrangement of atoms or molecules. Its optical analogue is the photonic crystal (also known as photonic bandgap materials), which enables researchers to tailor the properties of light. Like electrons being stuck in potential wells, photons can also be confined in modulated layers of photonic crystals (PC). Even in nature this periodic structure is found in different forms of structural coloration and animal reflectors. In contrast to the natural crystals, in this optical analogue atoms or molecules are replaced by macroscopic media with differing dielectric constants and the periodic potential is replaced with a periodic dielectric function. PC has opened a gateway to confine light within a specified volume, or to propagate them in certain directions and most importantly it has introduced the process of engineering materials that will respond to light over certain frequencies by perfectly reflecting them. Photonic crystals (PC), a solution to the manipulation of light, can be designed with a periodic modulation of the refractive index that introduces a photonic bandgap.

(a)   (b)   (c)
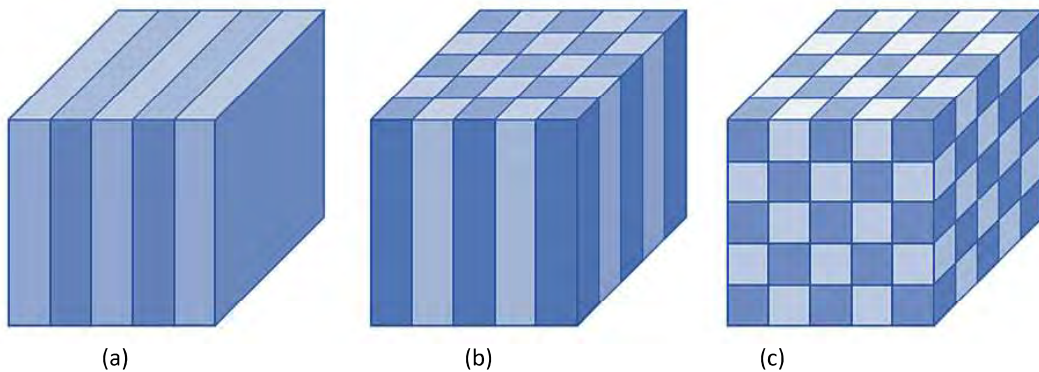
Figure 2-2: Examples of (a) 1D, (b) 2D and (c) 3D photonic crystals. The color contrast represents materials with different dielectric constants.

2.3.1 Structure and Category

PCs are categorized by the dimension of periodicity. Depending on the geometry of the structure, PCs are divided into three broad categories: (a) one-dimensional (1D) (b) two-dimensional (2D) (c) three-dimensional (3D) structures as shown in Figure 2-2.

In 1D PCs, the periodic modulation of the permittivity (refractive index) occurs in one direction only, while in two other directions the structure remains uniform. 1D PC is generally represented by the layered structure or a multilayer film. The very first analysis of optical properties of such a multilayer film was presented in Lord Rayleigh's work in 1887. The variation of the refractive index, layer's thickness and the number of layers within the period can obtain different periodic 1D structures [68]. A multilayer dielectric mirror or Bragg mirror is a well-known 1D photonic crystal where light wave is partially reflected at each interface and the destructive interference of the incident wave prohibit the forward propagation of waves. Dielectric feedback laser, Dielectric Fabry Perot Filters are also periodic in one dimension.

In 2D PC, permittivity is periodic along two directions, while in the third direction the medium is uniform. Periodically arranged system of dielectric rods in air is an example of 2D PC. They can also be found in nature. For instance, the pattern on the butterfly's wing and its rainbow play is caused by the light reflection from the microstructure on the wing [68]. The last category of PC i.e., the 3D PC is a dielectric structure that is periodic in all three directions. Drilled dielectric called Yablonovite, inverse opal, diamond lattice of air holes- are examples of 3D PCs.

(a)   (b)
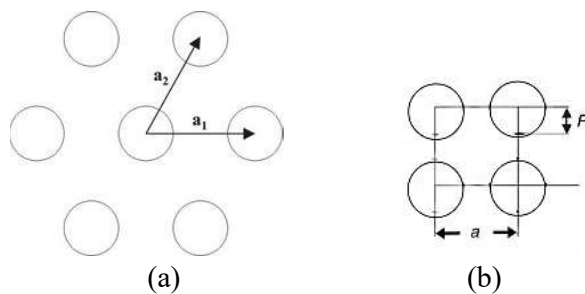
Figure 2-3: Unit Cell of a (a) Hexagonal lattice and (b) Square lattice of 2D PC. a_1 and a_2 define the sides of the unit cell for (a) and a defines the lattice constant for (b)

Like solid state crystals, the dielectric unit that is repeated over and over again to form the photonic structure is basically the unit cell of a photonic crystal. The permittivity or refractive index distribution

inside the PC and its shape define its unit cell. Figure 2-3 contains two examples of unit cell of a hexagonal and a square lattice. Unit cells in a reciprocal lattice space, which represents the spatial Fourier spectrum of the photonic crystal structure is defined as the Brillouin Zone of a PC. A detailed information regarding reciprocal lattice and Brillouin zone and their identification method is provided in references [1] [68].

This research is focused on certain kind of one and two dimensional PC constituting spherical particles. For 2D PC, both square and hexagonal lattice structures are studied and for each crystal the Brillouin zone and the wave vector set are defined differently based on their structures. Square lattice array has a square shaped Brillouin zone and the triangular inset is the irreducible Brillouin zone as displayed in Figure 3. The three special points that define the irreducible Brillouin zone of a square shaped lattice are: Γ, X and M. If $k_\parallel$ is the in plane wave vector, then Γ, X and M correspond to $k_\parallel=0$, $k_\parallel = \frac{\pi}{a} \hat{x}$ and $k_\parallel = \frac{\pi}{a} \hat{x} + \frac{\pi}{a} \hat{y}$. The k-paths for both square and hexagonal lattice types are shown in Figure 2-4.
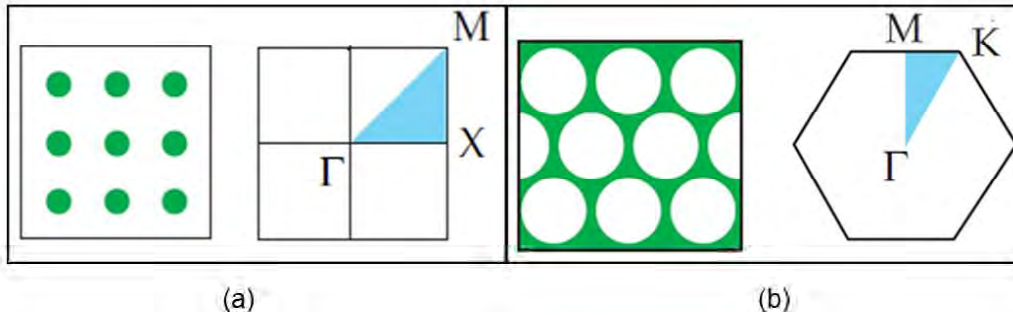
Figure 2-4: Reciprocal Brillouin zone (a) 2D square PC (b) Hexagonal PC. High symmetry points of the irreducible Brillouin zone is marked light blue [1]

2.3.2 Photonic Bandgap and Band structure:

Photonic crystals are also called photonic bandgap materials because of their unique feature- Photonic Bandgap. In a PC, multiple reflections from surfaces separated by a distance similar to the wavelength prevent an optical beam from propagating through the crystal. For example, in a1D mirror, forward and backward diffracted waves give rise to a standing wave in the structure as they reach their critical wavelength. As the waves cannot propagate, there remain no waves within a certain interval as shown in Figure 2-5, which is known as the **photonic bandgap** (PBG).

Photonic bandgap is the characteristic of PC that denotes the range of energy or frequencies where light is prevented from propagation in certain directions with specified frequencies [1]. Within this range of energies or frequencies PC cannot have any allowed mode [1][68]. When the propagation is

prohibited in any direction from any source and for any polarization the bandgap is termed as a complete bandgap for that certain frequency range [68]. In 1990 Ho et al. assumed a specific dielectric 3D periodic structure that can yield complete photonic bandgaps [1].

Band structure of a PC provides the most general information about the PC properties. The band structure shows the dispersion relations between the time frequency and the spatial frequency (wave number k). It is represented by a number of eigen-states or eigen-frequencies of an infinite periodic structure. Constructive and destructive interference between forward and backward waves causes either transmission or reflection of the radiation. The allowed frequencies within the PC structure are denoted as its eigen frequency [68]. In a PC band structure, depending on the concentration of the energy in the modes, the upper and lower region of bandgap is named separately.

2.3.3   Origin of Band Gap

The origin of bandgap lies in the distribution of electromagnetic energy inside the PC structure. A harmonic mode in a dielectric medium tends to concentrate its electric field energy in high dielectric region. According to the electromagnetic variational theorem which tends to minimize the following functional:

$$u_f(\mathbf{H}) = \frac{\left(\mathbf{H}, \widehat{\Theta}\mathbf{H}\right)}{(\mathbf{H}, \mathbf{H})}$$

$$u_f(\mathbf{H}) = \frac{(\nabla \times \mathbf{E}, \nabla \times \mathbf{E})}{(\mathbf{E}, \boldsymbol{\varepsilon}(\mathbf{r})\mathbf{E})}$$

$$= \frac{\int d^3\mathbf{r}\left|\nabla \times \mathbf{E}(\mathbf{r})^2\right|}{\int d^3\mathbf{r}\boldsymbol{\varepsilon}(\mathbf{r})|\mathbf{E}(\mathbf{r})^2|} \tag{2.15}$$

This expression reveals that to minimize the electromagnetic energy functional, u_f, the denominator needs to be maximized and for highest dielectric constant the minimum value of u_f can be obtained. Thus, to minimize u_f, electric field E concentrates in high $\boldsymbol{\varepsilon}$ region [1]. For dielectric contrast, the energy concentration in different bands become different and the bandgap basically arises for the difference in the field energy location. Generally, in one dimensional photonic crystals, bandgap arises between every set of bands [1].

2.3.4   Master Equation

Photonic bands are obtained by the similar procedure to solid state physics theory, i.e. a master equation which is obtained from the combination of Maxwell's equation. This equation is transformed

into an eigenvalue equation with a periodic boundary condition and computed based on the following four approximations [1]:

1. The field strengths are small enough and can be considered in the linear regime.
2. The material is macroscopic and isotropic so that electric field, $E(r, \omega)$ and displacement field, $D(r, \omega)$ are related by relative permittivity.
3. The material is dispersion free and a certain value of dielectric constant appropriate to the frequency range of the physical system is considered.
4. Materials are transparent, i.e., $\varepsilon(\omega)$ is real and positive.

Based on all these assumptions, the Maxwell's Equations can be written as:

$$\nabla \cdot \mathbf{H}(\mathbf{r}, \mathbf{t}) = 0 \tag{2.16}$$

$$\nabla \times \mathbf{E}(r, t) + \mu_0 \frac{\partial \mathbf{H}(r, t)}{\partial x} = 0 \tag{2.17}$$

$$\nabla \cdot [\boldsymbol{\varepsilon}(\mathbf{r})\mathbf{E}(\mathbf{r}, \mathbf{t})] = 0 \tag{2.18}$$

$$\nabla \times \mathbf{H}(\mathbf{r}, \mathbf{t}) - \varepsilon_0 \varepsilon(\mathbf{r}) \frac{\partial \mathbf{E}(\mathbf{r}, \mathbf{t})}{\partial x} = 0 \tag{2.19}$$

For mathematical convenience, the harmonic modes of both magnetic and electric fields are expressed as a spatial pattern times a complex exponential:

$$\mathbf{E}(\mathbf{r}, \mathbf{t}) = \mathbf{E}(\mathbf{r})\exp(-i\omega t)$$

$$\mathbf{H}(\mathbf{r}, \mathbf{t}) = \mathbf{H}(\mathbf{r})\exp(-i\omega t)$$

Inserting the above equations into the Maxwell Equations, the following forms of the divergence equations are obtained:

$$\nabla \cdot \mathbf{H}(\mathbf{r}) = 0$$

$$\nabla \cdot [\boldsymbol{\varepsilon}(\mathbf{r})\mathbf{E}(\mathbf{r})] = 0$$

Then using Fourier domain, the two curl equations can be expressed in the following manner:

$$\nabla \times \mathbf{E}(\mathbf{r}) = i\omega\mu_0\mathbf{H}(\mathbf{r})$$
$$\nabla \times \mathbf{H}(\mathbf{r}) = -i\omega\varepsilon_0\varepsilon(\mathbf{r})\mathbf{E}(\mathbf{r})$$

Dividing second equation by $\varepsilon(\mathbf{r})$ and then again taking curl on both sides the Master Equation can be obtained:

$$\nabla \times \left(\frac{1}{\varepsilon(\mathbf{r})}\nabla \times \mathbf{H}(\mathbf{r})\right) = -i\omega\varepsilon_0(\nabla \times \mathbf{E}(\mathbf{r}))$$

$$\nabla \times \left(\frac{1}{\varepsilon(\mathbf{r})} \nabla \times \mathbf{H}(\mathbf{r}) \right) = -i\omega\varepsilon_0 (i\omega\mu_0 \mathbf{H}(\mathbf{r}))$$

$$\nabla \times \left(\frac{1}{\varepsilon(\mathbf{r})} \nabla \times \mathbf{H}(\mathbf{r}) \right) = \omega^2 \varepsilon_0 \mu_0 \mathbf{H}(\mathbf{r})$$

$$\boxed{\nabla \times \left(\frac{1}{\varepsilon(\mathbf{r})} \nabla \times \mathbf{H}(\mathbf{r}) \right) = \frac{\omega^2}{c^2} \mathbf{H}(\mathbf{r})} \qquad (2.20)$$

This is the master equation where, the vacuum speed of light, $c = 1/\sqrt{(\mu_0\varepsilon_0)}$ .This equation can be presented as an Eigen value problem: $\widehat{\Theta}\mathbf{H}(\mathbf{r}) = \frac{\omega^2}{c^2}\mathbf{H}(\mathbf{r})$

Where $\widehat{\Theta}$ is the linear differential operator identifying the left side of the master equation in the following manner:

$$\widehat{\Theta}\mathbf{H}(\mathbf{r}) \triangleq \nabla \times \left(\frac{1}{\varepsilon(\mathbf{r})} \nabla \times \mathbf{H}(\mathbf{r}) \right) \qquad (2.21)$$

The above equation can be interpreted as: if $\mathbf{H}$ is an eigenfunction of some periodic structure which is defined by periodic dielectric function $\varepsilon(\mathbf{r})$, the influence of the operator $\widehat{\Theta}$ upon this function is equal to the multiplication of this function by the constant which is called the eigen-value [68]. The eigenvectors, $\mathbf{H}(\mathbf{r})$ represent the spatial pattern of the harmonic modes while the eigen values $\frac{\omega^2}{c^2}$ are proportional to the squared frequencies of those modes. Since the operator $\widehat{\Theta}$ is a Hermitian operator, they have real eigen values which are orthogonal and they can be obtained from variational theorem [1].

2.3.5 Bloch Theorem & Photonic Crystal Spectrum

Block theorem asserts that the solution in a periodic potential is always a product of two terms:

- A periodic function
- A plane wave

According to Bloch's theorem, the electromagnetic modes i.e. the eigenvector, $\mathbf{H_k}(\mathbf{r})$ can be expressed as a plane wave modulated by a periodic function that shares the periodicity of the optical lattice :

$$\mathbf{H_k}(\mathbf{r}) = e^{i\mathbf{k}.\mathbf{r}}\mathbf{u_k}(\mathbf{r}) \qquad (2.22)$$

where $\mathbf{u_k}(\mathbf{r})$ is the periodic function on the lattice.

The photonic crystal spectrum is nothing but the presentation of all the eigen values derived from the Master equation. The eigen waves obtained from this equation are allowed to propagate along z through the periodic structure and these EM waves are called the modes of the photonic crystal.

For a photonic crystal with discrete periodicity, all the information of its modes are contained within the periodic Bloch function $\mathbf{u_k}(\mathbf{r})$ and the wave vector $\mathbf{k}$. To solve for $\mathbf{u_k}(\mathbf{r})$, the Block states need to be inserted into the Master equation [1]:

$$\widehat{\Theta}\mathbf{H_k} = \frac{\omega(\mathbf{k})^2}{c^2}\mathbf{H_k}$$

$$\nabla \times \frac{1}{\varepsilon(\mathbf{r})}\nabla \times e^{i\mathbf{k}.\mathbf{r}}\mathbf{u_k}(\mathbf{r}) = \frac{\omega(\mathbf{k})^2}{c^2}e^{i\mathbf{k}.\mathbf{r}}\mathbf{u_k}(\mathbf{r})$$

$$(i\mathbf{k} + \nabla) \times \frac{1}{\varepsilon(\mathbf{r})}(i\mathbf{k} + \nabla) \times \mathbf{u_k}(\mathbf{r}) = \frac{\omega(\mathbf{k})^2}{c^2}\mathbf{u_k}(\mathbf{r})$$

$$\widehat{\Theta}_\mathbf{k}\mathbf{u_k}(\mathbf{r}) = \frac{\omega(\mathbf{k})^2}{c^2}\mathbf{u_k}(\mathbf{r}) \tag{2.23}$$

The above equation is helpful to determine $\mathbf{u_k}$, i.e., the mode profiles. Here $\widehat{\Theta}_\mathbf{k} \triangleq (i\mathbf{k} + \nabla) \times \frac{1}{\varepsilon(\mathbf{r})}(i\mathbf{k} + \nabla) \times$, the new Hermitian operator which depends on $\mathbf{k}$ has been substituted.

Here $\mathbf{k}$ is a continuous parameter and for each value of $\mathbf{k}$, it is possible to find an infinite set of modes with discretely spaced frequencies that are labeled as band index n. For a given n, a continuous variation of k yields a similar variation in frequency and thus a set of continuous function $\omega(k)$ or the mode profiles are obtained. The information derived from these functions are mainly termed as the band structure of the photonic crystal [1].

For three different lattice type, band structures are plotted in Figure 2-5. Two different forms of reduced Maxwell equation i.e., TM and TE are considered based on different radiation polarization. TM polarization has non zero Ez, Hx and Hy and TE polarization has Hz, Ex, Ey components of the field. These polarizations are defined based on which field vector has the component perpendicular to the plane of photonic crystal.
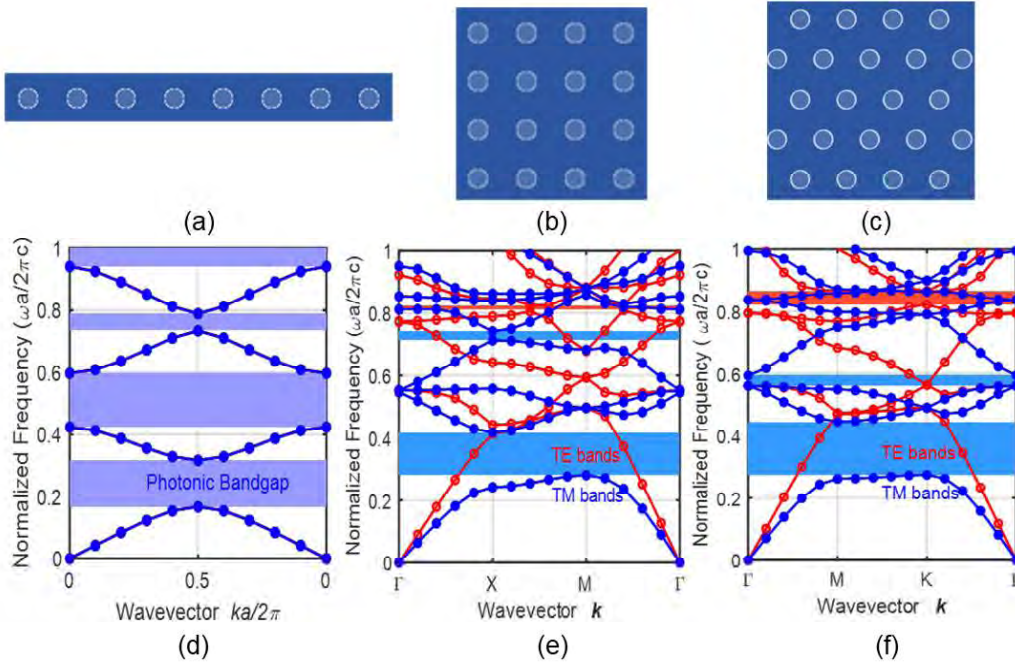
Figure 2-5: (a) 1D array, (b) 2D square array, (c) 2D hexagonal array and (d-f) their band structures. Particle permittivity:12 and radius: 0.2a.

As already mentioned depending on the modulation of permittivity, at some specific range of frequencies, the radiation cannot propagate inside the PC and in Figure 2-5 for all three cases there are significant amount of gap is observed in between the bands marked with solid fill of colors. These are the complete band gaps for each kind of crystal.

2.4   Whispering Gallery Mode Resonator

Whispering gallery modes (WGM) or waves are the electromagnetic surface oscillation in optical cavity that correspond to waves circling around the periphery. The circulating waves interfere constructively when the resonance condition (after one roundtrip they return to the same point with the same phase (modulo 2π) is met and hence form standing waves. High Q-factors, low mode volumes, small size, the ability to operate at optical (and telecommunication) frequencies of light and the ease of fabrication and on-chip integration- are some of the intriguing features of WGM resonators. [69]

2.4.1 Historical Background

The term "whispering gallery waves" was introduced by Lord Rayleigh in the 19th century to explain the phenomenon of the whispering gallery located under the dome of St. Paul's cathedral in London [2][69][70]. Whispering gallery mode resonators were named after the path that the resonant light follows as it circulates in the cavity. It was known that a sound (a whisper) uttered at one end of the dome could still be heard loudly at the opposite end of the dome, a large distance away from the source. By direct experiments using a whistle as a sound source and a burning candle as a detector, Lord Rayleigh described this phenomenon as: sound seemed to cling to the rigid reflector like dome of St. Pauls' and creep only inside a narrow layer near the surface of the concave wall of the gallery [Figure 2-6]. The smooth, curved walls guiding the sound waves around the periphery of the gallery made it possible. Also, in this case sound should decay in intensity only as the inverse of the distance while in free space sound intensity decreases proportionally to the square of the distance from the source radiating in all directions. Because of this slower decay rate in free space, whispers became audible near the edges of the gallery. Sound waves taking any other path to the listener generally get dissipated or scattered en route. [70]
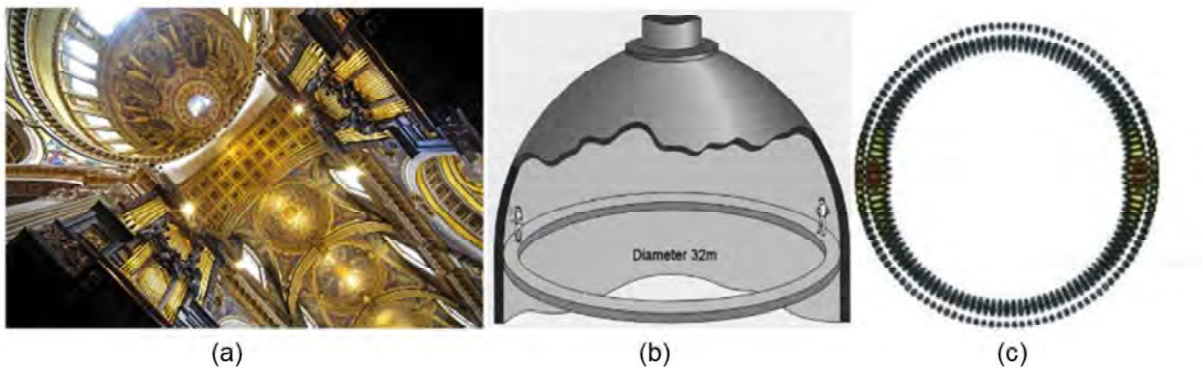
Figure 2-6: (a) A view of the dome of St Pauls Cathedral from below. (b)A sketch of the whispering gallery and (c) the sound intensity profile showing the whispering gallery phenomenon that Lord Rayleigh studied [69]

In the beginning of the 20th century its was found that like sound waves, WGMs also exist for light waves where specific resonances (or modes) of a wave field get confined inside a given resonator (cavity) with smooth edges due to continuous total internal reflection (TIR). So in other words, WGM optical resonators are dielectric structures capable of trapping light in paths around the periphery like the one happened in St Pauls' [70].

Apart from light waves, whispering-gallery waves have also been demonstrated for other electromagnetic waves such as radio waves, microwaves, terahertz radiation, infrared radiation, ultraviolet waves and x-rays. [71].

2.4.2 Modeling WGM Resonator

A circular cross section can typically contain WGM enabling light to be trapped as it propagates near the periphery. Electromagnetic whispering gallery waves propagate in the concave region if it has larger permittivity than the surrounding region. In order to excite WGMs, there should necessarily be a concave interface between two dielectric media with different permittivities defined as $\varepsilon_1 = \varepsilon_1' - i\varepsilon_1''$ and $\varepsilon_2 = \varepsilon_2' - i\varepsilon_2''$. For example, a dielectric cylinder with $\varepsilon_1' > 1$ surrounded by air with $\varepsilon_2'=1$ can sustain WGM. To excite WGM, the interface must have a shape of the solid of revolution, i.e., rod, sphere, hemisphere, toroid or cone [71].
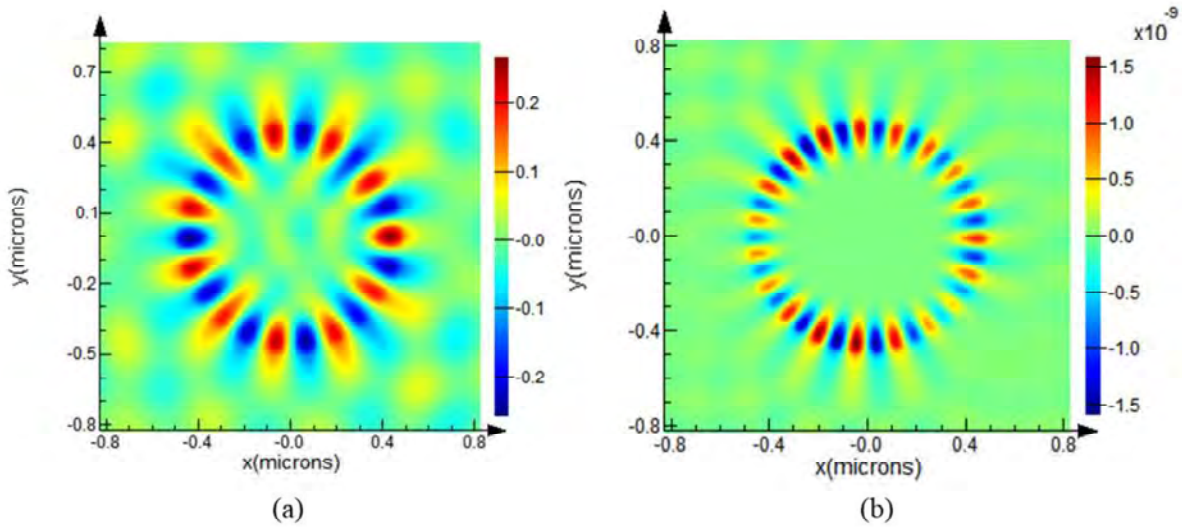
Figure 2-7: Magnetic Field profile (Hz) of a 1um Polystyrene microsphere in air medium at (a) 341 nm (b) 370 nm. Particle is illuminated by point dipole source.

For a 1um polystyrene microsphere whispering gallery mode profile is observed as shown in Figure 2-7. The difference between the refractive index at the interface between the particle and surrounding medium is met as the particle is kept in air medium.

22

2.4.3 Resonance:

Whispering gallery modes have extraordinary optical field intensity and their energy is mainly confined to the region near the boundary. Total internal reflection at the interface between the resonator and the surrounding medium confines light in WGM resonators as displayed in Figure 2-8.

In a spherical structure, optical resonance occurs for light that has an optical path length to complete a round trip in the sphere as a multiple integer of the light wavelength, λ. So, for a sphere with refractive index n and equatorial radius R, resonance condition is met when

$$2\pi Rn \approx m\lambda \tag{2.24}$$

where m is an integer representing the azimuthal mode number and m>>1 [71]. Constructive interference occurs under these conditions, allowing the circulating intensity to grow until the rate at which light is coupled into the cavity is balanced by the rate at which it is lost. This phenomenon is referred to as resonance and the electromagnetic field profile that describes the path the resonant light takes is called the mode.

(a)   (b)
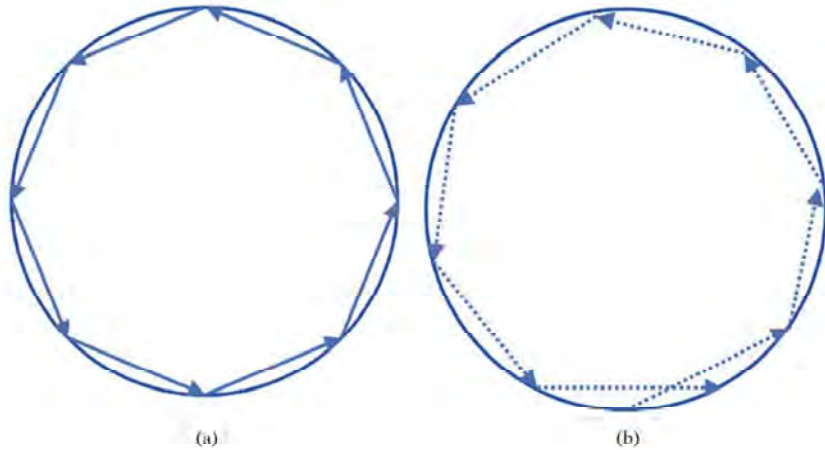
Figure 2-8: Ray of light propagation by TIR in a spherical cavity. (a) on resonance (b) off resonance

Any change in R and n affects the resonant wavelength in the following manner [71]:

$$\frac{dR}{R} + \frac{dn}{n} = \frac{d\lambda}{\lambda} \tag{2.25}$$

Thus, any perturbation of the refractive index or cavity path length will change the resonance wavelength of the WGM resonator. Since the spatial field profile depends on the wavelength of light, the effective refractive index changes as well as the mode number for a certain resonator. In Figure 2-7, for two different resonance wavelength, WGM profile shows two different mode number for a 1um

polystyrene particle in air medium. The change in the effective index profile accounts for this phenomenon and it supports the above equation.

For more accurate consideration of the distribution of optical intensity that spans both the resonator and the surrounding medium, n in equation (2.24) can be replaced with n_{eff} which is defined as:

$$n_{eff} = \frac{\int n(r)E(r)^2 dr}{\int E(r)^2 dr}$$

(2.26)

2.4.4 WGM Mode Structure

The true mode frequencies within a circular resonator are given by the eigenvalues of the appropriate wave equation. In this regard, an example of scalar wave can be considered in an idealized whispering gallery namely a 2D circular cavity of radius R [Figure 2.9]. The electromagnetic field profile for such a WGM resonator with refractive index n can be described by the Helmholtz equation:

$$\nabla^2 E + \frac{\omega^2 n^2}{c^2} E = 0$$

(2.27)

The resonator is placed in a medium that affects its field profile. For a WGM cavity like the one shown in Figure 04, a jump in n(r) results in two separate Helmholtz' equation: [2][69][72]

$$\nabla^2 E + \frac{\omega^2 n_1^2}{c^2} E = 0 \text{ for } r < R$$

$$\nabla^2 E + \frac{\omega^2 n_2^2}{c^2} E = 0 \text{ for } r > R$$

(2.28)

n_1 and n_2 are the refractive index of the resonator and the surrounding medium. The above equations can be written in terms of H also.
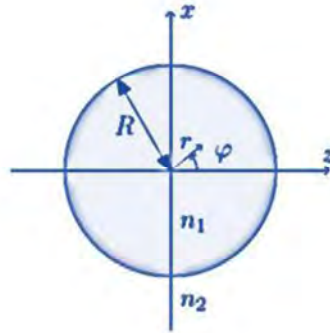
Figure 2-9: A disc with radius R and refractive index n_1, refractive index of the background medium: n_2

Time harmonic oscillation of the field is a mandatory assumption to obtain the resonant solution to the equation of a whispering gallery profile and this oscillating behavior is defined by a time dependence of $e^{-i\omega t}$, in this case ω can be a complex number. Since the field of such a cavity is generally lossy, the physically relevant solution should have the same decaying nature. Therefore to obtain the desired

decay, the real part of $-i\omega t$ will be negative with a positive imaginary part of ω. For the target wavelength λ, the relationship between ω and λ can be expressed as: $Re(\omega) = \frac{2\pi c}{\lambda}$.

For a circularly symmetric structure, the fields can be expressed in terms of cylindrical coordinates (r, φ). To get the desired resonance the fields should be exactly equal to the original fields after making one roundtrip. This results in an angular dependence $e^{im\phi}$ of the electric field, where m is an integer. Hence, the electric field associated with TE polarization (E_y, H_x and H_z) has the form E(r; φ; t) = $E_y(r)e^{i(m\phi - \omega t)}$. Substituting this into the Helmholtz equation of equation 2.27 [70]:

$$\left[\frac{\partial^2}{\partial r^2} + \frac{1}{r}\frac{\partial}{\partial r} + \frac{\omega^2 n^2}{c^2} - \frac{m^2}{r^2}\right] E_y(r) = 0 \tag{2.29}$$

Multiplication of the above equation by r^2 gives the Bessel equation

$$\left[r^2\frac{\partial^2}{\partial r^2} + r\frac{\partial}{\partial r} + r^2\frac{\omega^2 n^2}{c^2} - m^2\right] E_y(r) = 0 \tag{2.30}$$

Solutions of this equation are the Bessel functions J and Y. Based on the boundary conditions, a suitable combination of the fundamental solutions J and Y has to be chosen for each region. A detailed description of the mode equation and its solution can be found in reference [2][70].

2.4.5   Optical Modes and Mode numbers:

Electromagnetic modes that are of whispering gallery type have the property that their energy is mainly confined to the region, i.e. highly localized near the boundary. Due to the effect of total internal reflection these modes are much better confined inside the cavity (higher Q-factor) than (most) other eigen modes of the cavity [2][69].

The spatial structure and the resonance frequency of each WGM is characterized by a unique set of numbers, i.e. the polar, the azimuthal, and the radial mode number l, m, and n, respectively. l corresponds to angular mode number that depends on the equatorial length, expressed in number of wavelengths, m is azimuthal mode number and n represents the number of maxima along the radial direction [73]. Figure 2-10 and 2-11 show the mode profile of two different sized microsphere. In Figure 2-10 the azimuthal mode number varies with the effective refractive index of the cavity. In Figure 2-11 for a slightly larger polystyrene particle different mode numbers are observed with evolution of resonance wavelength.
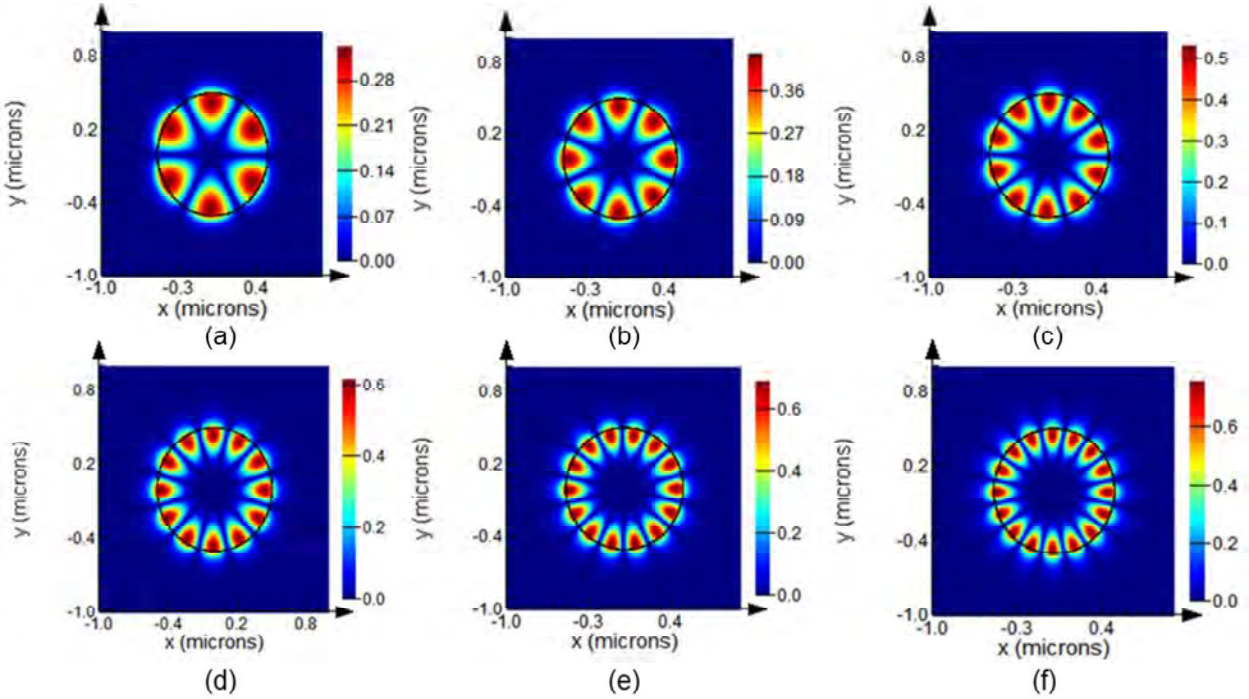
Figure 2-10: Whispering Gallery Eigen mode profile across the cross section of a 1μm polystyrene microparticle. Azimuthal mode number, m (a)6, (b)8, (c)10 (d)12, (e)14, (f)16.
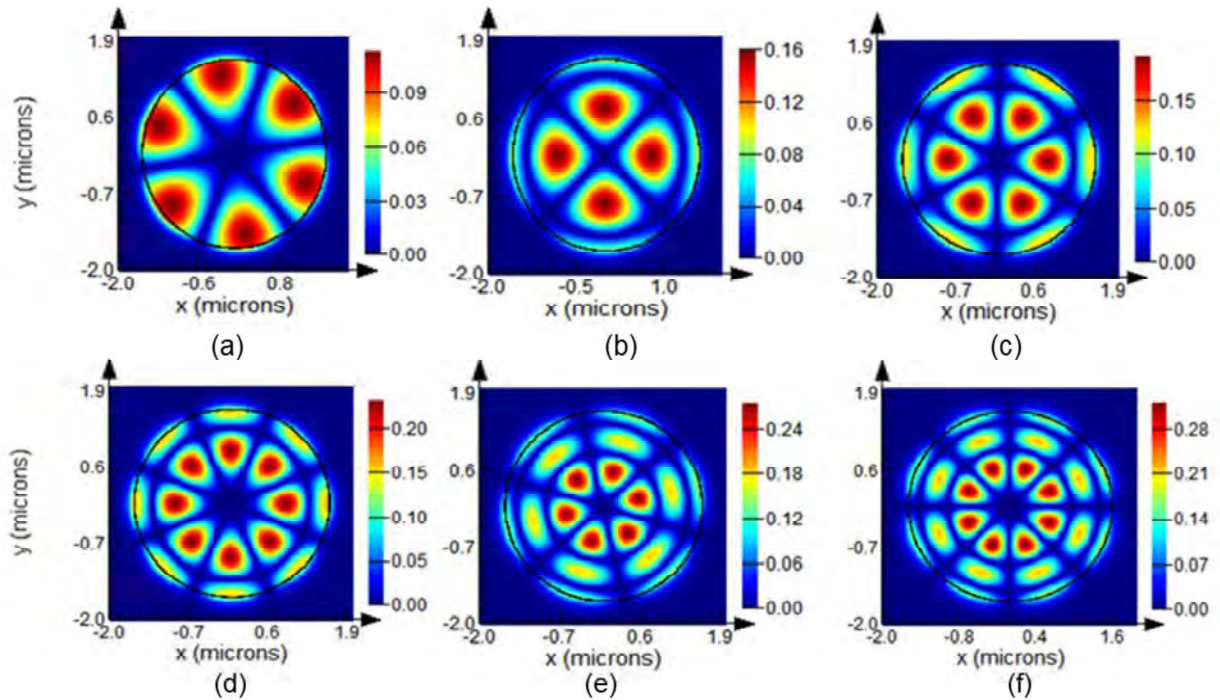
Figure 2-11: Electric Field Profile of a Polystyrene sphere (refractive index=1.574) in water medium, radius 1.6μm. Mode number and resonant wavelength(λ_R): Top row: (a) m=6,n=1,λ_R= 2.62μm;(b) m=4,n=2, λ_R= 3.9μm; (c) m=6, n=2, λ_R= 2.58μm. Bottom row : (d) m=8, n=2, λ_R= 1.92μm; (e) m=6, n=3, λ_R= 2.53 μm; (f) m=8, n=3, λ_R= 1.88μm.

26

2.4.6 Resonator Parameters

The resonant parameters of a WGM resonator quantifies different aspects of the resonant cavity and help to describe its spectrum obtained from the eigen frequencies.

2.4.6.1 Quality Factor:

To determine the efficiency of a resonator for confinement of light and the optical intensity in the resonant cavity of a WGM, the quality factor Q acts like a figure of merit. The Q factor is proportional to the decay time of the waves, which in turn is inversely proportional to both the surface scattering rate and the wave absorption in the medium making up the gallery. It can be defined as:

$$Q = \omega_0 \frac{\text{Stored Energy}}{\text{Power Loss}} = \omega_0 \tau = \frac{\omega_0}{\Delta \omega_{FWHM}}$$

where $\omega_0 = 2\pi \nu_0$ is the angular frequency, here ν_0 is the frequency of the resonance, τ is the time required for the field intensity to decay by a factor e, $\Delta \omega_{FWHM} = 1/\tau$ is the linewidth of the full width at half maximum of the resonance peak.

Since Q factor provides an estimation of the decay time of the energy stored inside the resonator in terms of the number of total field oscillation (times 2π), high-Q basically denotes a longer decay time for the electromagnetic field stored within the resonator cavity [69]. In a WGM resonator, a high value of Q is generally obtained as total internal reflection ensures almost perfect guiding of the light waves near the periphery of the resonator cavity [69]. This means, the higher the Q factor, the higher the energy stored inside the resonator.

The limiting factors of Q are dielectric, metal and radiation losses [71]. Different loss mechanics that can impact the Q factor can be expressed as [69]:

$$\frac{1}{Q} = \frac{1}{Q_{mat}} + \frac{1}{Q_{surf}} + \frac{1}{Q_{scatt}} + \frac{1}{Q_{bend}}$$

Q_{mat}: describes intrinsic material absorption

Q_{surf}: surface absorption losses (due to surface coatings or adsorbed material, for example due to adsorbed water or due to other contaminants)

Q_{scatt}: scattering losses (intrinsic and inherent to the surface of the cavity, such as imperfections in the form of surface-roughness).

Q_{bend}: bending loss (or whispering gallery or tunnel or radiation loss). WGM is generally termed as a leaky mode as incomplete total internal reflection ultimately results in transmitted waves that leak in the lower refractive index region.

2.4.6.2 Mode Volume:

Apart from temporal confinement of light defined by Q-factor, mode volume is an important performance parameter that defines the extent of spatial confinement of a WGM mode. Small mode volume is a requirement for a good WGM resonator. The ratio of energy stored inside the resonator in that mode to the maximum energy density of that mode is termed as the mode volume of a field eigenmode in a resonator [69][74]

$$V_{Mode} = \frac{\text{Stored Energy Density}}{\text{Maximum Energy Density}} = \frac{\int \varepsilon(r)|E(r)|^2 d^3 r}{\max(\varepsilon(r)|E(r)|^2)}$$

CHAPTER 3

MODEL AND GEOMETRY DESCRIPTION

3.1 Maxwell Stress Tensor and Optical Force

The time averaged optical force acting on a particle due to harmonic fields may be calculated from the Maxwell Stress Tensor (MST) which is already mentioned in Chapter 02. In this work, the net force on individual microparticle is computed by integrating the MST over a closed surface surrounding the particle.

MST is a symmetric second-order tensor used in classical electromagnetism that models the interaction between electromagnetic forces and mechanical momentum. This is one of the most extensively used methods in calculating optical force and torque functioning on an illuminated object. MST method is based on the conservation laws of electromagnetic wave momentum involving the current densities of linear and angular momentum [76-77]. For a trapped spherical particle, the total electromagnetic force may be determined by applying MST in the space surrounding the particle [77].
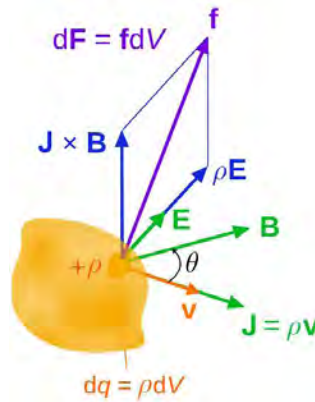
Figure 3-1: Lorentz force (per unit -volume) f on a continuous charge distribution (charge density ρ) in motion. The current density J corresponds to the motion of the charge element dq in volume element dV and varies throughout the continuum.

MST is derived from the Lorentz force law. According to this law, the total electromagnetic force, F on the charges in volume V is expressed as:

$$\mathbf{F} = q\,(\mathbf{E} + v \times \mathbf{B}) \tag{3.1}$$

Dividing equation (3.1) by V, Force per unit volume is obtained as:

$$\mathbf{f} = \rho(\mathbf{E} + v \times \mathbf{B}) = \rho\mathbf{E} + \mathbf{J} \times \mathbf{B}$$

Eliminating ρ and J using Maxwell's equations (2.1) and (2.4):

$$\mathbf{f} = \varepsilon_0(\nabla.\mathbf{E})\mathbf{E} + \left(\frac{1}{\mu_0}(\nabla \times \mathbf{B}) - \varepsilon_0\frac{\partial \mathbf{E}}{\partial t}\right) \times \mathbf{B}$$

Now, using the law of vector products:

$$\frac{\partial}{\partial t}(\mathbf{E} \times \mathbf{B}) = \frac{\partial \mathbf{E}}{\partial t} \times \mathbf{B} + \mathbf{E} \times \frac{\partial \mathbf{B}}{\partial t}$$

And also from Faraday's Law:

$$\frac{\partial \mathbf{B}}{\partial t} = - \nabla \times \mathbf{E}$$

So,

$$\frac{\partial}{\partial t}(\mathbf{E} \times \mathbf{B}) = \frac{\partial \mathbf{E}}{\partial t} \times \mathbf{B} - \mathbf{E} \times (\nabla \times \mathbf{E})$$

Thus,

$$\mathbf{f} = \varepsilon_0[(\nabla.\mathbf{E})\mathbf{E} - \mathbf{E} \times (\nabla \times \mathbf{E})] - \frac{1}{\mu_0}[\mathbf{B} \times (\nabla \times \mathbf{B})] - \varepsilon_0\frac{\partial}{\partial t}(\mathbf{E} \times \mathbf{B})$$

Just to make things look more symmetrical, a new term is introduced since: $\nabla.\mathbf{B} = 0$

And from product rules:

$$\nabla(\mathbf{E}^2) = 2 (\mathbf{E}.\nabla)\mathbf{E} + 2\mathbf{E} \times (\nabla \times \mathbf{E})$$

$$\mathbf{E} \times (\nabla \times \mathbf{E}) = \frac{1}{2}\nabla(\mathbf{E}^2) - (\mathbf{E}.\nabla)\mathbf{E}$$

And the same goes for **B.** So now f can be rewritten as:

$$\mathbf{f} = \varepsilon_0\left[(\nabla.\mathbf{E})\mathbf{E} - \frac{1}{2}\nabla.(\mathbf{E}^2) + (\mathbf{E}.\nabla)\mathbf{E}\right] + \frac{1}{\mu_0}\left[(\nabla.\mathbf{B})\mathbf{B} - \frac{1}{2}\nabla.(\mathbf{B}^2) + (\mathbf{B}.\nabla)\mathbf{B}\right] - \varepsilon_0\frac{\partial}{\partial t}(\mathbf{E} \times \mathbf{B})$$

$$= \varepsilon_0[(\nabla.\mathbf{E})\mathbf{E} + (\mathbf{E}.\nabla)\mathbf{E}] + \frac{1}{\mu_0}[(\nabla.\mathbf{B})\mathbf{B} + (\mathbf{B}.\nabla)\mathbf{B}] - \frac{1}{2}\nabla\left[\varepsilon_0(\mathbf{E}^2) + \frac{1}{\mu_0}(\mathbf{B}^2)\right] - \varepsilon_0\frac{\partial}{\partial t}(\mathbf{E} \times \mathbf{B})$$

It can be simplified by introducing the Maxwell stress tensor [78]:

$$\mathbf{T} = \varepsilon_0\left[E_iE_j - \frac{1}{2}\delta_{ij}E^2\right] + \frac{1}{\mu_0}\left[B_iB_j - \frac{1}{2}\delta_{ij}B^2\right] \tag{3.2}$$

where: i, j = x, y, z or 1, 2, 3; i.e. the i, j indices of Maxwell's stress tensor physically correspond to the x, y, z components of the E & B-fields.

It can also be expressed in the following form:

$$\overleftrightarrow{T} = \begin{pmatrix} T_{xx} & T_{xy} & T_{xz} \\ T_{yx} & T_{yy} & T_{yz} \\ T_{zx} & T_{zy} & T_{zz} \end{pmatrix} = \begin{pmatrix} T_{11} & T_{12} & T_{13} \\ T_{21} & T_{22} & T_{23} \\ T_{31} & T_{32} & T_{33} \end{pmatrix}$$

The Kronecker delta, δ_{ij}, is 1 if the indices are the same ($\delta_{ij} = \delta_{xx} = \delta_{yy} = \delta_{zz} = 1$) and zero otherwise ($\delta_{ij} = \delta_{xy} = \delta_{yz} = \delta_{zx} = 0$).

$$T_{xx} = \frac{1}{2}\,\varepsilon_0\left(E_x^2 - E_y^2 - E_z^2\right) + \frac{1}{\mu_0}\left(B_x^2 - B_y^2 - B_z^2\right)$$

$$T_{xy} = \varepsilon_0\left(E_x E_y\right) + \frac{1}{\mu_0}\left(B_x B_y\right)$$

The divergence of $\overleftrightarrow{T}$ has its jth component:

$$\nabla.\overleftrightarrow{T} = \varepsilon_0\left[(\nabla.\mathbf{E})E_j + (\mathbf{E}.\nabla)E_j\right] + \frac{1}{\mu_0}\left[(\nabla.\mathbf{B})B_j + (\mathbf{B}.\nabla)B_j\right] - \frac{1}{2}\nabla_j\left[\varepsilon_0(\mathbf{E}^2) + \frac{1}{\mu_0}(\mathbf{B}^2)\right]$$

Thus the force per unit volume, f can be written in the much simpler form:

$$\mathbf{f} = \nabla.\overleftrightarrow{T} - \varepsilon_0\frac{\partial}{\partial t}(\mathbf{E} \times \mathbf{B})$$

Then the total force, F on the charges in V is evidently:

$$\mathbf{F} = \int_V \nabla.\overleftrightarrow{T}\, dV - \varepsilon_0\frac{\partial}{\partial t}(\mathbf{E} \times \mathbf{B})$$

The first term of the force equation can be transformed into a surface integral using divergence theorem:

$$\mathbf{F} = \oint_S \overleftrightarrow{T}.\mathbf{n}\, dS - \varepsilon_0\frac{\partial}{\partial t}(\mathbf{E} \times \mathbf{B})$$

The field momentum is zero when it is averaged over one oscillation period. In the static case the second term drops out and so the time averaged electromagnetic force on the charge configuration can be expressed entirely in terms of the stress tensor at the boundary.

So, the time averaged optical force:

$$\langle \mathbf{F} \rangle = \oint_S \langle \overset{\leftrightarrow}{\mathbf{T}} \rangle . \mathbf{n} \, dS \tag{3.3}$$

$\mathbf{n}$ is the unit normal of the closed surface S.

The force is entirely determined by the electric and magnetic fields on the surface dS. It is interesting to note that no material properties enter the expression for the force; the entire information is contained in the electromagnetic field. The only material constraint is that the body is rigid. If the body deforms when it is subject to an electromagnetic field the electrostrictive and magnetostrictive forces need to be included [60].

3.2   Numerical Solution of Maxwell Equations and FDTD method

In this thesis work, electric field distributions of all the systems considered are computed in the near field employing Finite Difference Time Domain (FDTD) analysis of Maxwell's equation of electromagnetics. The obtained field distributions are then applied to Maxwell Stress Tensor in order to estimate three dimensional (3D) optical forces acting on individual particles [79].

Finite-difference time-domain or Yee's method is one of the simplest and most popular numerical techniques, in electromagnetics for modeling nanophotonic devices, processes, and materials which provides the solution of Maxwell's equations in the time domain. The technique was first proposed by K. Yee and then improved by others in the early 70s. The time-dependent Maxwell's equations (in partial differential form) are discretized using central-difference approximations to the space and time partial derivatives. The resulting finite-difference equations are solved in a leapfrog manner: first the electric fields, then the magnetic fields, are computed at each step in time; calculation is continued until all field values have decayed to essentially zero (at least 60dB down from the peak) or a steady-state condition has been reached. In addition to time domain, FDTD can also obtain the frequency solution by exploiting Fourier transforms, thus a full range of useful quantities can be calculated [79][80].
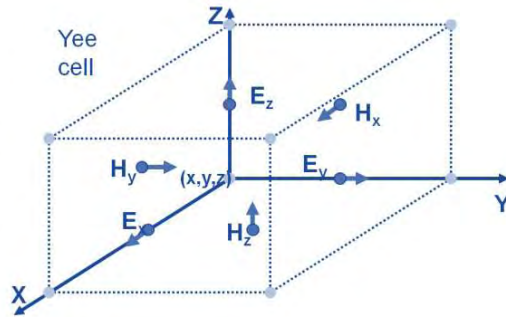
Figure 3-2: Yee cell for FDTD method

As already mentioned, the FDTD method solves Maxwell equations on a discrete spatial and temporal grid. Each field component is solved at a slightly different location within the grid cell (Yee cell). Each FDTD cell has six field values associated with it: three electric fields and three magnetic fields. Additionally, each cell has six flags associated with it to indicate the material type present at each of the six field locations. When many FDTD cells are combined together to form a three-dimensional volume, the result is an FDTD grid or mesh. FDTD simulation uses a rectangular, Cartesian style mesh. Fundamental simulation quantities (material properties and geometrical information, electric and magnetic fields) are calculated at each mesh point. The FDTD solver provides a number of features, including the conformal mesh algorithm, that provides accurate results, even when using a relatively coarse mesh.
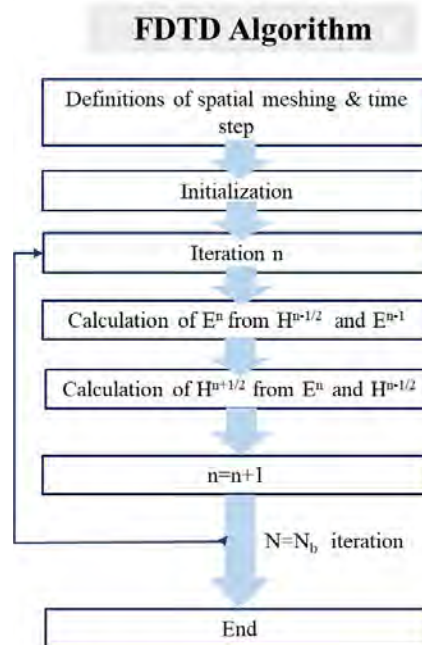
Figure 3-3: FDTD Algorithm

33

Thus the objects are discretized in space using Cartesian Grid, then using FDTD cell called Yee cell the locations of Field components are defined. Then the continuous derivatives are replaced with differences i.e., the derivatives in time and space are approximated as differences. By time marching difference equations solution evolves. This method is known as leapfrog algorithm [79]-[81]. Figure 3-3 shows schematically the algorithm and Figure 3-4 presents the MST based optical force computation technique used in this research.

Dual Gaussian Beam Induced Optical Force Computation

Gauss's Law	$\nabla . \mathbf{E} = \dfrac{\rho}{\varepsilon_0}$
Gauss's Law for Magnetism	$\nabla . \mathbf{B} = 0$
Maxwell–Faraday equation	$\nabla \times \mathbf{E} = -\dfrac{\partial \mathbf{B}}{\partial t}$
Ampere's Circuital Law	$\nabla \times \mathbf{B} = \mu_0 \mathbf{J} + \varepsilon_0 \mu_0 \dfrac{\partial \mathbf{E}}{\partial t}$

FDTD Modeling

$$\mathbf{T} = \varepsilon_0 \left[E_i E_j - \frac{1}{2}\delta_{ij}E^2 \right] + \frac{1}{\mu_0}\left[B_i B_j - \frac{1}{2}\delta_{ij}B^2 \right]$$

Maxwell Stress Tensor

Time Averaged Optical Force:
$$\langle \mathbf{F} \rangle = \frac{1}{2}\left\{ \int_S <\vec{T}>. \mathbf{n} dS \right\}$$
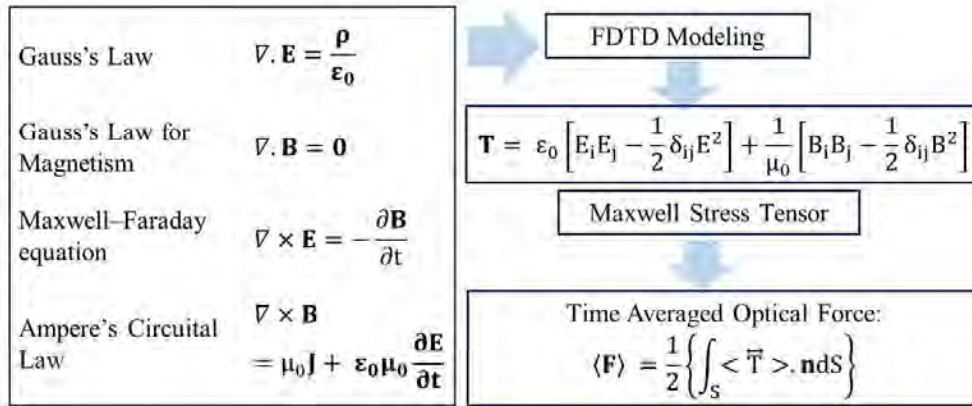
Figure 3-4:Maxwell Stress Tensor based Optical Force computation technique.

When calculating MST by the FDTD method, the structures are surrounded by Perfectly Matched Layers in all three directions, x, y and z directions. After FDTD modeling of the Maxwell's equations, MST is computed based on the calculated electric and magnetic fields Lumerical FDTD is used to carry on all FDTD simulations required for this research.

3.3 Geometry Description

The influence of optical force is considered for the reorganization of the following configurations. For all periodic and rotationally symmetric structures, the PS micro particles with diameter 1μm are considered. Based on the dispersion calculation for PS, the particle refractive index, n_p is considered 1.574 at 980nm [82]. The refractive index of the surrounding medium is water with refractive index, n_m of 1.33.

3.3.1 Geometry of Polystyrene (PS) Photonic Crystal

Polystyrene(PS) microparticle based on one and two-dimensional periodic arrays submerged in a liquid medium are considered for photonic crystals. For both 1D and 2D PC, the investigation on their reconfiguration process using optical force is carried out for PS particles with diameter of which is of

the same order of magnitude as the wavelength of the trapping Gaussian laser beam. The illumination wavelength is denoted as $\lambda_0 = 0.980\mu m$.

For a 1D PC, a 1D periodic array is considered which consists N no of PS particles aligned along the beam axis submerged in liquid medium, water ($n_m = 1.33$). For an array consisting 2N+1 particles, the center particle is placed at (0,0) point and named "M". The particles to the right of "M" are marked as R1, R2,……,RN and the ones to the left of "M" are marked as L1,L2,L3,………,LN. The set-up used for 1D PS PC is displayed in Figure 3-4.
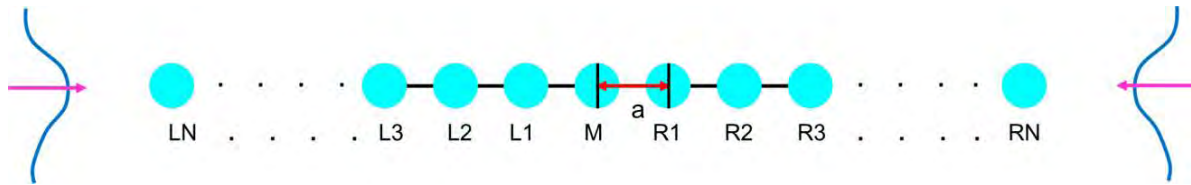
Figure 3-5: 1D array of 2N+1 no of PS particles in a dual Gaussian beam system. "a" is the interparticle spacing between the PS spheres. M is the center particle.

For 2D PC, two dimensional (2D) arrays of NxN PS particles arranged in a square are considered and submerged in water (background medium refractive index, $n_m = 1.33$). In Figure 3-5, a PS 2D PC is demonstrated which is periodic along x and y direction and homogenous along z. This material consists of square lattice of columns consisting PS spheres with diameter 1μm. For 2D PS PC, two different sets of polarization are taken into account: TE and TM modes unlike 1D. In TE mode, H is normal to the plane of PC while for TM polarization E is normal to the xy plane.
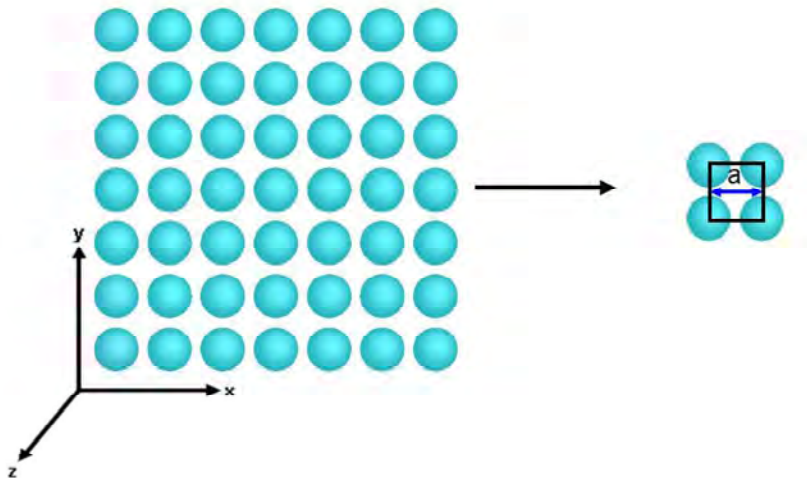
Figure 3-6: 2D Square PC with PS particles submerged in water medium. It is periodic along x and y with lattice constant a. The square black box denotes the unit cell of the square lattice and the blue arrow marks the lattice constant, a. Particle radius is 0.5μm

Three different set of arrays: 3x3, 5x5 and 7x7 are investigated to study their reconfiguration process in presence of light force exerted from dual Gaussian Beam system. For a NxN square array of PC microparticles, the middle row is always aligned with the beam axis. The only difference from 1D set up is that now the particles are not confined only in one direction rather in two. The interparticle spacing, a now denotes the center to center distance from each other in both x and y directions. Figure 3-6 shows the arrangement used for exerting optical force on 2D square arrays using monochromatic Faussian beam light sources illuminated from two opposite ends.
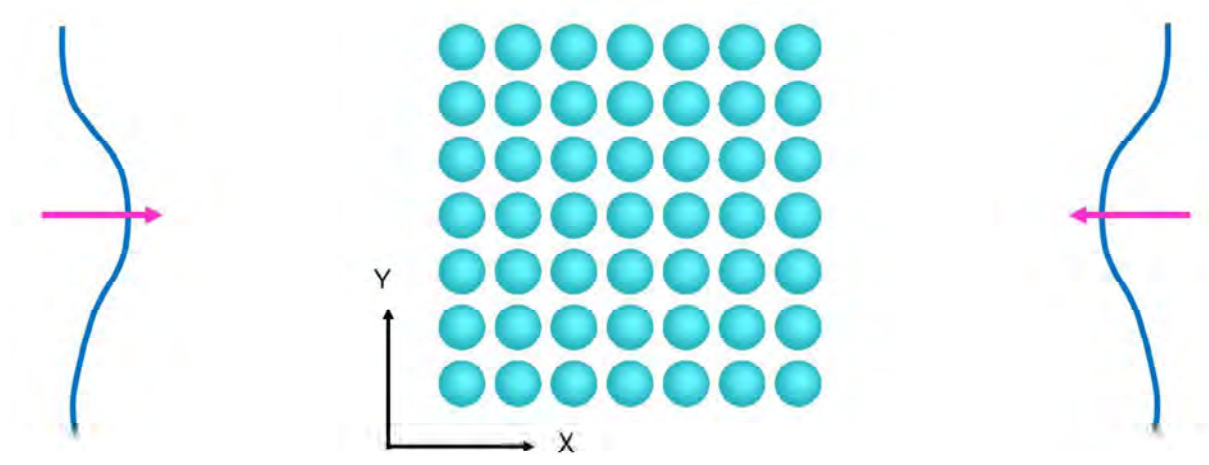
Figure 3-7: A N by N Arrow of PS (n_p=1.574) particles in a dual Gaussian beam system. Particles are submerged in water (n_m=1.33) medium. The array is periodic along x and y direction. Particle radius 0.5um. In this case, N=7.

3.3.2   Geometry of Polystyrene (PS) Whispering Gallery Mode Resonator

Whispering Gallery mode resonators are designed using similarly submerged rotationally symmetric arrays of PS microparticles. Also a 2D hexagonal array of PS particles are considered to study their resonant characteristics.

Whispering gallery mode (WGM) resonators are designed using similarly submerged rotationally symmetric arrays of PS microspheres. For observation of the impact of optical force in a dual Gaussian beam system, the unit cell of such a large WGM consisting PS microparticles arranged in a rotationally symmetric manner is taken into account. Figure 3-8 shows such an arrangement for 7 PS microparticles arranged in a hexagonal manner with a particle at the center position. The centered row aligns with the dual beam axis.
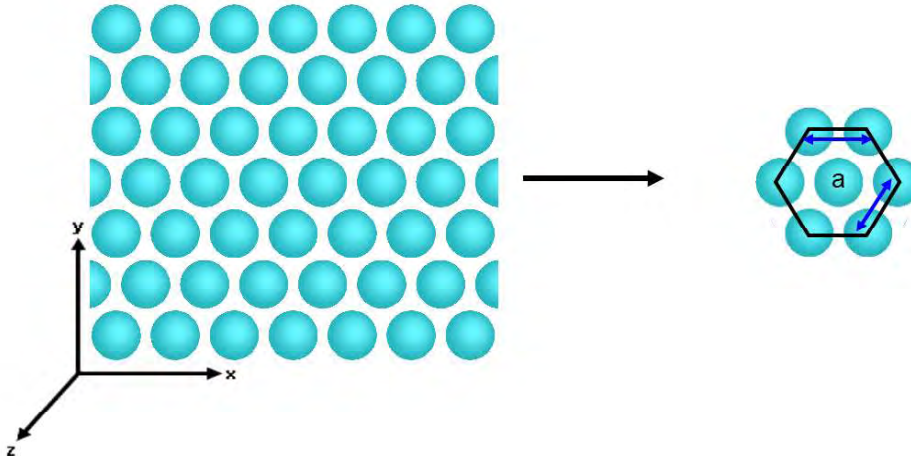
Figure 3-8: 2D hexagonal PC with PS particles submerged in water medium. It is periodic along x and y with lattice constant a. The hexagonal black box denotes the unit cell of the hexagonal lattice and the blue arrow marks the lattice constant, a. Particle radius, r=0.5μm.

Figure 3-9: Unit Cell of a hexagonal photonic crystal placed in a dual counter propagating Gaussian Beam. The centered array is aligned with the beam axis. Particle radius: 0.5μm.

For all the geometries studied in this thesis, the interparticle spacing "a" mainly points to the center to center distance between particles.

3.4 Counter propagating Dual Gaussian Beam System

In order to exert optical force, the counter propagating monochromatic Gaussian beams with equal power are used. Each of them has a beam waist, ω_0= 3μm. The beam waists are separated by a finite amount, D.

In our set up of counter propagating dual Gaussian beam [Figure 3-9], X axis is termed as the beam axis connecting the two beams. Gaussian beams are aligned with centers at x=−D/2 for the forward field and x=D/2 for the backward field, where D denotes the distance between beam waists. In this set up D is 160μm and the beams are identical except their propagation direction is opposite to each other.

37

The dielectric sphere is illuminated by time harmonic incident EM field, $E_{inc} = E_0 \hat{x} \exp(ikz - i\omega t) + E_0 \hat{x} \exp(-ikz - i\omega t)$ modeled by the Gaussian monochromatic beams of the same intensity, with angular frequency ω and wave vector, k=ω/c.
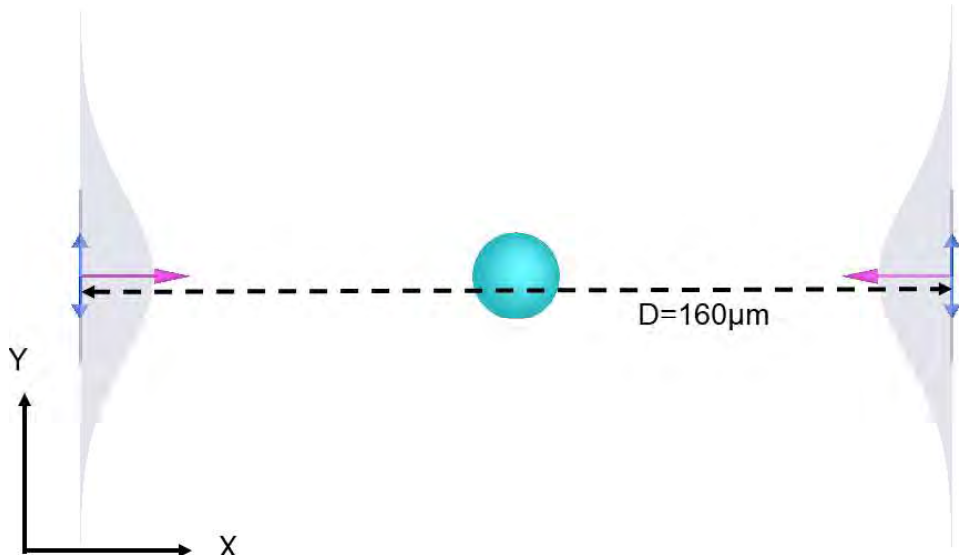
Figure 3-10: A single polystyrene microparticle placed in between two Gaussian Beam with D=160μm. Propagation direction is along X axis. Polarization angle: 0 degree.

All the structures considered for analysis are placed in between the dual beam system. Commonly, the illumination intensity of each beam is taken to be 127.6mW/μm^2. A generalized idea of the Gaussian beam waist radius is displayed in Figure 3-10.
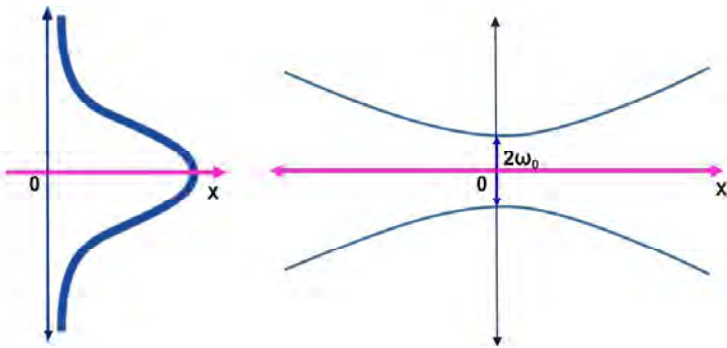
Figure 3-11: Gaussian laser beam profile showing the beam waist as a function of distance from focal plane. The X axis is the propagation axis. The beam waist or the spot size is 2ω_0, In our set up. waist radius, ω_0=3μm.

CHAPTER 4

RESULTS AND DISCUSSION

According to the models and formulations described in the previous chapter, optical force tuned reconfiguration of the Polystyrene(PS) microsphere based periodic and rotationally symmetric structures is analyzed. In this chapter the behavior of optical forces acting on the geometries mentioned in Chapter 2 are investigated and their resonant characteristics with and without the effect of optical force are discussed with illustrations.

4.1   Optical Force Tuned One Dimensional (1D) Polystyrene Array

In this section the behavior of optical forces acting on 1D array of periodic dielectric microparticles in a dual counter propagating dual Gaussian beam system are studied.

4.1.1   Monosphere Optical Trap
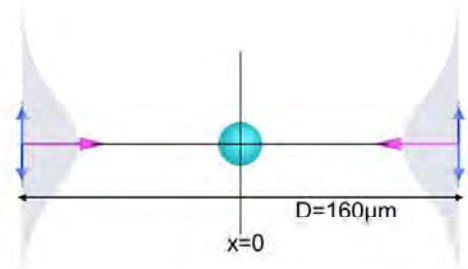
Figure 4-1: A single PS microparticle at the center of dual Gaussian Beam with D=160μm. Particle radius: 0.5um and refractive index, n_P=1.574. The particle is fully submerged in water.

At first the optical force acting on a single PS particle is computed using Gaussian beam system exerting wavelengths of light within the range of 0.4μm to 1μm. For the configuration showed in Figure 4-1, the force components acting along x, y and z direction are plotted in Figure 4-2. As the particle is placed along the beam axis, the y and z components of force are almost negligible. This supports the fact that the Gaussian input beams supply strong enough confinement to direct the motion of the sphere motion along the beam axis [2] and so the x component of the force becomes the point

of interest in 1D case. Here, positive Fx denotes a force acting along positive x direction and negative Fx means the opposite. This plot infers that for light above 850nm, the magnitude of optical force is almost zero and the current position of the single PS particle, i.e., x=0 is its equilibrium position in this dual beam trap.
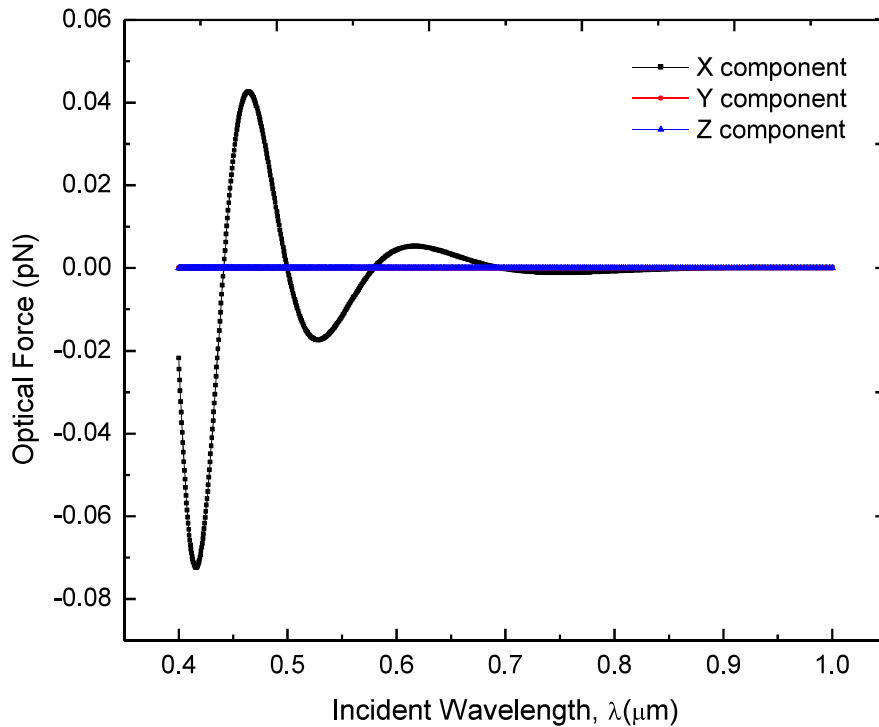
Figure 4-2: Optical Force acting on a PS microsphere in a dual Gaussian Beam and submerged in water. Black, red and blue lines represent X, Y and Z component of the Optical Force.

To check the force dynamics with the variation of particle position from -6um to 6um i.e., from negative x axis to positive x position the optical force acting on this mircoparticle is computed for monochromatic illumination of λ_0 = 980 nm with same light intensity. Figure 4-3 shows that at x=0 position, the force along x direction is perfectly zero. The equal segments of positive and negative force marked by the green dotted arrow also marks x=0 as the stable position of this single microparticle in dual beam trap. It also conforms to Figure 4-2 as it shows that an illumination wavelength of 980 nm can stabilize a single PS particle at the center of the dual beam trap. The alternating attractive-repulsive nature of force is the indication of the phase of the EM fields that evolves with the particle position [83].

40
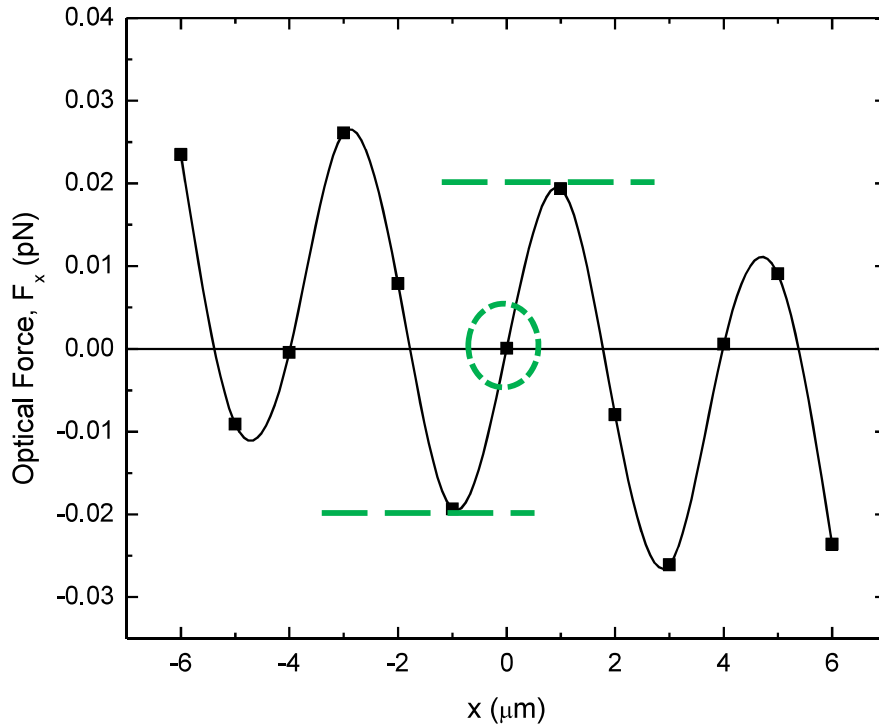
Figure 4-3: X component of Optical Force, Fx at various position of X axis. The symbols represent the computed value and the solid line represents the interpolated values. Green dotted circle marks the stable position of the particle.

4.1.2   Equilibrium Positions of N-particle array

Before discussing the reconfiguration process of a N particle 1D array by the application of optical force, a set of three particles is considered at the first stage. The PS micrsopheres are arranged along the counter-propagating beam axis with initial interparticle spacing, a=2μm with the same configuration of light source [Figure 4-4].
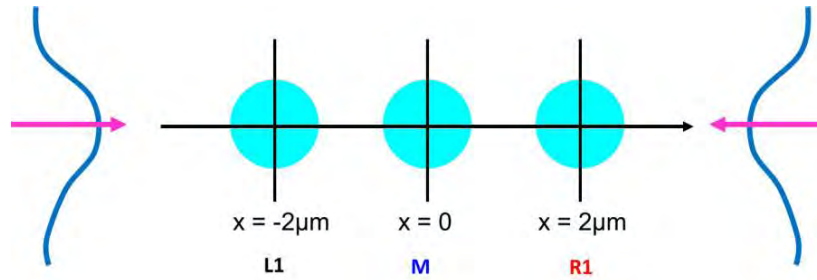
Figure 4-4: Three particle array of PS particles in a dual beam system. Particles are submerged in water.

The value of a is varied from 2 μm to 20μm with an interval, Δ of 2μm and the force acting on M, R1 and L1 positioned particles are computed for each "a" and plotted in Figure 4-5. The force on the middle particle is negligible and so the center position is the stable position of the particle marked M. The forces on the other two particles (L1 and R1) are symmetric. They provide multiple zero crossing points as they alternate sign. The interplay of the scattered photons by the three particles influence each other's stable position followed by the redistribution of the incident light [57]. Therefore, the force acting on each particle becomes different in presence of other two particles. Since the equilibrium spacing for an N particle array are obtained by calculating the optical force as a function of interparticle spacing and locating a point where the optical forces are zero and dFx/dx<0 [41][83], the same procedure is followed for this 3 particle array.

Stable positions marked using green arrow in the Figure 4-5 correspond to zero-force positions but the more stable case is when a=4.2μm around which the negative and positive force segments are equivalent. An increase in the interparticle separation from the stable position would induce an attractive restoring force, whereas a reduction would induce a repulsive restoring force as illustrated in Figure 4-6. Initially at a=2μm R1 faces a positive force while L1 faces a negative Fx. So they try to move away from each other weakening this repulsion. At around 4.2μm, the photoinduced force on all three particles become zero and they remain stable at this point. If the interparticle spacing is changed from 4.2μm to 6μm an attractive force is induced on the R1 and L1 particles that act along the negative and positive x direction respectively and draw them toward M.
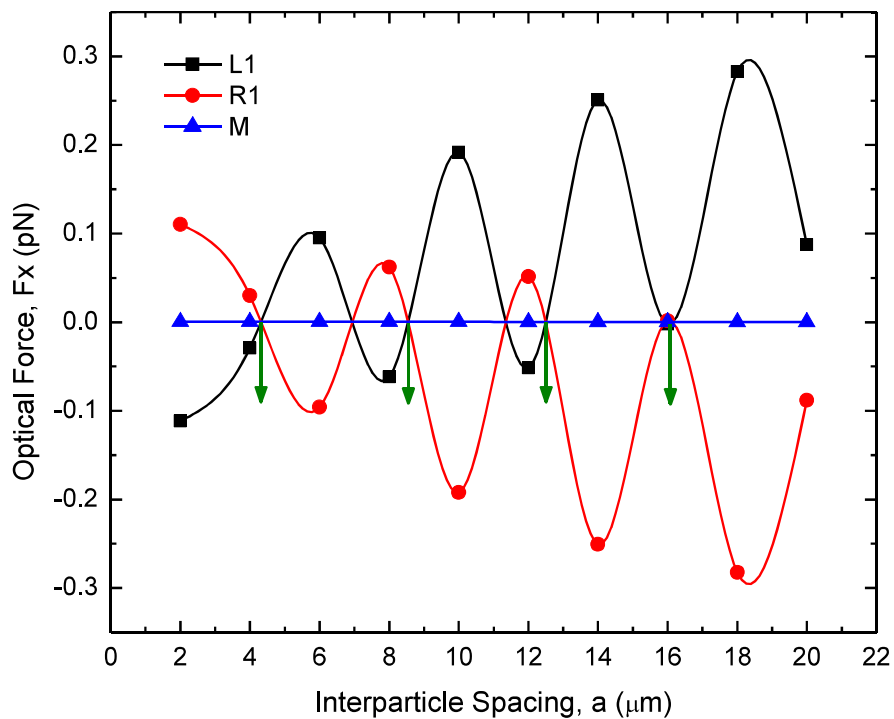
Figure 4-5: Optical force along X direction, F_x as a function of distance between neighboring particles in a 3 particle PS array. Stable positions are indicated by green arrow.
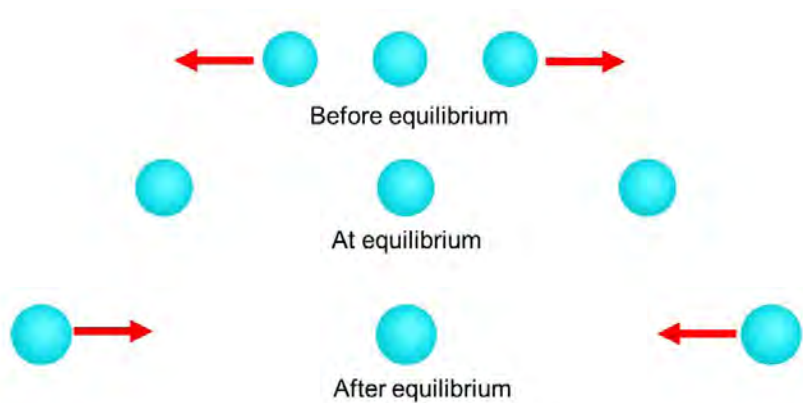
Figure 4-6: Force direction in a 3 particle system. The top row presents the direction of force before reaching equilibrium position, the middle row shows the equilibrium position and the bottom row presents the force direction after crossing the equilibrium position.
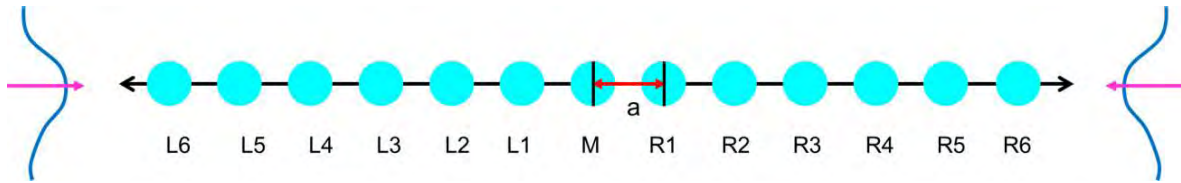
Figure 4-7: 1D array of 13 PS particles in a dual Gaussian beam system. Here, a : Interparticle spacing between the PS spheres. The ones along right of center particle, M are marked as R1, R2, R3..... and those are left are as L1, L2, L3....and so on..
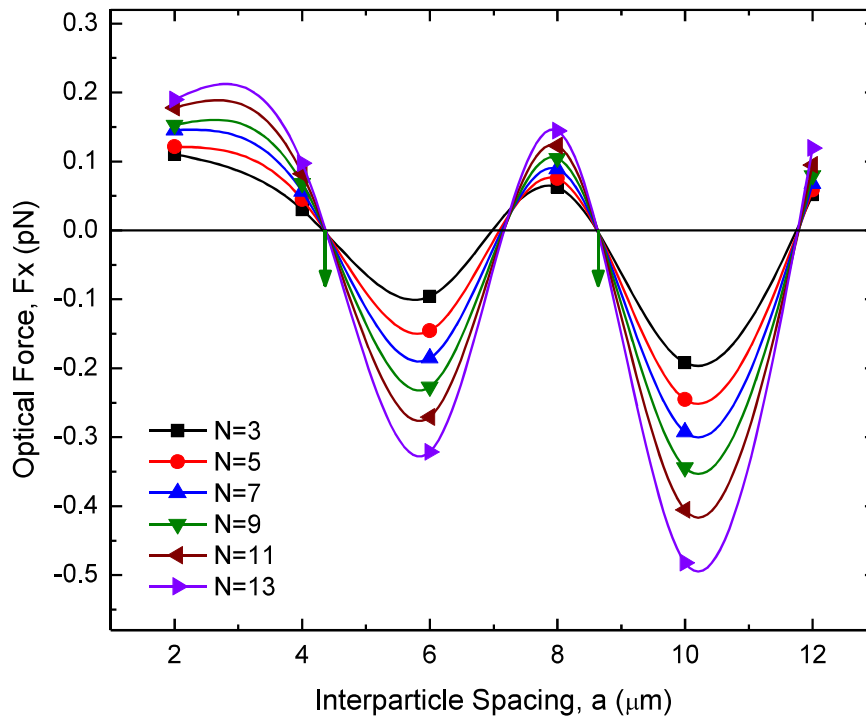
Figure 4-8: Optical Force as a function of interparticle spacing. Here, Fx is the X component of force acting R1 positioned PS particles and, N=no of particles in the system. Stable positions are indicated by green arrow.

Now the equilibrium positions of an array consisting more than three-particles are investigated. For increasing N from 3 to 13, the force magnitude goes higher accordingly as displayed in Figure 4-8 to 4-13. For symmetric nature of optical force, only the force components acting along x direction and on right hand sided particles are plotted. As there are more number of scatterers in the system, the force magnitude of each particle goes up for the additional contribution from the new scatterer introduced in the system. For each N in the dual beam trap, the stable interparticle spacing, "a" is identified using the same method described above.

44

Figure 4-8 records the Fx on all R1 positioned particles for N=3,5,7,9,11 and 13. Within the considered range, two zero crossing points are obtained for the same R1 particle.
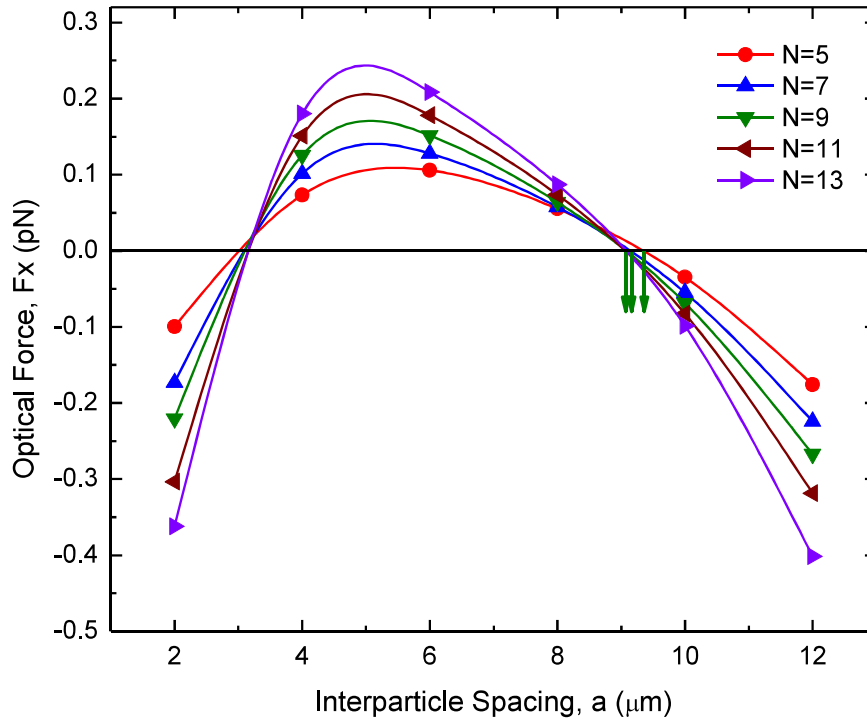
Figure 4-9: Optical Force as a function of interparticle spacing. Here, Fx is the X component of force acting R2 positioned PS particles and, N=no of particles in the system. Stable positions are indicated by green arrow.

As shown in Figure 4-9, all the force curves obtained for R2 positioned PS microparticles go from positive to negative near a=8.5μm. The curves change their shape from the ones obtained for R1 particles. It is an indication that the electromagnetic(EM) waves change phase from particle to particle depending on their position from the source and also from the center of the beam axis.

The pattern of optical force changes for R3 particles too but there is a similarity of the pattern of optical force curves with the one obtained for R1 particles in Figure 4-8. According to Figure 4-10, around a=4.47μm there is one equilibrium position for all R3 positioned particles in the systems with N= 7,9,11 and 13.
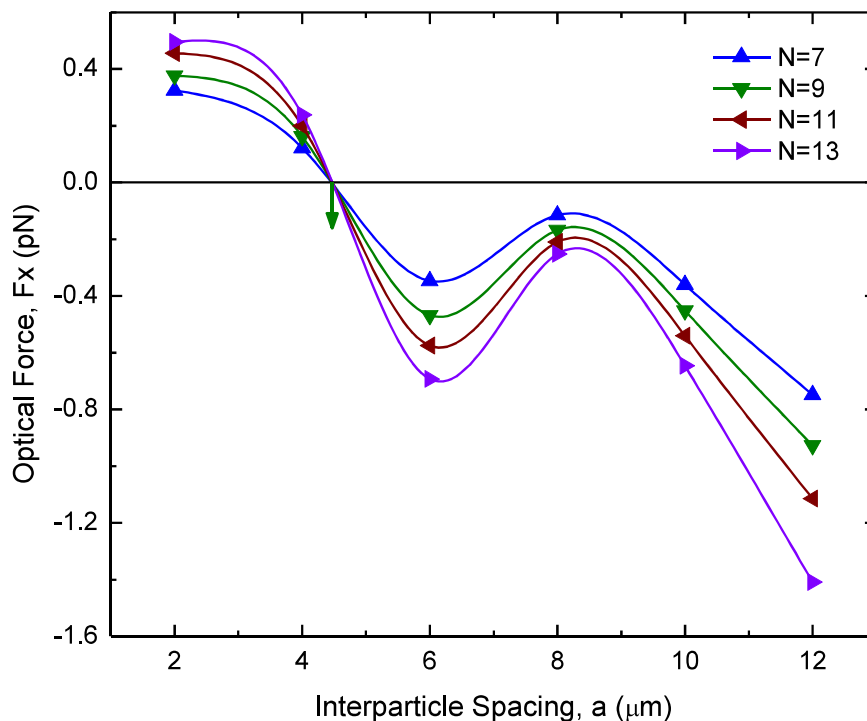
Figure 4-10: Optical Force as a function of interparticle spacing. Here, Fx is the X component of force acting R3 positioned PS particles and, N=no of particles in the system. Stable positions are indicated by green arrow.

Figure 4-11 portrays the change in optical force acting on R4particles when the size of the 1D array is 9,11 and 13. It shows that the curves interpolated from the data points computed for R4 positioned particles with different "a" shows similar trend as the ones obtained for R2 positioned microspheres. Observing such trends of optical force in a 1D array, it can be inferred that the shape of the force curves repeats itself in a periodic manner along with the change in phase of EM waves depending on the particle position.
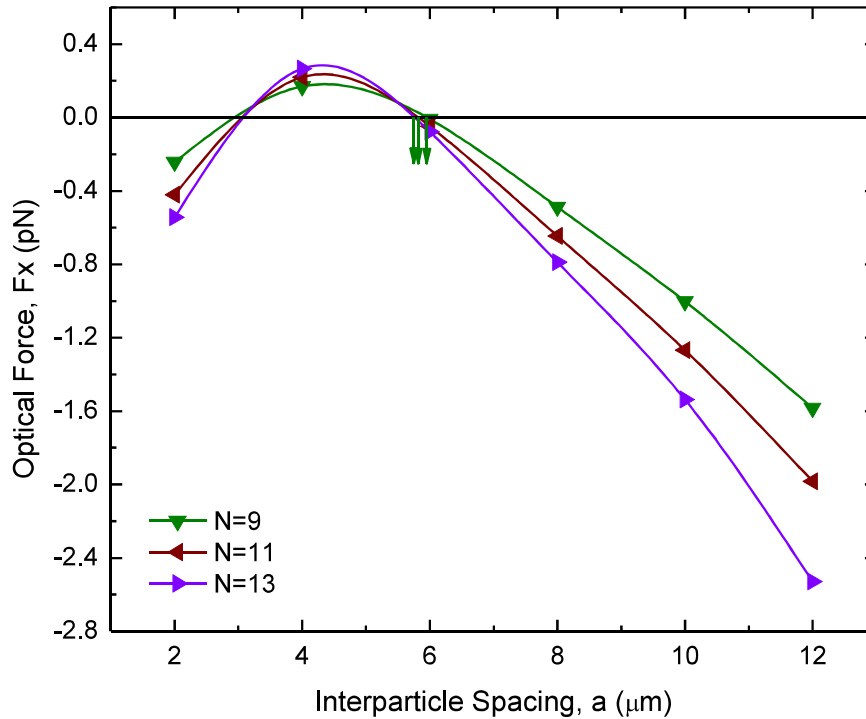
Figure 4-11: Optical Force as a function of interparticle spacing. Here, Fx is the X component of force acting R4 positioned PS particles and, N=no of particles in the system. Stable positions are indicated by green arrow.

For two 1D arrays with N=11 and 13, Fx component of optical force is plotted as a function of interparticle spacing in Figure 4-12. It shows that for "a" $\approx 4.73\mu m$, the R5 positioned particles become stable in a dual beam configuration. And also in a similar manner the shape of the interpolated curves obtained for R5 particles match the ones plotted for R1 and R3.

Next in Figure 4-13, the Fx component of optical force acting on R6 positioned particle resembles the shape observed for R2 and R4. When N=13, Fx becomes zero with a negative slope when their interparticle spacing is around 4.9μm.

From all the force components plotted above, one thing is evident that depending on the position of each particle in the system the force directions i.e., phase of the electromagnetic waves change but this change maintains a repetitive nature. Also this investigation points to the fact that, a certain particle depending on its position from the center of the beam axis, always maintains same stable interparticle spacing irrespective of the total number of particles present in the 1D structure. But there might be several possible equilibrium positions for the same microsphere as was observed by v. kar´asek et al.

47

in their Coupled Dipole Method based force model [84]. Based on these stable points predicted from the force curves, Figure 4-14 is plotted for N=13 which exhibits inhomogeneous spacing of the particles.
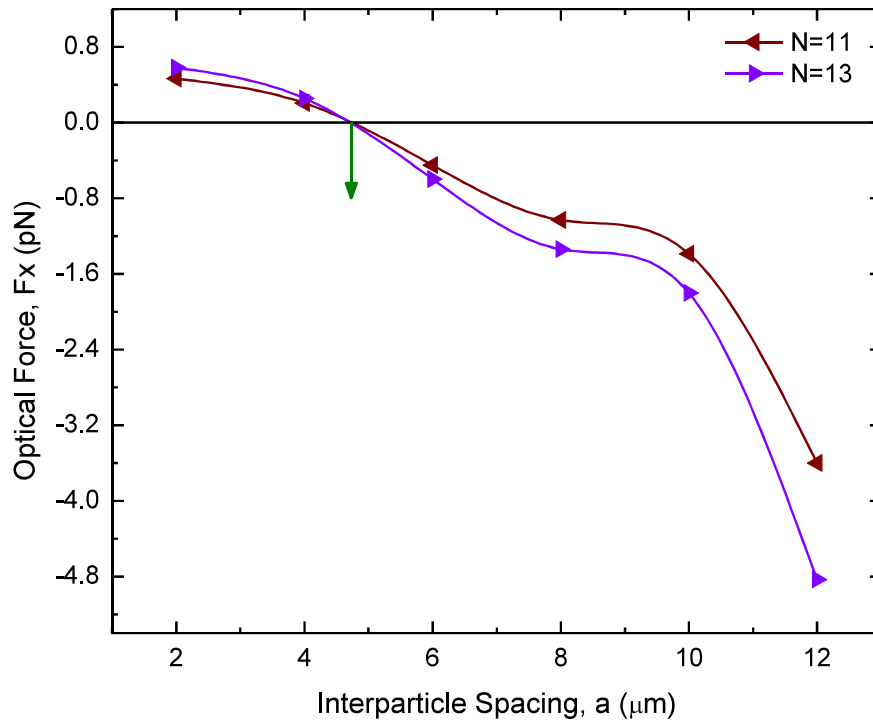
Figure 4-12: Optical Force as a function of interparticle spacing. Here, Fx is the X component of force acting R5 positioned PS particles and, N=no of particles in the system. Stable positions are indicated by green arrow.

Dielectric objects like PS particle with a refractive index larger than the index of the surrounding liquid (in our case water) are drawn toward the high field intensity region, so each particle behaves like a seeker of local intensity maximum of the electromagnetic field nearby [41]. However, apart from the combination of two force components exerted by the two counter propagating, slightly divergent light beams emerging from the two opposing ends, another force component termed as the scattering force play a key role in this regard.

In a multiparticle configuration, each particle acts as a scatterer and rearranging itself in the light field, each object changes the field distribution for the other objects in the trap. Thus the objects eventually

rearrange themselves in patterns of low potential energy with respect to the gradient force in a self-organized way. In our case the particles placed along the beam axis align axially and are suspended in space by the application of light force exerted by the counter propagating laser beams [41].
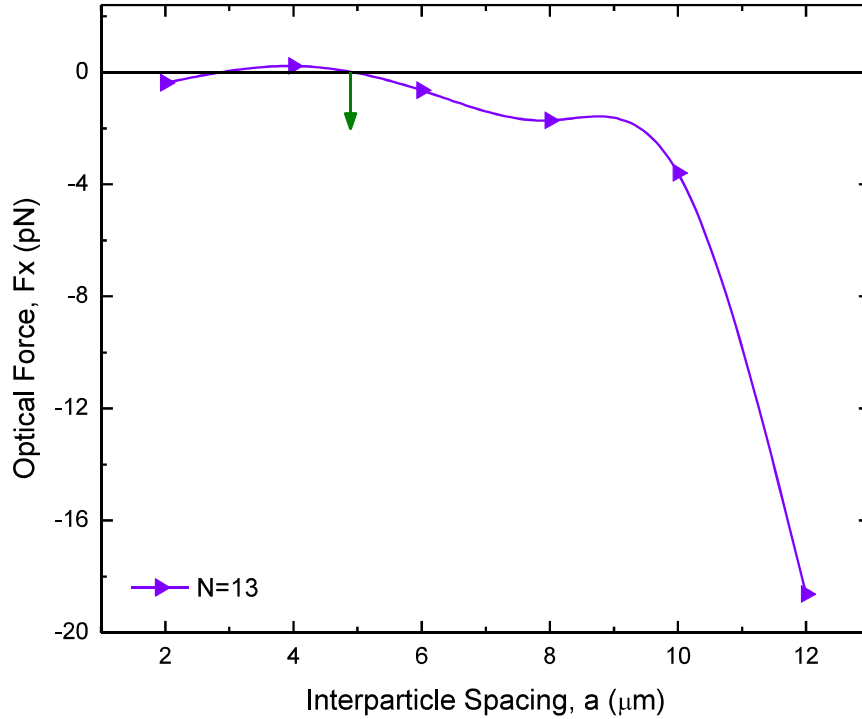
Figure 4-13: Optical Force as a function of interparticle spacing. Here, Fx is the X component of force acting R6 positioned PS particles and, N=no of particles in the system. Stable positions are indicated by green arrow.

Two force components: scattering and gradient force result from the beams from the two opposite ends and also by the spherical particles present in the system. The reflection of photons at the boundary of the particles cause them to move along the beam direction. This is termed as longitudinal trapping while the gradient force is responsible for transverse trapping that arises due to the refraction of photons. Gradient force holds the particles on the beam axis. When a single PS particle ($2r \approx \lambda$) is considered to be submerged in water medium, the contribution of these two forces push the particle at the center of the two beams as shown in Figure 4-2 and 4-3.
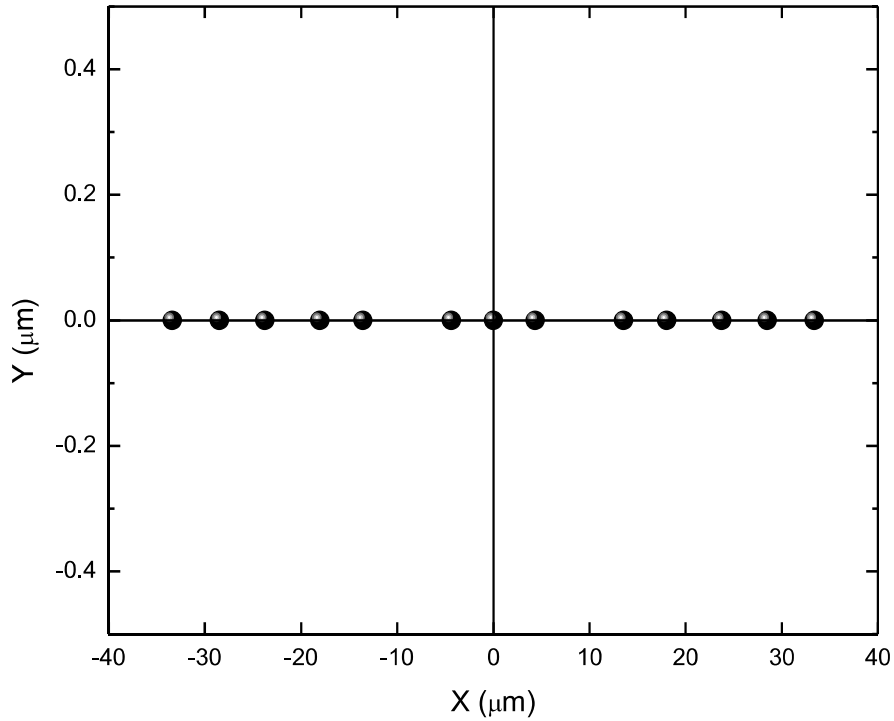
Figure 4-14: Stable positions of a 1D array of 13 PS particles (n_P=1.574) submerged in water medium. Illumination Wavelength: 980nm.

As the number of particles in the system is increased, N from 1 to 3 to 13, there are now more number of scatteres of the incident beam. Therefore, the built-in feedback mechanism between the distribution of the particles and the distribution of the light field align them in a self-consistent manner that corresponds to the minimal energy solution realized by the system [41]. The PS spheres spaced with a certain interval within the water medium acts like a diffraction grating whose grating constant is the interparticle spacing, a. In fact, the refractive index contrast between the PS and water creates a modulated potential function and the self-consistent approach leads a to value so that each sphere is located in an optimally shaped potential minimum [41]. However, it is observed that the zero crossing points do not point to the same "a" for each particle in the system. Therefore, if a periodic array of PS particles submerged in water medium is illuminated by dual Gaussian wave of 980nm, it will eventually be rearranged in an aperiodic manner in presence of photo-induced forces provided that other parameters like background Brownian motion, medium viscosity, thermal expansion are neglected.
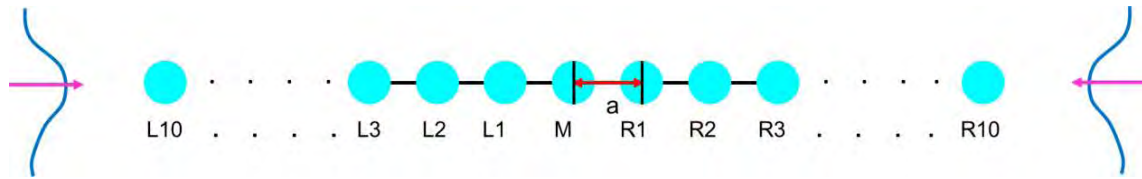
Figure 4-15: An Array of 21 PS particle submerged in water medium in a dual Gaussian Beam trap. All the particles are not explicitly displayed.

As a second attempt, an array of 21 particles submerged in water medium [Figure 4-15] is illuminated with light of same intensity and wavelength. But this time, the value of Δ is reduced to 0.5µm for better resolution and better prediction of the stable positions. Figure 4-16 shows that for both N=3 and 21 the stable points coincide for R1 positioned particle whereas instead of one stable points within the same interval now 3 possible points are obtained. In a similar manner the other equilibrium points are computed and plotted in Figure 4-17 for all other particles present in a 1D array of 21 microspheres.
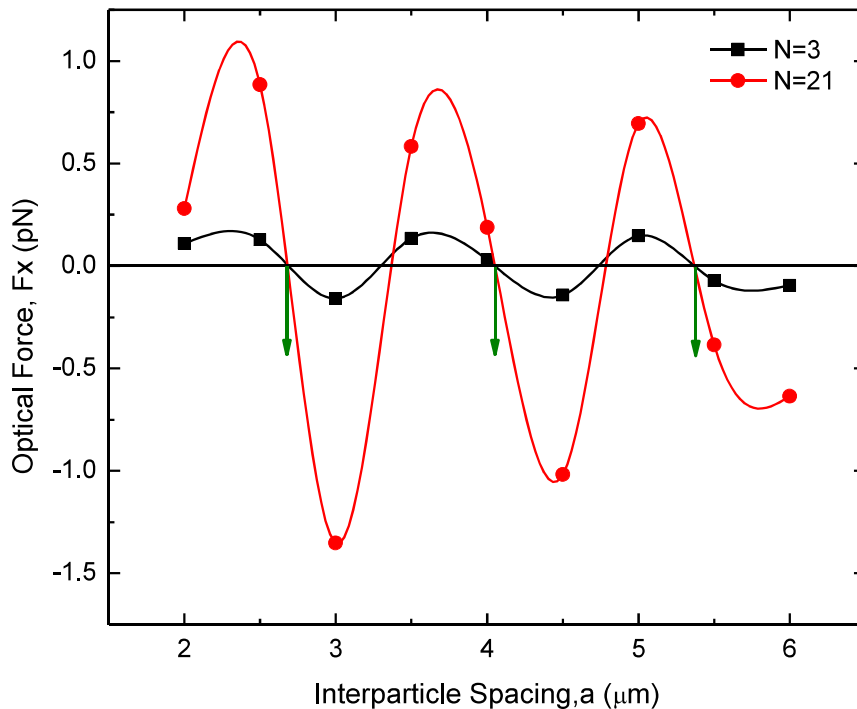
Figure 4-16: Optical Force, Fx of R1 positioned particle in the 1D array of 21 PS particles (n_p=1.574) submerged in water medium. Illumination Wavelength: 980nm. Here, gap between each data point, Δ=0.5µm. The black and red symbols represent data points for N=3 and 21 PS particles in the system.
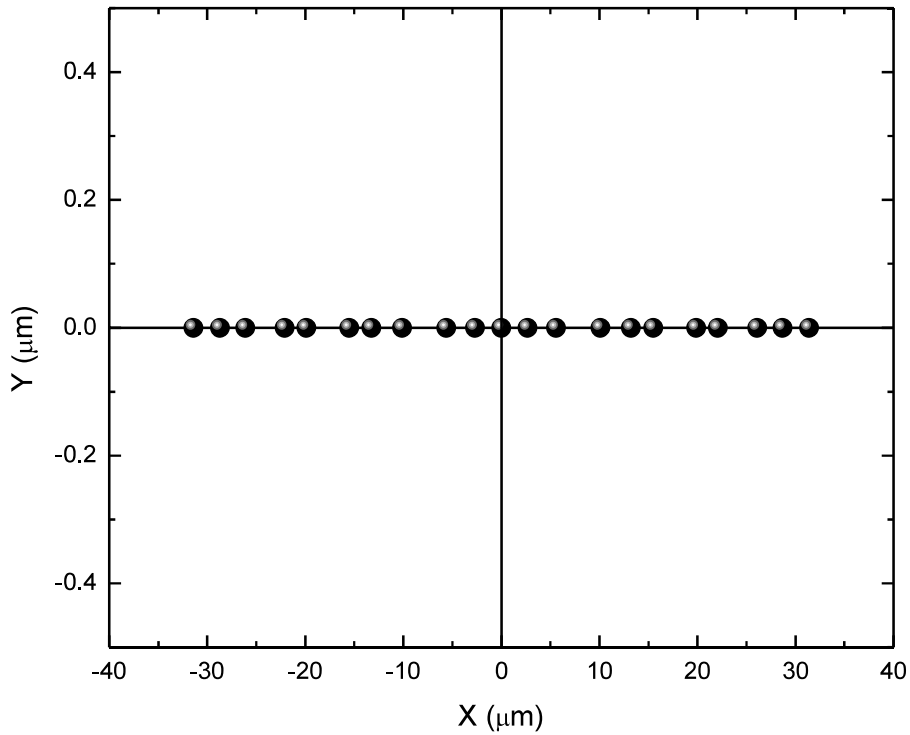
Figure 4-17: Stable positions of a 1D array of 21 PS particles (n_P=1.574) submerged in water medium. Illumination Wavelength: 980nm.

Both Figure 4-14 and 4-17 represent aperiodic arrangement of the PS microparticles due to the exertion of optical force upon them. This phenomenon points to the fact that, no matter how closely spaced the stable points are, the reconfiguration process under 980 nm illumination cannot yield a periodic configuration.

4.1.3 Intensity Profile of Optical Force in a 1D array

The light induced force is considered to be proportional to the intensity of the incident light [83] Incident light intensity is related to the Electric field by : $I = \frac{1}{2}c\varepsilon_0 n_m E^2$, where E is the magnitude of the electric field of the incident light, n_m is the refractive index of the background medium and c is the velocity of light.
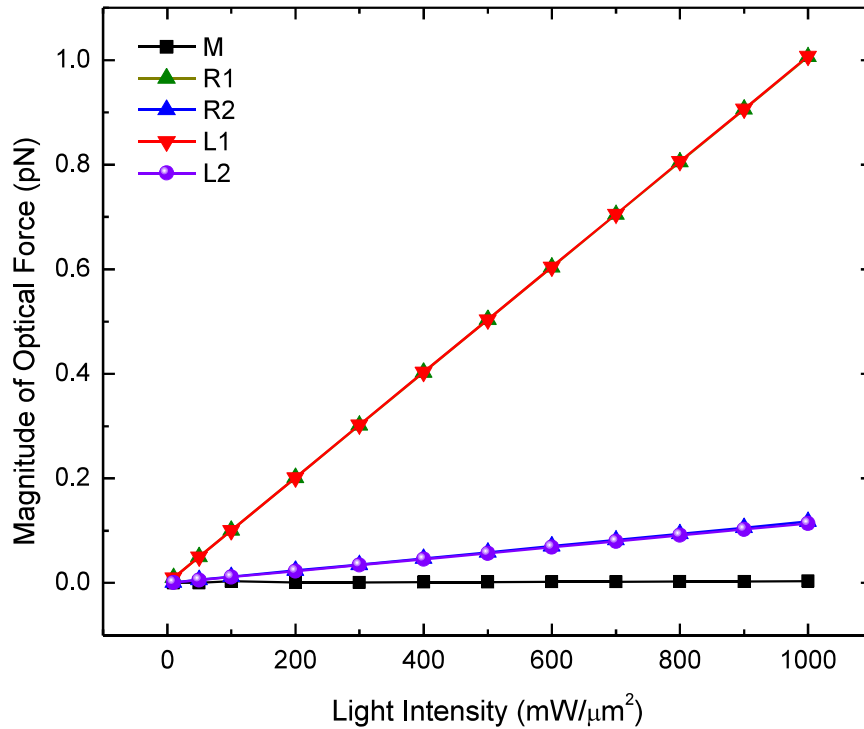
Figure 4-18: Optical Force vs Incident Light Intensity in a 5 particle system. Particles are arranged in a row with a=1.5μm and particle radius is 0.5 um. Incident light wavelength is 980nm.

To investigate the change in photon induced force with increased light intensity Figure 4-5 is presented where a periodic array of 5 PS microspheres with a=1.5μm are placed in the dual beam set up and illuminated by 980 nm light but with different intensities. The magnitude of force is recorded for all 5 particles. When the incident light intensity is increased from $10mW/\mu m^2$ to $1000mW/\mu m^2$, the magnitude of light force increases in a linear manner. A similar phenomenon is observed when the array is extended to a 21 PS microspheres submerged in water medium. Figure 4-19 shows the change in Fx for various intensities of incident light on R1. Both Figure 4-18 and 4-19 represent that increasing intensity leads to a larger magnitude of optical force. But the zero crossing points coincide for all

incident light intensities. Ultimately, this proves the fact that intensity variation of the axial beam profile does not influence the longitudinal optical binding [57] and hence the reconfiguration process of a 1D array.
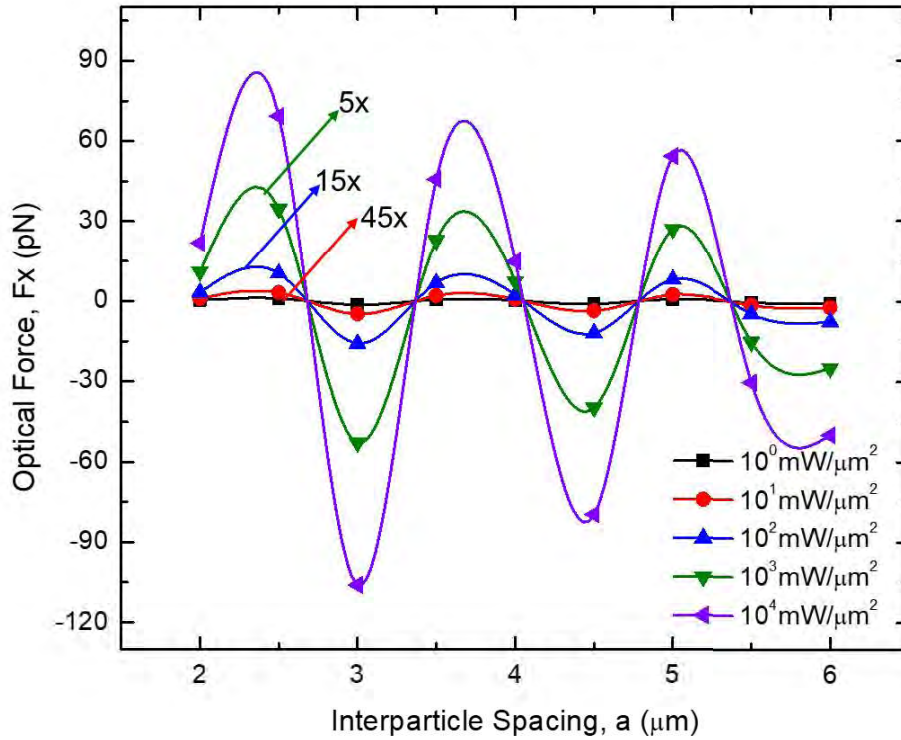
Figure 4-19: Optical Force, Fx acting on R1 positioned particle as a function of Interparticle spacing for different incident light intensities. The blue, green and violet curves are 45x, 15x and 5x zoomed for better representation. Here N=21 and n_m=1.33 (water).

This is further illustrated in Figure 4-20 which shows that even after increasing the intensity from $1 mW/\mu m^2$ to $10^4 mW/\mu m^2$, the equilibrium positions remain same and results in the same aperiodic configuration as is obtained for 127.6 $mW/\mu m^2$ illumination.
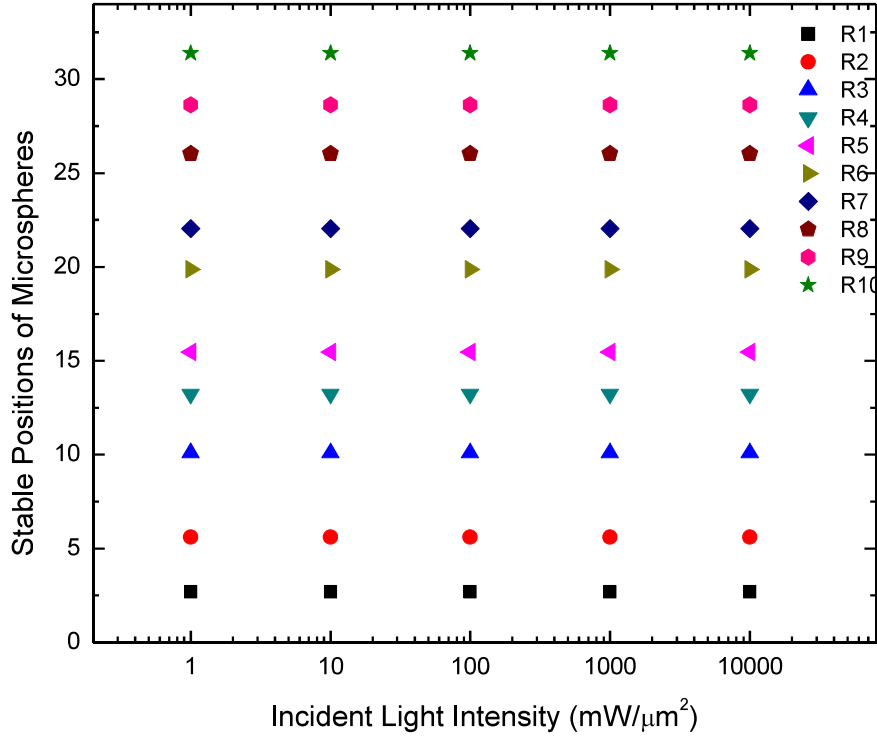
Figure 4-20: Stable Positions of different Microspheres after applying Optical Force of Different Intensity. N=21 and n_m =1.33. For symmetry considerations L1, L2………L10 particle positions are not shown.

4.1.4   Different Background Medium and Reconfiguration of 1D array

Difference in refractive index between the microparticle and background medium is an important optical parameter to be considered for the reconfiguration of a periodic structure. The variation in "a" for different n_m is displayed in Figure 4-21. The average interparticle spacing, $a_{av=}\dfrac{a_1+a_2+a_3+a_4+a_5+a_6+.....+a_N}{N}$ and the standard deviation, $\sigma=\sqrt{\dfrac{\Sigma(a-a_{av})^2}{N}}$ from the mean value are plotted for a 1D array of 21 PS microspheres illuminated by 980nm wavelength of light with an intensity 127.6mW/μm^2. For all values of n_m, the particles are considered periodic with an "a" of 2μm before the exertion of optical force from the dual beam system.

55

Since the redistribution of light depends very much on the refractive index of the background medium, the computed optical force changes accordingly. In fact, the distribution of potential minimum, i.e., the equilibrium positions of microparticles are dictated mostly by the difference between n_p and n_m.
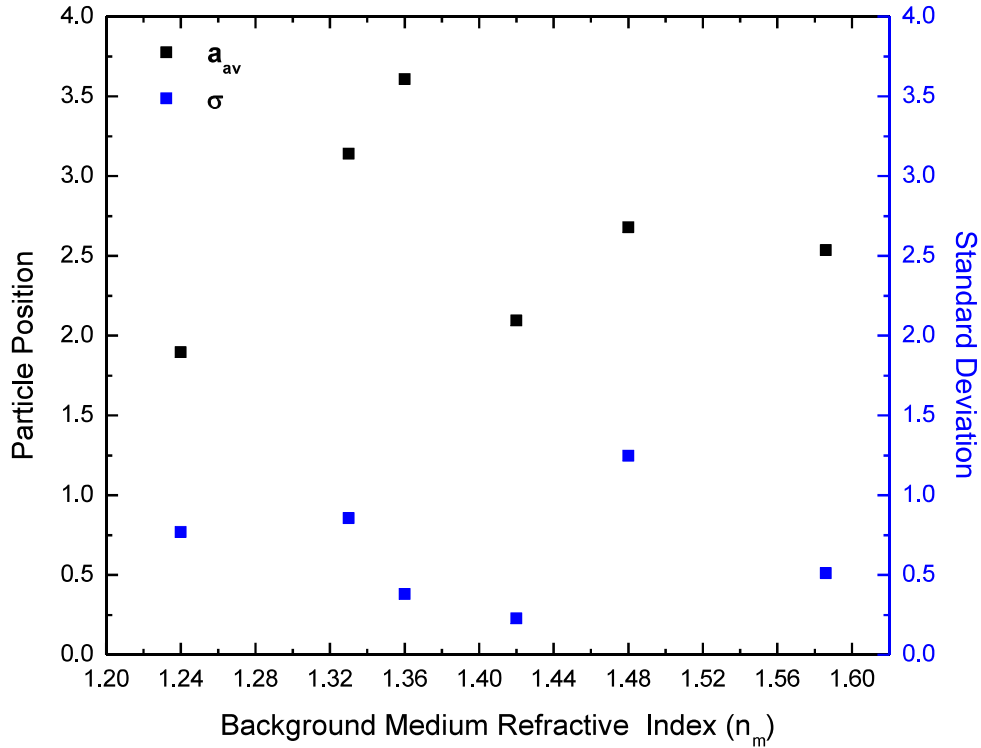
Figure 4-21: Average Stable Position, a_{av} and Standard deviation, σ of their stable positions for different background index in a Dual Gaussian Beam System. For each case, N=21, Illumination Wavelength, λ_0=980 nm. Initial a=2μm.

As a result, the value of a_{av} and σ become different for different n_m. For changing the background medium within the range of 1.24 to 1.6, no certain trend is observed in the stable configurations and the aperiodic nature of the reconfigured 1D array still exists. However, among all the data points, n_m=1.42 yields the minimum standard deviation and can obtain an almost periodic structure for a 1D PS microsphere array after applying 980nm light using the dual beam system.

4.1.5   Different Illumination Wavelength and Reconfiguration of 1D array
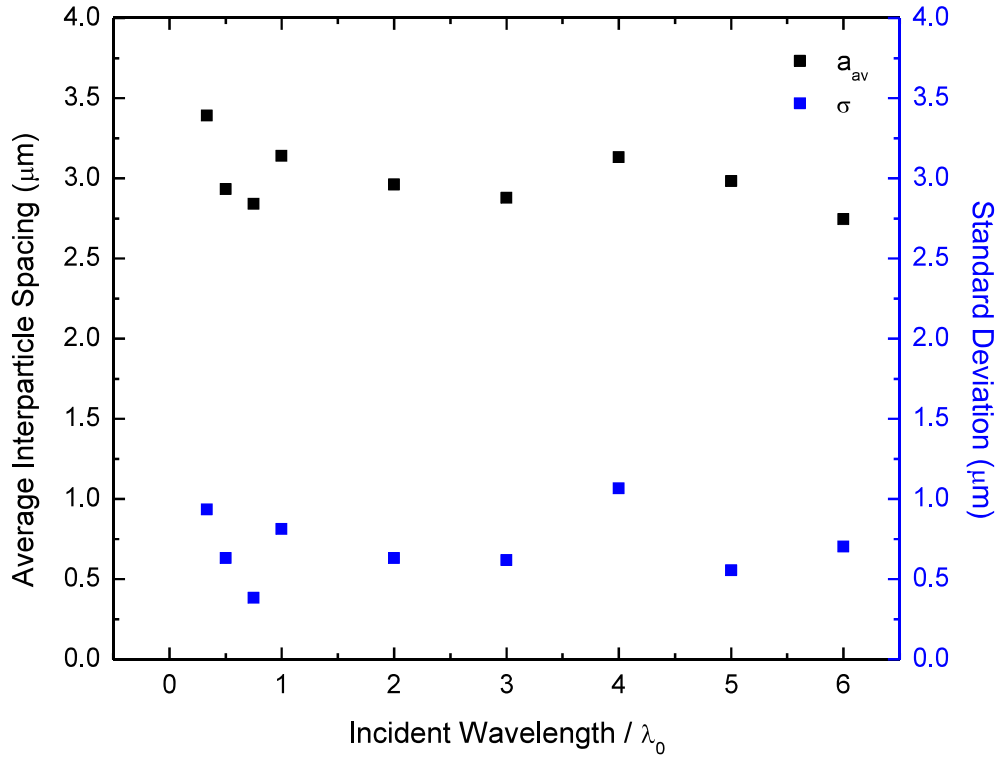
Figure 4-22: Average Stable Position, a_{av} and Standard deviation, σ of their stable positions for different incident wavelength of light in a Dual Gaussian Beam System. For each case, N=21, Here λ_0=980 nm. The left column represents a_{av} and the right column shows σ. Initial a=2μm.

Next the change in reconfiguration process is studied for incident light of different wavelengths. So far the investigations are carried out in the Mie regime as the PS microparticle of 1μm in diameter is comparable to the incident wavelength, λ_0 = 980 nm. For different multiples of λ_0, the average stable interparticle spacing, a_{av} and the standard deviation from a_{av}, σ are computed and presented in Figure 4-22. For variation of illumination wavelength, σ almost follows a_{av}. For wavelength below λ_0, the a_{av} exhibits a downward trend but for higher multiple of λ_0, there is an almost sinusoidal trend. For, $3\lambda_0/4$=735nm σ is the lowest and for this wavelength of light a quasiperiodic structure is obtained with the least amount of deviation from a_{av}. However, to reconfigure a periodic array into another periodic structure applying optical force, a different approach needs to be followed.
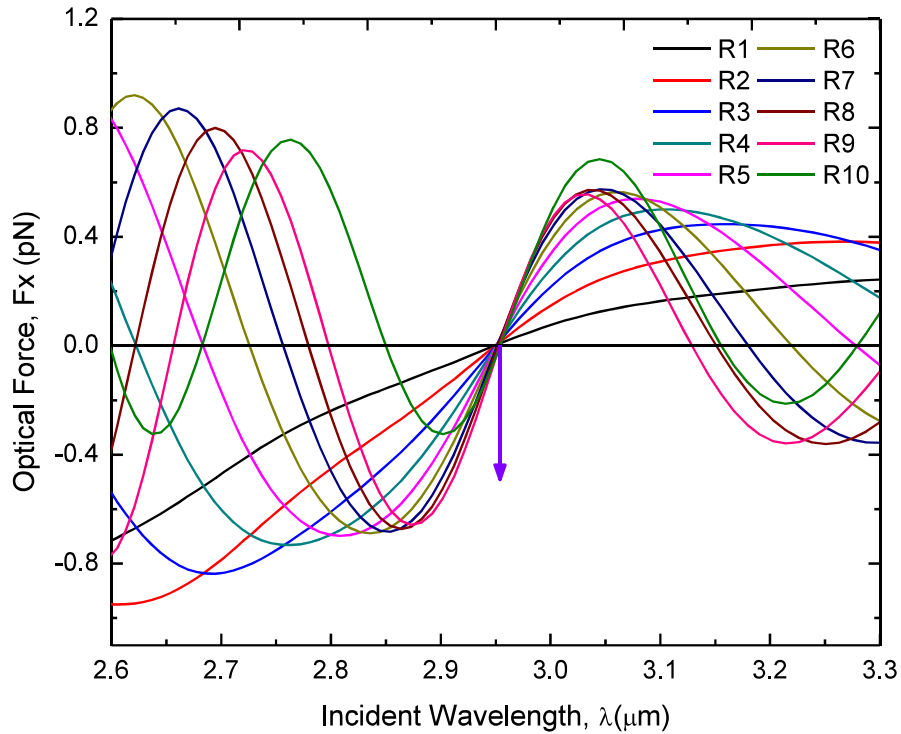
Figure 4-23: Optical Force as a function of Illumination Wavelength. The X component of force is plotted for right hand particles of an array of 21 PS particles in water medium. The violet arrow points to the stabilizing wavelength for a= 1.1µm.

Instead of changing illumination wavelength as a multiple of λ_0, a certain incident wavelength is searched for that can stabilize the particles in their own periodic position rather moving them. Figure 4-23 and 4-24 represent optical force, Fx as a function of the incident wavelength in dual beam system. These graphs show that a periodic array of 21 PS particles maintain their interparticle spacing, a at 1.1 and 1.5µm respectively if they are illuminated by 2.95µm and 4.01µm monochromatic light.
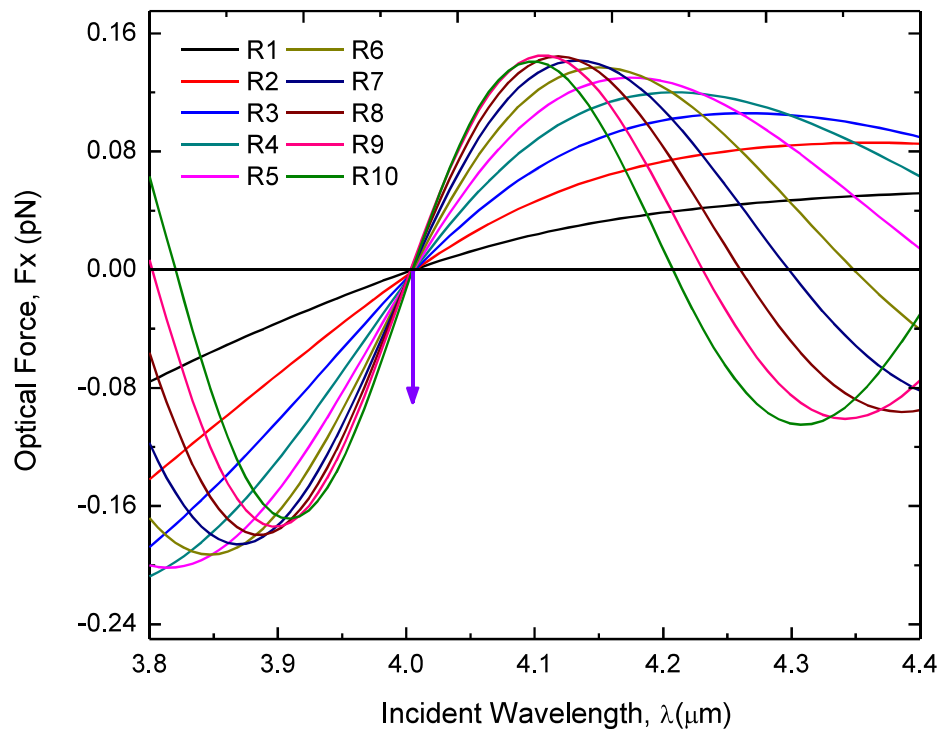
Figure 4-24: Optical Force as a function of Illumination Wavelength. The X component of force is plotted for right hand particles of an array of 21 PS particles in water medium. The violet arrow points to the stabilizing wavelength for a= 1.5μm.

When "a" is varied from 1.1μm to 1.5μm, there is a red shift in the stabilizing wavelength. So to obtain a stable periodic structure with a=2μm, the stable point is searched within a higher wavelength range. As shown in Figure 4-25, instead of one zero crossing points, a small range of wavelengths is obtained illumination by which can lead the particles to a stable condition. So for higher value of "a", it is difficult to maintain the periodicity of the PS particles in water medium using monochromatic illumination. Therefore, to reconfigure a certain periodic array within small range of "a" i.e. for nanoscale interparticle spacing, these wavelength profiles are helpful to identify what monochromatic light can help us achieve a certain periodicity in 1D PS microsphere structure. Moreover, to tune the lattice constant of a 1D periodic array using the optical force tuned reconfiguration process this observation can play a significant role.
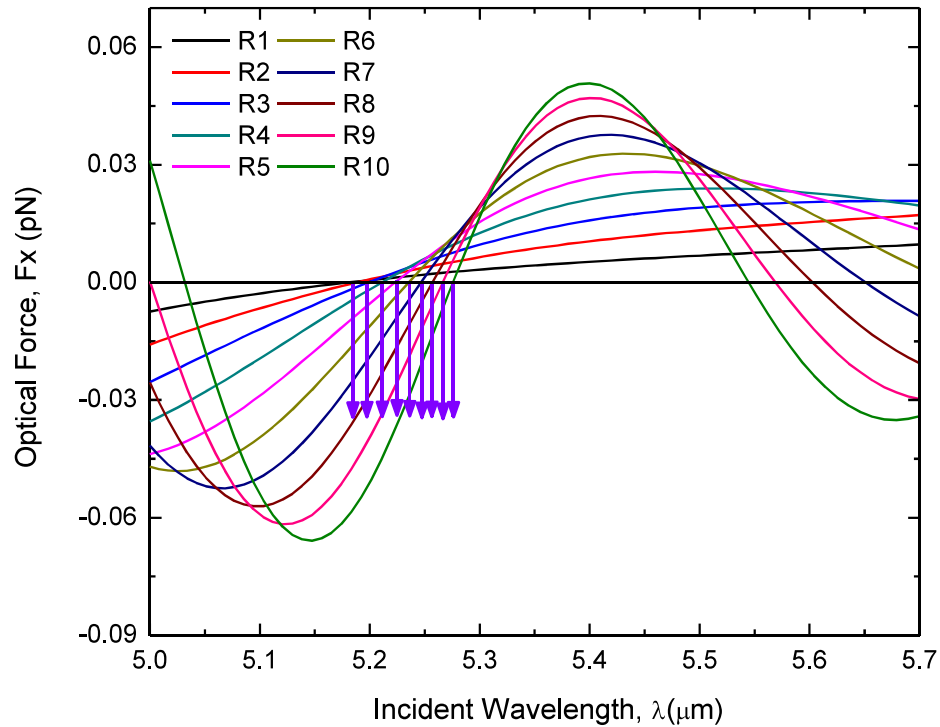
Figure 4-25: Optical Force as a function of Illumination Wavelength. The X component of force is plotted for right hand particles of an array of 21 PS particles in water medium. The violet arrows point to the stabilizing wavelength for a= 2μm.

4.1.6   Resonant Characteristics of 1D Polystyrene (PS) Photonic Crystal (PC) and Impact of Optical Force:

The 1D periodic arrays of PS microparticles discussed so far constituted a finite amount of N. In this section 1D PC consisting PS microparticles with infinite N is analyzed. Computing definite frequency eigen states of Maxwell's equations using MIT Photonic-Bands (MPB), the photonic band structures of these 1D PS PCs are determined.

For changing the interparticle spacing of water submerged PS PC, i.e. the center to center distance, "a" between 1.05μm to 10μm, the nature of bandgap between the first two bands are recorded in Figure 4-26.

When the particles are in touching condition i.e. for r/a =0.5, there is no gap between band 1 and 2. The peak is obtained when r/a is around 0.25 i.e. when the lattice constant is approximately 2μm. For this value of "a", the highest percentage of gap is found between Band 1 and 2

60
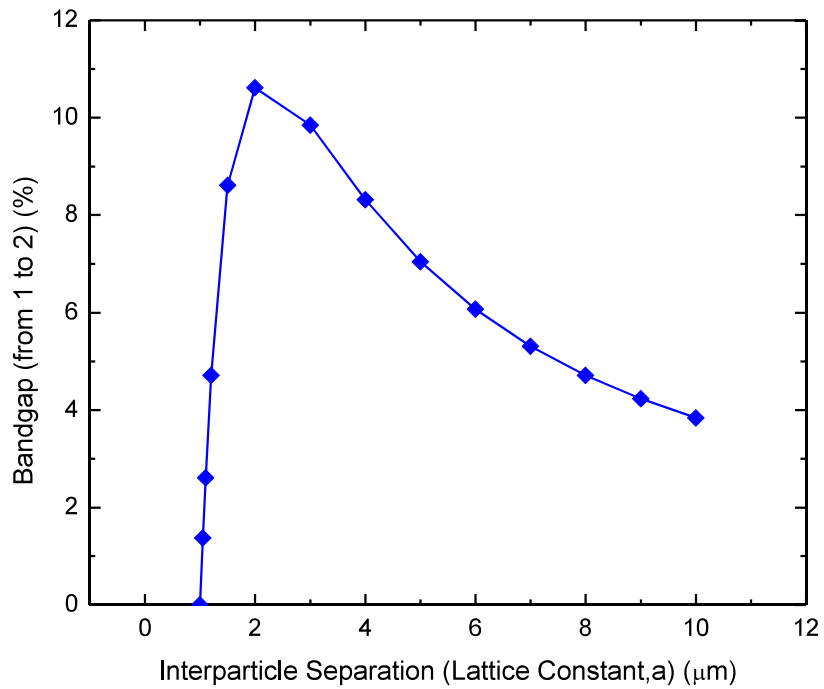
Figure 4-26: Percentage of Bandgap as a function of interparticle distance of a 1D PS array. Background Medium is water (1.33). The percentage is given for Bandgap between Band 1 and 2. The radius of each particle is 0.5μm.

.
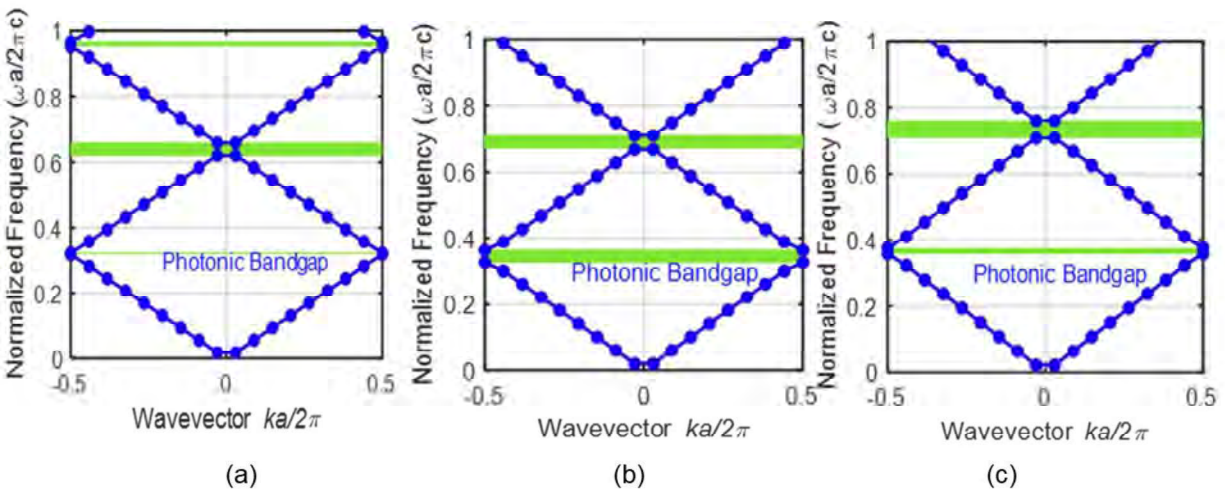
Figure 4-27: Band structure of a 1D PC consisting PS particles in water medium with lattice constant (a)a= 1.05 μm (b) a=2μm (c) a=8μm. The light green shade marks the region of bandgap in each case.

The band structures of the 1D PS PC computed for three different lattice constants: 1.05μm, 2μm and 8μm are plotted in Figure 4-27. As already shown in Figure 4-27, there is a very narrow bandgap for

the first case which is marked by the light green line between band 1 and 2 in Figure 4-2. When the lattice constant increases from 1.05 to 2μm, around 10.62% band gap arises between the first two bands. Next for increasing the interparticle separation to 8μm, the percentage of bandgap goes down as shown in the right column of Figure 4-27.

Now, the effect of refractive index of background medium on the band structure is checked for a 1D PS PC where for each case "a" is considered fixed at 2μm. Only the background index, n_m is varied from 1 to 3 with an irregular interval. It is already known higher refractive index contrast between the particle and submerging medium yields higher percentage of Bandgap [1]. For further illustration, the band structures calculated for three different background index are shown in Figure 4-29. For the left column, the bandgap is much higher than the case with water as submerging medium. The band gap vanishes when the medium has a refractive index of 1.6 and again the bandgap appears when the refractive index is 3 as displayed in the center and right column of Figure 4-29.
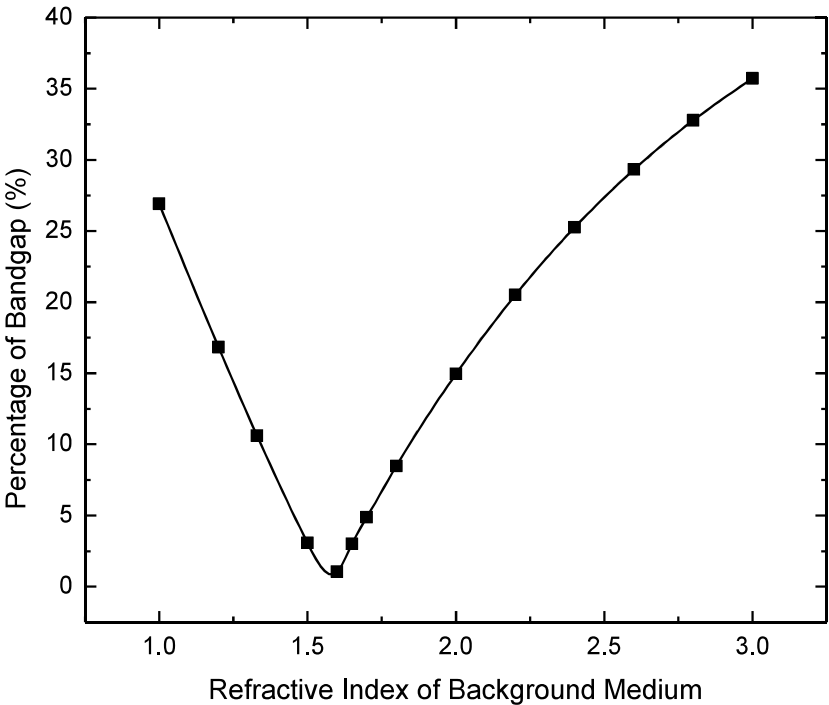
Figure 4-28: Percentage of Bandgap as a function of refractive index of the background medium. The interparticle separation is 2μm and the particle radius is 0.5μm.
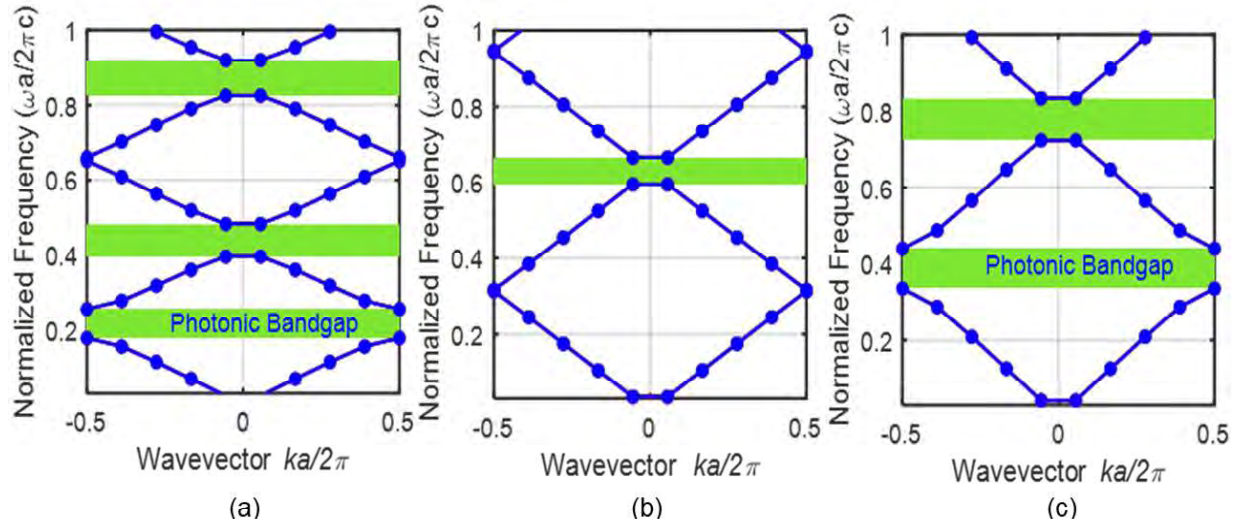
Figure 4-29: Band structure of the 1D PS PC with lattice constant 2μm and particle radius 0.5μm. The refractive index of the background medium is (a) 1 (b) 1.6 and (c) 3. The particles are identical in each case.

Next the resonance frequency obtained from the band structure computed for the case stated above is compared with the one obtained from the following approximation and it yields Figure 4-30. Here the resonance frequency denotes the midgap frequency which is the frequency at the middle of the first band gap and also termed as the resonant frequency. Based on the generalized equation provided by Joannopoulos et al. [1] for a multilayer stack consisting two materials, one with refractive index n_p and the background index n_m, the midgap frequency is given by:

$$f_m = \frac{n_p + n_m}{4n_p n_m} \times \frac{c}{a} \qquad (4.1)$$

where a is the lattice constant of the 1D PC, and for a PC consisting PS particles n_p is the particle refractive index and n_m is the medium refractive index. Here the value of n_p is 1.574. Figure 4-30 shows that the results obtained from the computed band structure using MIT photonic band and the one calculated using the approximation in equation (4.1) almost coincide. As the theoretical approximation is for multilayer slabs and the 1D PC considered in this case contain spherical particles, the results show slight variation.
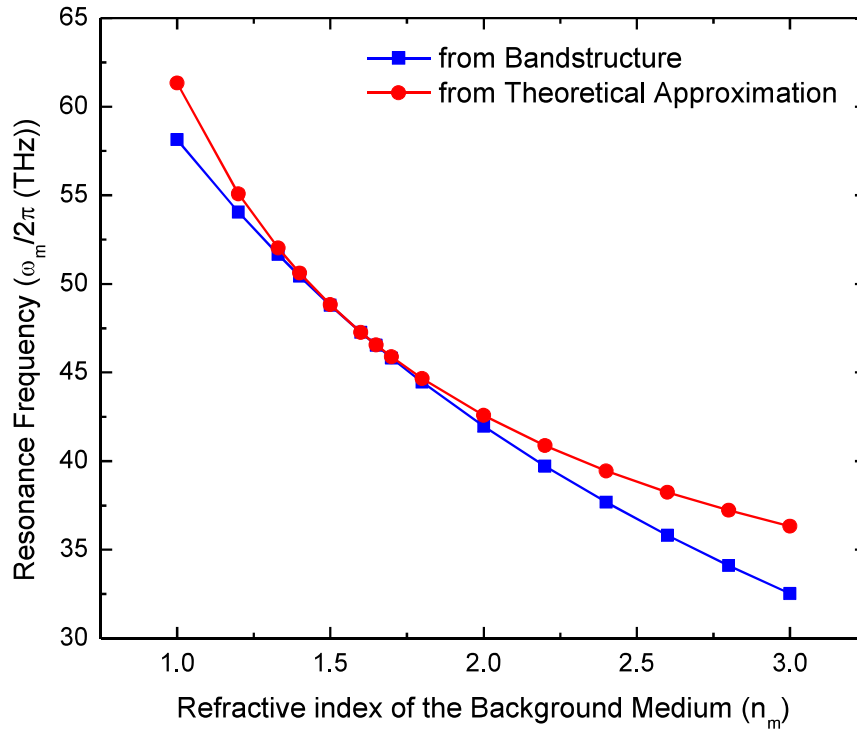
Figure 4-30: Resonance Frequency as a function of the background medium of the 1D PC. The interparticle separation is 2μm and the particle radius is 0.5μm.

Now the previous discussion is resumed from here where spherical particles are fully submerged in water medium. For this structure the Resonance frequency, f_m and corresponding resonance wavelength, λ_m are shown in Figure 4-31 for different "a". The results conform with equation (4.1) where the midgap frequency i.e., the resonance frequency is found to be inversely proportional to the lattice constant. So for higher interparticle separation the resonance frequency decreases in an exponential manner while the resonance wavelength linearly goes higher.

64
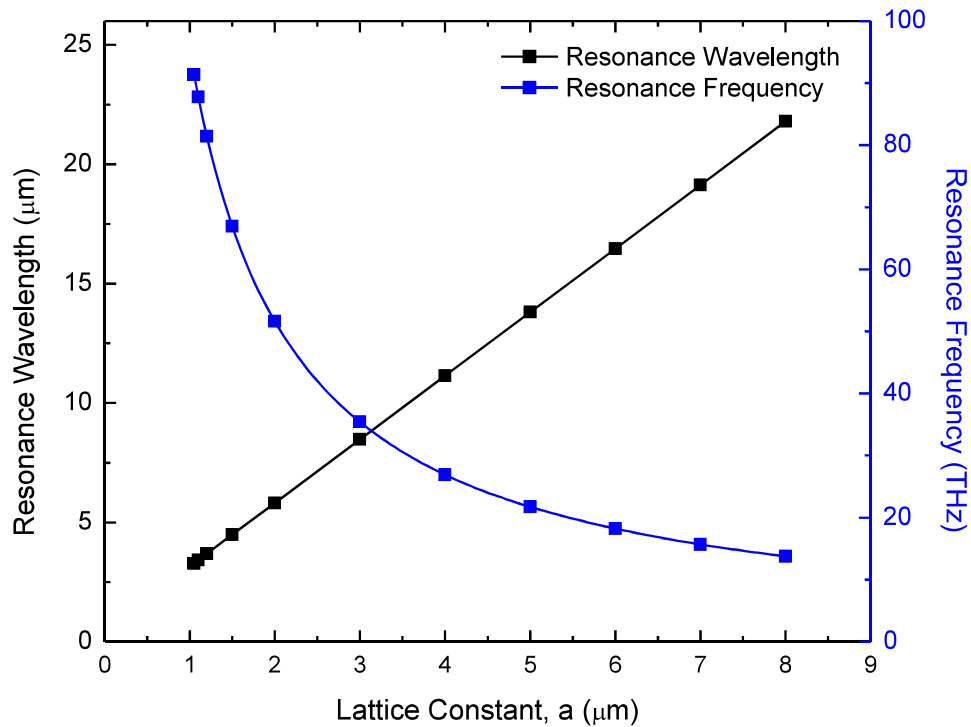
Figure 4-31: Resonance characteristics of the 1D PS PC with water as background medium. The left side scale of Y axis (black) is resonance wavelength and the right scale (blue) is resonance frequency. Particle radius is 0.5μm.

To verify the resonant behavior of the 1D PS PC obtained from Figure 4-31, the transmission and reflection spectra are investigated for a 1D periodic array of 27 identical PS particles submerged in water medium. When "a" is 2μm, a normalized plane wave is incident along the direction of the array and the recorded transmission and reflection curves are plotted in Figure 4-32. As for normally incident light, T=1-R, T=0 means 100% reflectance. At around 5.71μm, there is a dip in the normalized transmission curve and at this point there is almost 100% reflection obtained from this structure. From Figure 4-31, the value of λ_m is found to be around 5.8μm for a=2μm. So the resonant behavior obtained from the study of transmittance reflectance coincide with the ones derived from the photonic band structure computations.
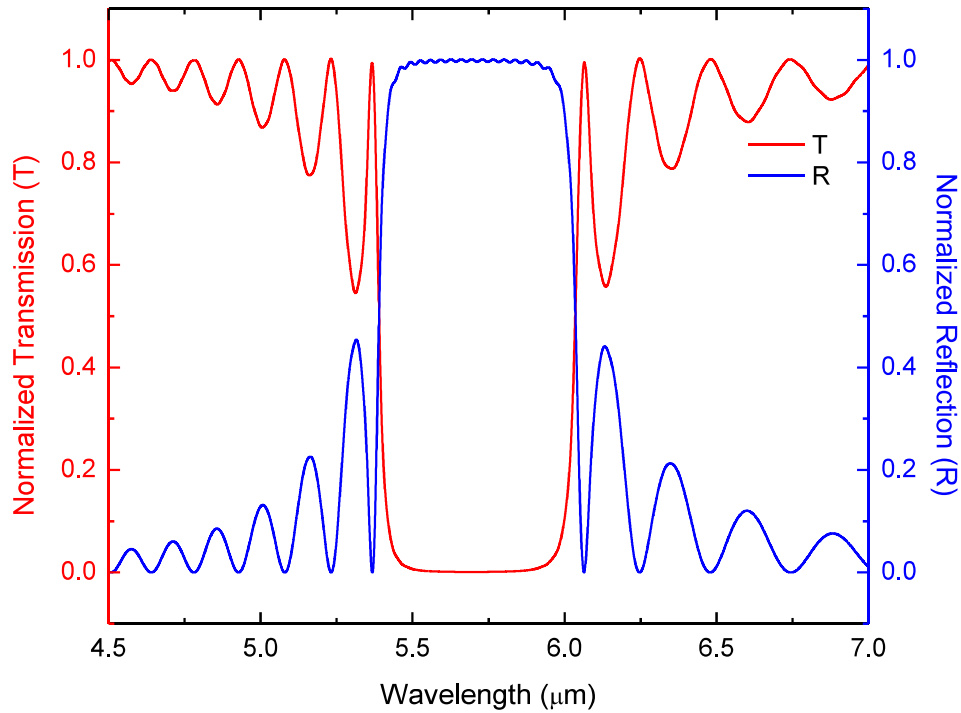
Figure 4-32: Normalized Transmission and Reflection Spectra of a 1D PS PC with 27 spherical particles in an array. The lattice constant "a" is 2μm. The left Y scale (marked red) denotes normalized transmission and the right Y scale (marked blue) is the reflection spectrum. n_m=1.33 and n_p=1.574.

For various interparticle gap, the transmittance curves are recorded in Figure 4-33 which shows that for increasing separation the resonance wavelength red shifts. This phenomenon supports the results plotted in Figure 4-31. For further illustration a comparative picture is presented in Figure 4-34 where the resonant wavelengths obtained from both the bandstructures and the transmission characteristics are displayed as a function of the interarticle gap in a 1D array. An identical linear trend is prominent for both cases. So to obtain resonance at higher wavelength the variation in interparticle separation can play a significant role.
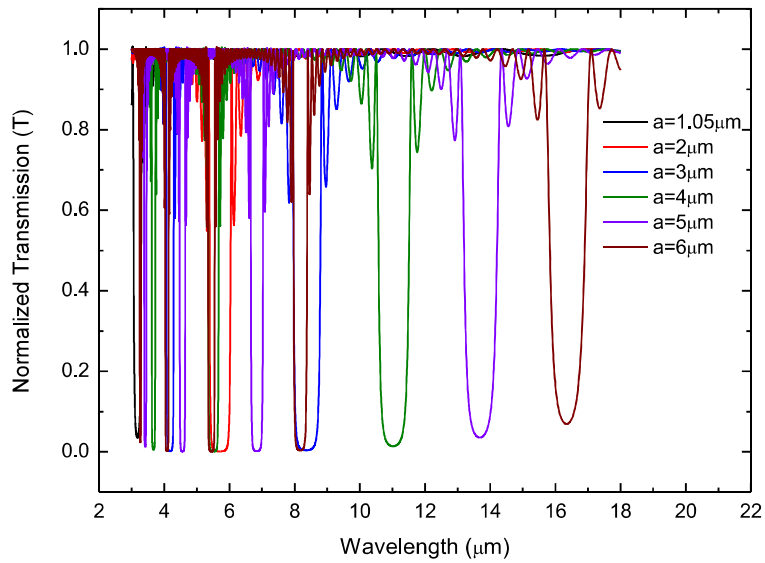
Figure 4-33: Transmission spectra of 1D PS array of 27 particles for different a. The solid curves are the normalized transmission curves and the dip denotes reflection at that wavelength.
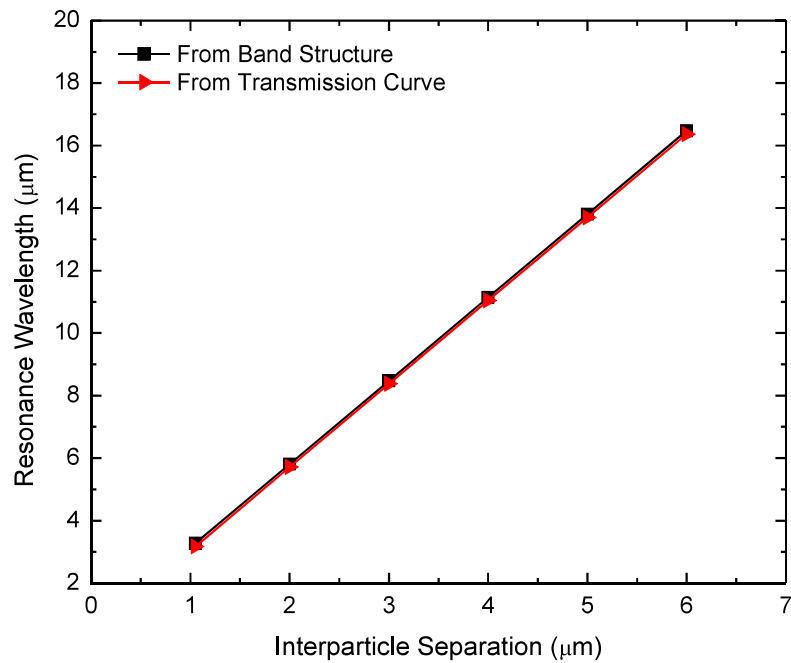
Figure 4-34: Resonance Wavelength as a function of interparticle separation a. The black and red lines are respectively the resonance wavelength obtained from band structure and the Transmission spectra.
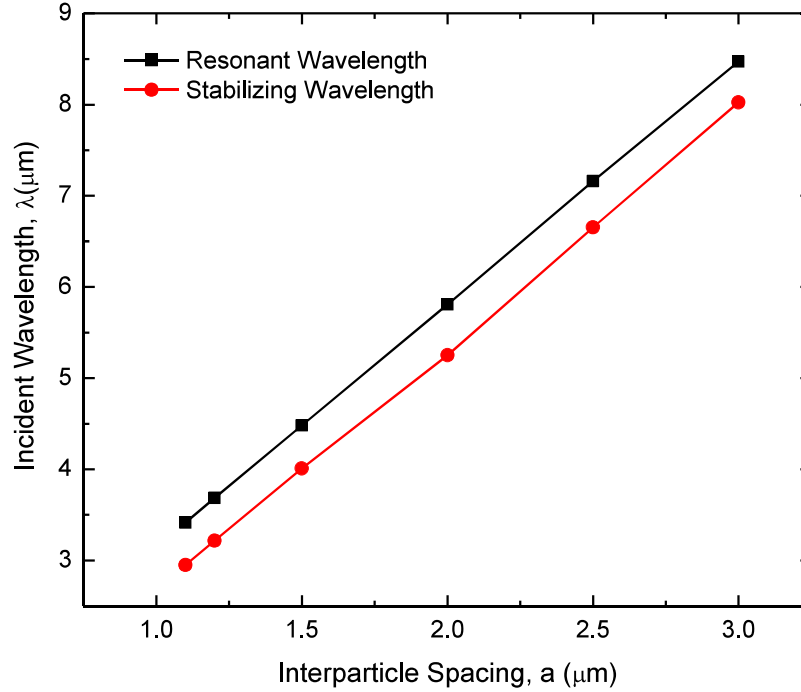
Figure 4-35: Relationship between stabilizing wavelength and resonant wavelength of a 1D PS photonic crystal.

In the previous discussion on the wavelength profile of optical force in dual Gaussian beam system, a similar red shift was observed in the stabilizing wavelength for increasing "a". In Figure 4-35, a relation between the resonant wavelength obtained from Figure 4-34 for a 1D Polystyrene PC in water and the stabilizing wavelength obtained from the study of wavelength profile of optical force is presented. It reveals that to reconfigure a PS PC using Optical force, an incident wavelength almost 0.5µm (which is equal to particle radius) less than its resonant wavelength needs to be applied from the dual Gaussian source.

4.2   Optical Force Tuned Two Dimensional (2D) Polystyrene Array

The self-assembly of polymers like PS can form 2D PC [47]. This section mainly focuses on 2D PC constituting PS microparticles of 0.5µm in radius.

4.2.1   Band structure of 2D Square Lattice Polystyrene (PS) Photonic Crystal (PC)

For PS particles submerged in water medium and arranged in 2D square lattice, no complete band gap is found rather it shows a narrow partial band gap within the region from X to M in its Brillouin zone. Figure 4-36 demonstrates the band structures for three different lattice constant a. For all three cases it is observed that there is no complete bandgap like the 1D case. The low refractive index contrast between PS (n_p=1.574) and water (n_m=1.33) in this 2D system does not possess a complete band gap but a partial band gap. In 2D layers of colloidal particles, the EM field in the layers become considerably delocalized depending on the sphere size and strong interparticle coupling of the EM field. This might be one possible reason for not getting any gap between the consecutive bands of 2D PS square lattice [12]. The relatively small refractive index difference between n_p and n_m($\Delta n \approx 0.244$) also accounts for the narrow partial gap [1] as shown in Figure 4-36.
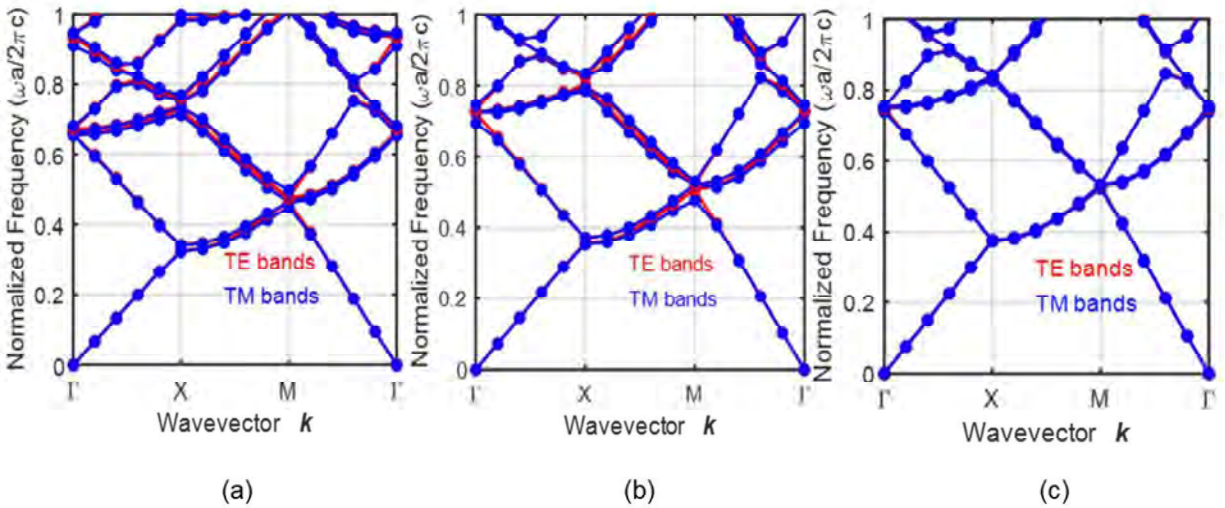
Figure 4-36: Band structure of 2D Square PS PC (a) a= 1.05μm (b) a= 2μm (c) a=6μm. The red lines are for TE bands and blue curves are TM bands.

As the small intrinsic dielectric contrast between the PS microparticles precludes the formation of large photonic band gaps in such materials [44][83], the minimum dielectric contrast is identified for which bandgap appears in this 2D model. Figure 4-37 shows the effect of the variation of refractive index of the background medium on the band gap of the 2D square PC. Increasing the dielectric contrast between n_p and n_m changes the amount of reflection occurring within the 2D plane and for n_m=3.9 and TM polarization there is a very narrow complete bandgap found in PS periodic structures which is almost 0.025%. So to obtain band gap a minimum refractive index contrast, $\Delta n \approx 2.33$ is required between the background medium and the PS particles. When the background index is 4.1 the bandgap

in both TM and TE mode is around 1% and it denotes that to obtain a complete bandgap for both TE and TM polarization the value of Δn needs to be 2.53. As the background index is increased from 4.1 to 12, the contrast between the percentage of gap found for TM and TE polarizations gradually increases for this 2D square PC. But in practical cases, no such high value of n_m is possible.
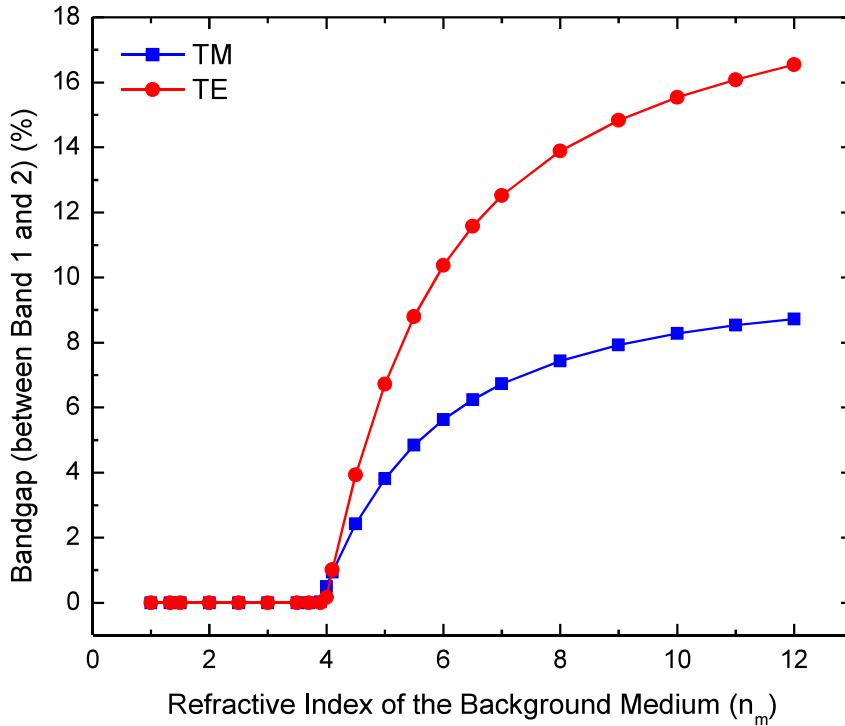
Figure 4-37: Percentage of Bandgap as a function of the refractive index of the background medium of 2D square PC consisting of PS spheres. Lattice constant, a = 1.2μm and particle radius, r=0.5μm. Here the bandgap between the first two bands are computed. Red and blue curves represent TE and TM polarization respectively.

Based on the plot shown in Figure 4-37, band structures for three different background medium are plotted in Figure 4-38. The left panel shows when the PS particles are placed in a medium with n_m=1(air). The center panel show the band structure for n_m=4.1 and the right panel shows structure for n_m=7. As already mentioned in Figure 4-37, for higher refractive index contrast the amount of band gap for TM and TE polarizations become higher and the position of this gap changes.
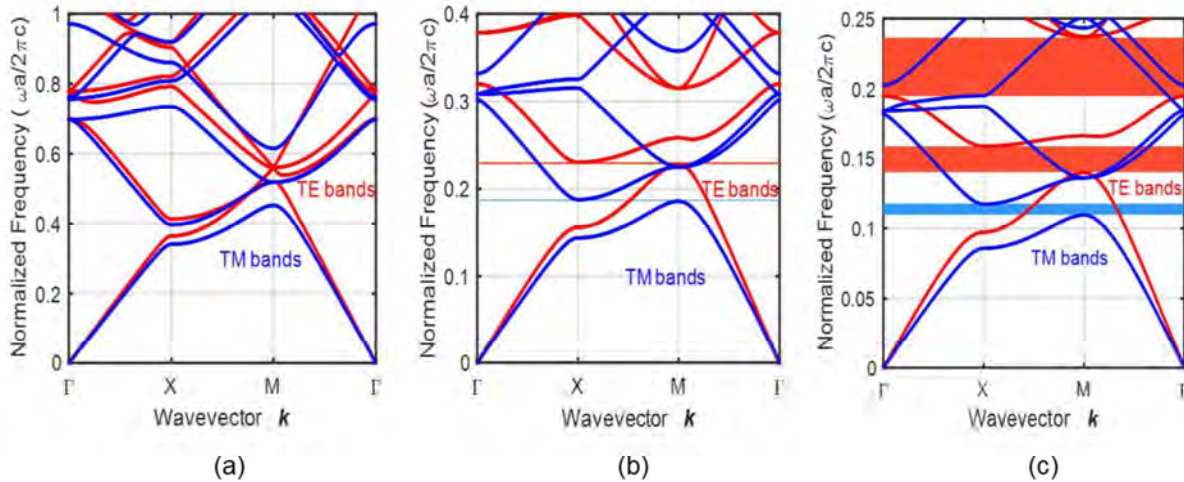
Figure 4-38: Band structures of 2D PS square lattice with three different background index (a) n_m=1 (b) n_m=4.1 (c) n_m=7. The blue lines represent TM bands and red lines present TE bands. The blue and red filled area represent the bandgap from TM and TE polarization respectively.

4.2.2 Optical Force Tuned Reconfiguration of 2D Square Array

As it is observed that one-dimensional optically coupled array of colloidal particles is formed by two counterpropagating Gaussian light beams, the discussion is now moved to two dimensional (2D) arrays of PS particles arranged in a square lattice. In the beginning, a 3x3 array of PS particles is considered and mark them based on the array position as shown in Figure 4-39. The particles have the same dimension and they are fully submerged in water medium as before. The interparticle spacing, "a" now denotes the center to center distance from each other in 2-D.
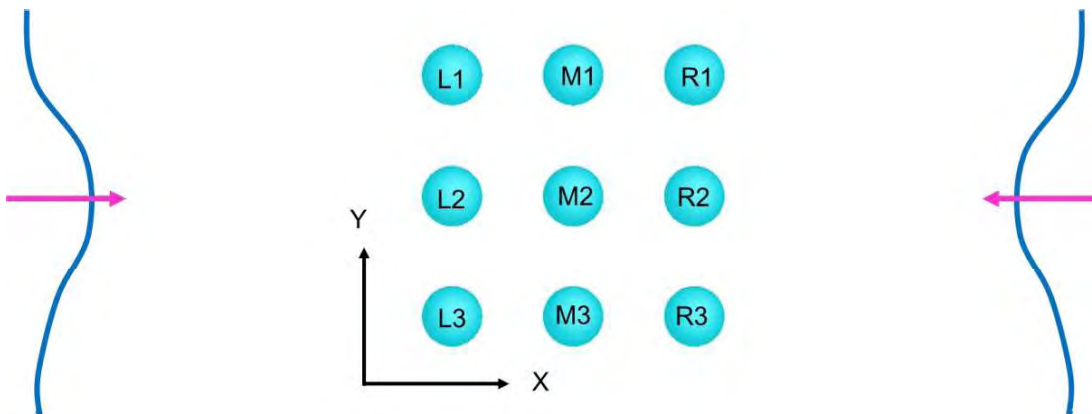
Figure 4-39: A 3by3 Arrow of PS (n_p=1.574) particles submerged in water (n_m=1.33) medium. Particle radius 0.5um. Here "a" is the interparticle spacing that represents the center to center distance between spheres.

The 2D array is illuminated by the Gaussian beam from two opposite ends and both the X and Y component of photo induced force, F_x and F_y are plotted in Figure 4-40 and 4-41 respectively. Although the Gaussian beams are X-polarized, unlike 1D array there is a significant amount of force acting along Y direction in this case. The slightly divergent Gaussian beams now push the particles in a way so that they are confined in xy plane rather than in a single line aligning the beam axis. The number of scatterer plays a significant role in this case. The arrangement of the particles in the xy plane redistribute the light source and in a similar manner to the 1D case, the zero crossing points of both F_x and F_y are identified. Initially all 9 particles are arranged with a=2μm and for changing "a" from 2μm to 4.8μm several zero crossing points are obtained. Unlike 1D array, the potential is now modulated both in x and y axis and thus the stable conditions i.e., the (x,y) coordinates of the particle upon the application of optical force are now computed based on the zero crossing points of both Fx and Fy.
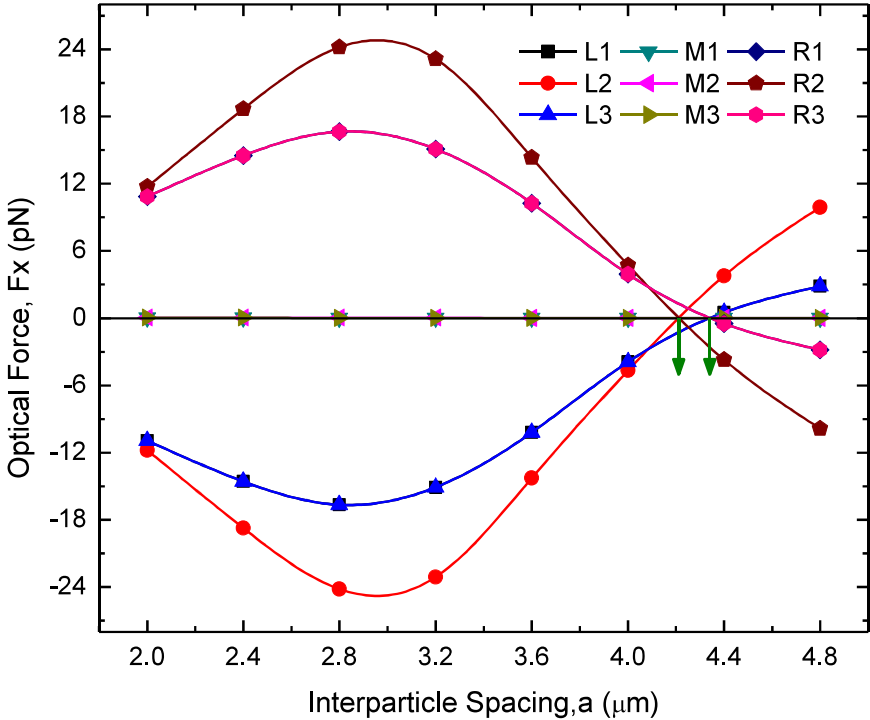
Figure 4-40: X component of Optical Force, Fx on a 3x3 PS Array in water medium. Illumination wavelength: 980nm. The green arrows represent the stable x coordinates.

From Figure 4-40, it is found that the particles along the centered column feel negligible amount of force acting along X axis. Therefore, the particles marked M1, M2, M3 will not change their position due to Fx. But the other particles will try to rearrange their position to reach their energy minimum. In Figure 4-41 that same situation occurs for Fy acting along the particle in the mid row. So L2, M2 and R2 particles do not move along y axis rather they remain confined to the x axis. For R1, R2, R3 (L1, L2, L3) when Fx goes from positive (negative) to negative (positive), stable conditions are achieved.
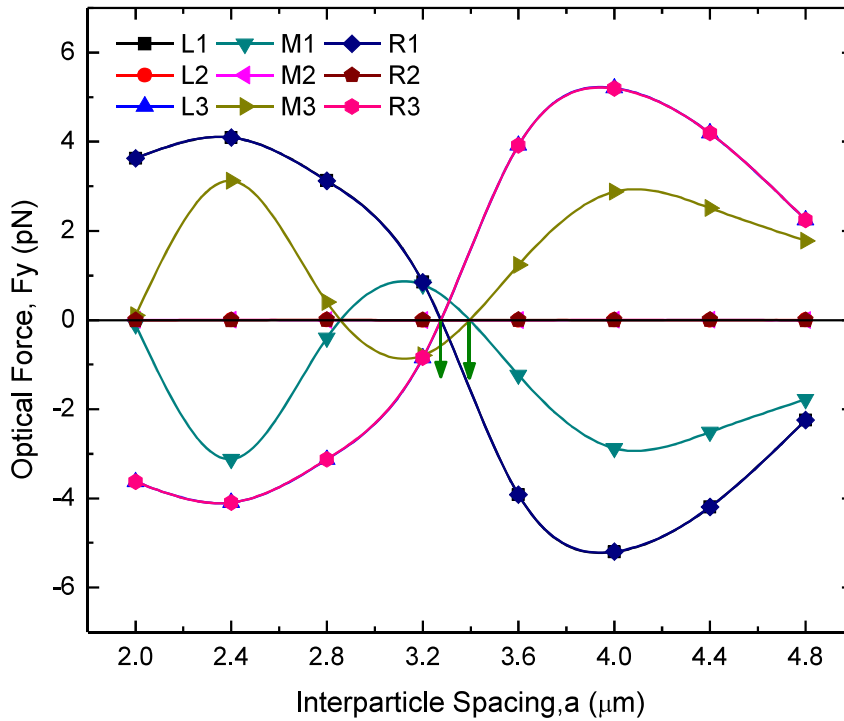
Figure 4-41: Y component of Optical Force, Fy on a 3x3 PS Array in water medium. Illumination wavelength: 980nm. The green arrows represent the stable y coordinates.

From Figure 4-42 it can be seen that the same value of a that obtains stable x coordinates in the previous case does not yield stable y positions of particles. Rather the green arrows in Figure 4-40 and 4-41 show that at (x,y)=(4.34, 3.28), R1 particle becomes stable. In the similar manner, other stable (x,y) coordinates are identified. Thus, upon illumination the square shape is not conserved anymore. Based on the results obtained from Figure 4-40 and Figure 4-41, Figure 4-42(a) provides a clear picture in

what direction the force components act just before the stable position and also the stable configuration obtained through the application of optical force is presented in Figure 4-42(b).
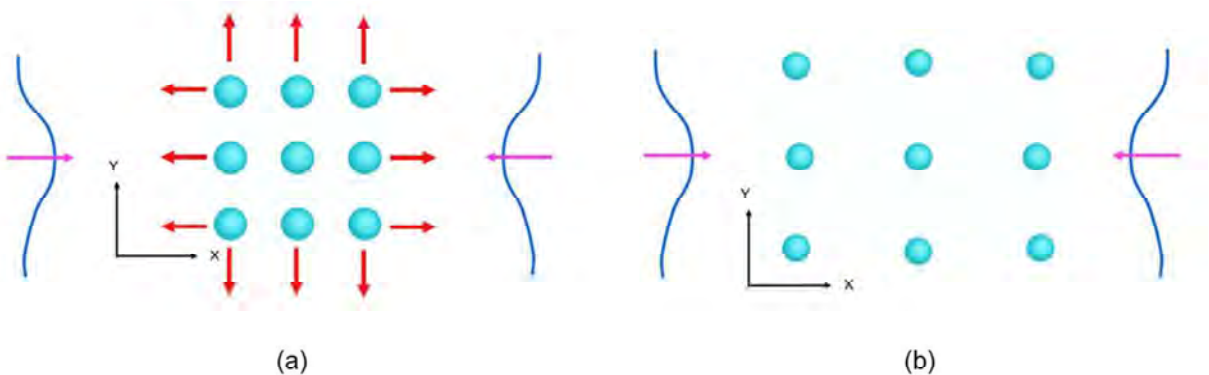
Figure 4-42: (a) Direction of Force acting on a 2D PS array. Particles are in xy plane. The two end beams are counter propagating Gaussian beams. The red arrows represent the force direction just before reaching the stable condition. (b) Stable configuration.
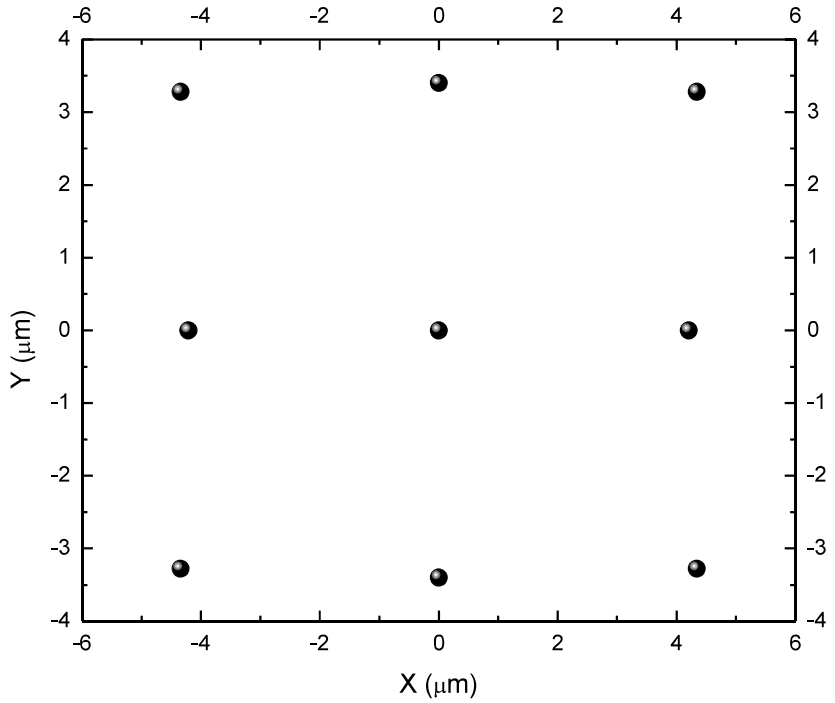
Figure 4-43: The stable 3x3 array of PS particles in water medium (n_m=1.33) after applying optical force. The Illumination wavelength: 980nm. Initial a: 2μm.Particle radius: 0.5μm.

After analyzing the 3x3 array of PS particles in presence of optical force, a 5x5 PS microparticle array is studied. Figure 4-44 shows the configuration containing the labels of particles used in this manner. The particles are arranged in a periodic 2D square lattice structure with an initial a=2μm and placed in between the dual Gaussian beam to apply the photoinduced force.
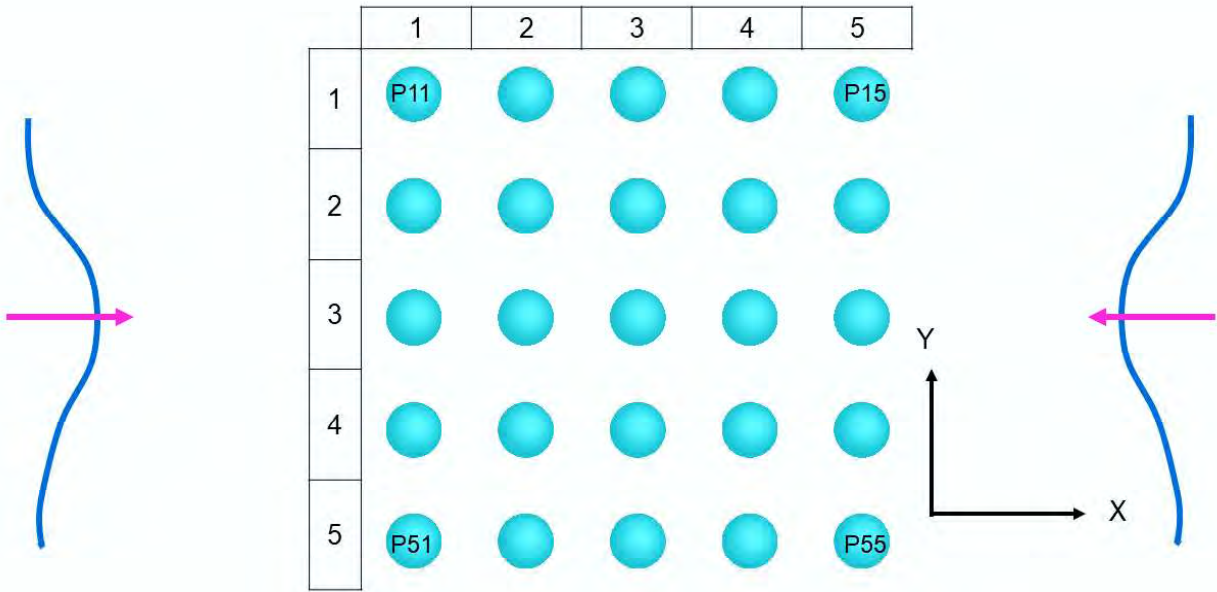
Figure 4-44: A 5by5 Arrow of PS (n_p=1.574) particles submerged in water (n_m=1.33) medium. Particle radius 0.5um. Here each row and column is marked in a matrix format. The first row is marked as P11,P12,…..P15 and second row as P21, P22,…..,P25 and the rest of them are marked accordingly.

Figure 4-45 to 4-49 record the Fx acting on each particle in the matrix after monochromatic illumination of 980nm wavelength. And in the next three figures: Figure 4-50 to 4-52 display the Fy component of the total optical force acting on the particles of periodic 5x5 array.
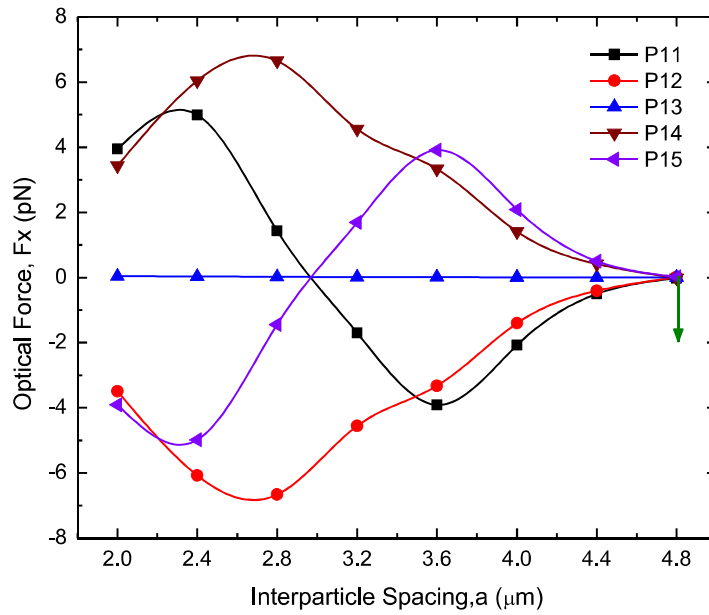
Figure 4-45: X component of Optical Force, Fx on the first row of particles (P11,…..,P15) a 5x5 PS Array in water medium. Illumination wavelength: 980nm. The green arrows represent the stable x coordinates.
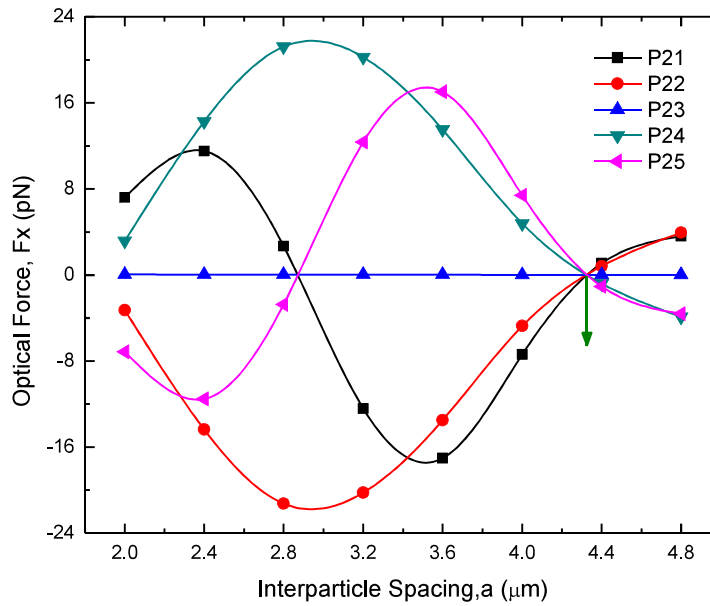
Figure 4-46: X component of Optical Force, Fx on the first row of particles (P21,…..,P25) a 5x5 PS Array in water medium. Illumination wavelength: 980nm. The green arrows represent the stable x coordinates.
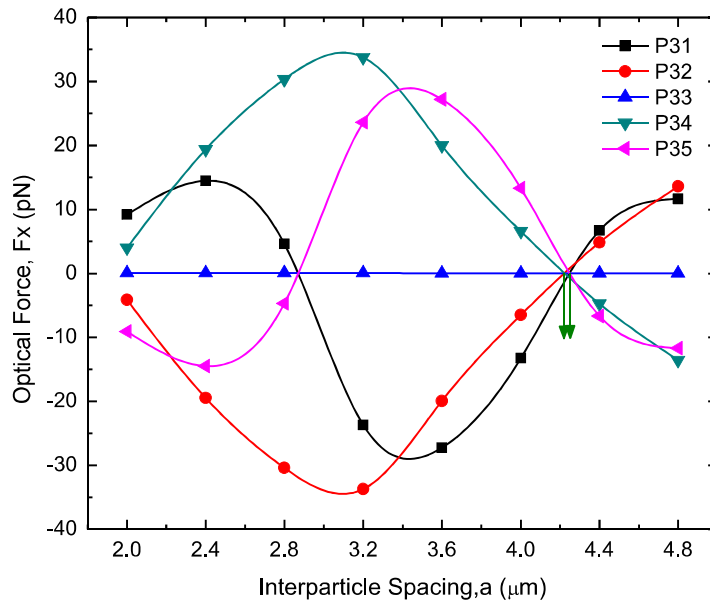
Figure 4-47: X component of Optical Force, Fx on the first row of particles (P31,…..,P35) a 5x5 PS Array in water medium. Illumination wavelength: 980nm. The green arrows represent the stable x coordinates.
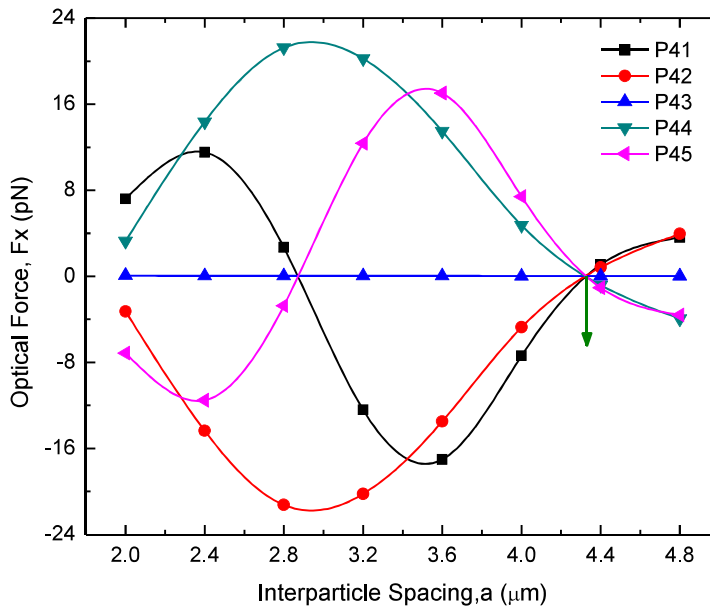
Figure 4-48: X component of Optical Force, Fx on the first row of particles (P41,…..,P45) a 5x5 PS Array in water medium. Illumination wavelength: 980nm. The green arrows represent the stable x coordinates.
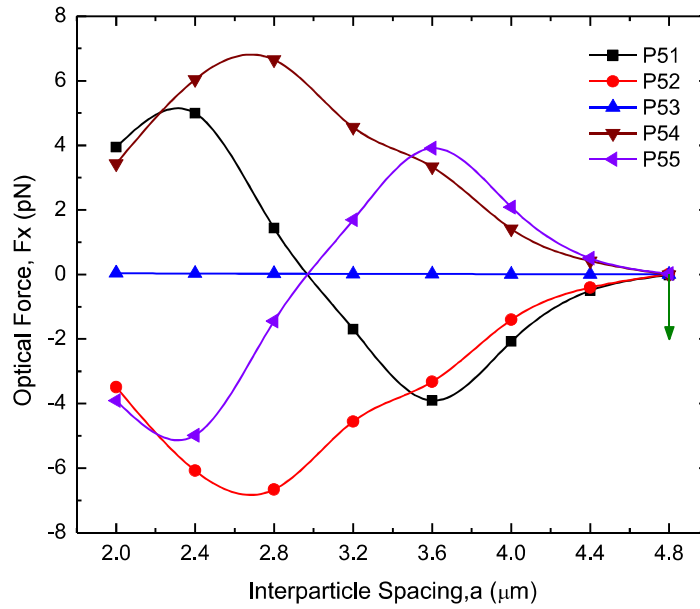
Figure 4-49: X component of Optical Force, Fx on the first row of particles (P51,.....,P55) a 5x5 PS Array in water medium. Illumination wavelength: 980nm. The green arrows represent the stable x coordinates.
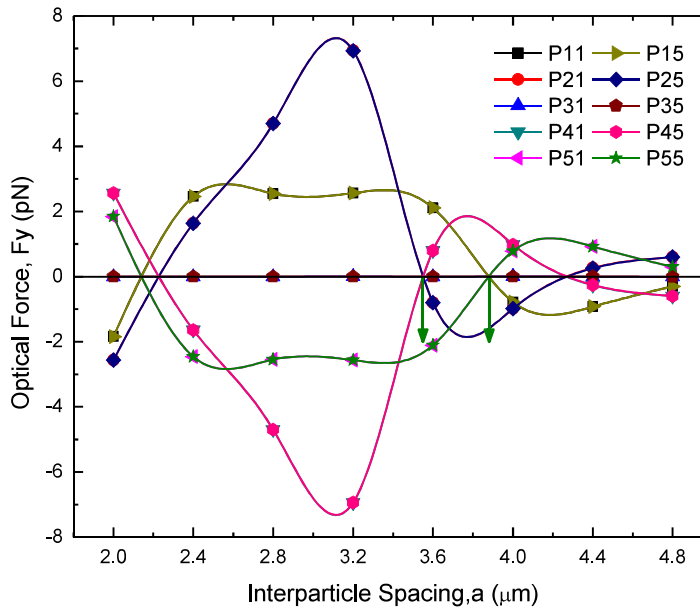
Figure 4-50: Y component of Optical Force, Fy on the particles (P11, P21, P31, P41, P51, P15, P25, P35, P45, P55) in a 5x5 PS Array in water medium. Illumination wavelength: 980nm. The green arrows represent the stable y coordinates.
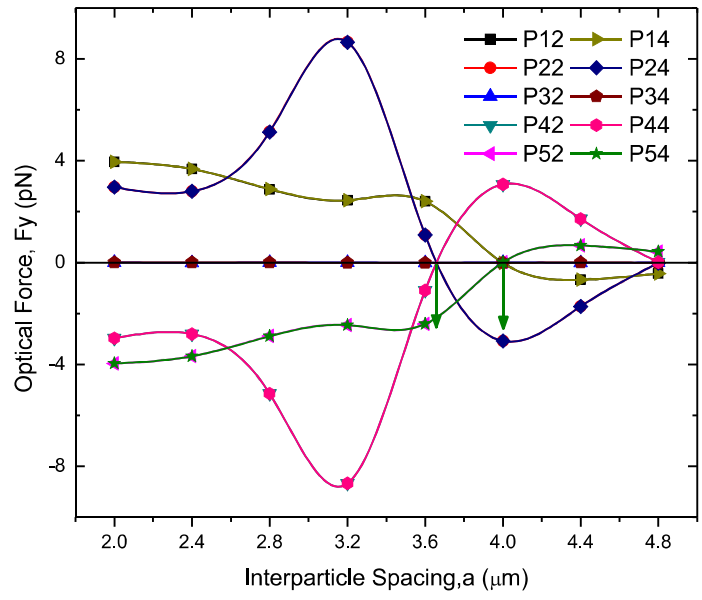
Figure 4-51: Y component of Optical Force, Fy on particles (P12, P22, P32, P42, P52, P14, P24, P34, P44, P54) in a 5x5 PS Array in water medium. Illumination wavelength: 980nm. The green arrows represent the stable y coordinates.
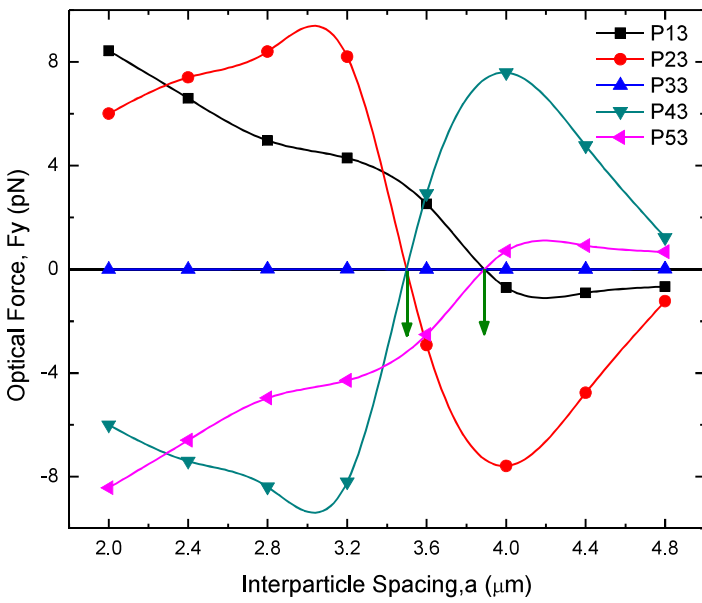
Figure 4-52: Y component of Optical Force, Fy on the particles (P13, P23, P33, P43, P53) in a 5x5 PS Array in water medium. Illumination wavelength: 980nm. The green arrows represent the stable y coordinates.

In a similar manner, all stable (x,y) coordinates of all 25 particles marked P11, P12,………P54, P55 constituting the 5x5 PS array are located. The new reconfigured array is presented in Figure 4-53 which shows a similar arrangement of PS particles to that shown in Figure 4-44. The reconfiguration of both 3x3 and 5x5 array reveal that the previous square configuration will now rearrange the particles in a slightly rectangular manner influenced by the photoinduced force. Following the same identification process, the equilibrium arrangement of a 7x7 array is studied and is shown in Figure 4-55.
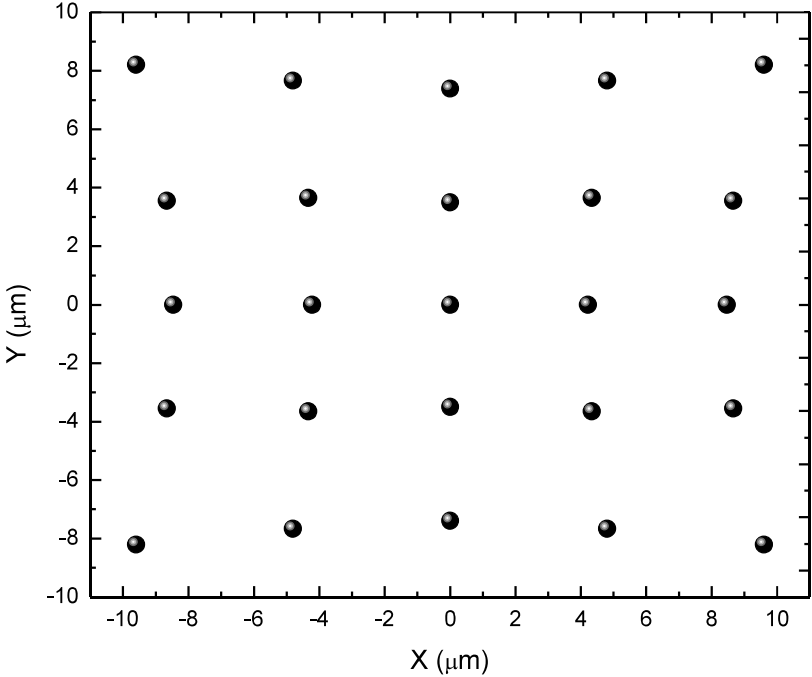
Figure 4-53: The stable 5x5 array of PS particles in water medium (n_m=1.33) after applying optical force. The Illumination wavelength: 980nm. Initial a: 2μm

Looking closely at the pattern of all three reconfigured structures displayed in Figure 4-43, 4-53 and 4-54, a common trend is observed that can help predict the stable structure of more than such small number of particles or of a larger 2D array. The center particle positions itself at (0,0), while the others are affected by the scattering caused by the presence of neighboring particles and the Gaussian source from two opposite ends. The intensity gradient holds the particles in the x-y plane and inhibit them to move along z direction. Since the dual beam resides along the beam axis, the particles remain more confined along x axis and the outermost particles gradually disperse as they go farther from the beam axis.
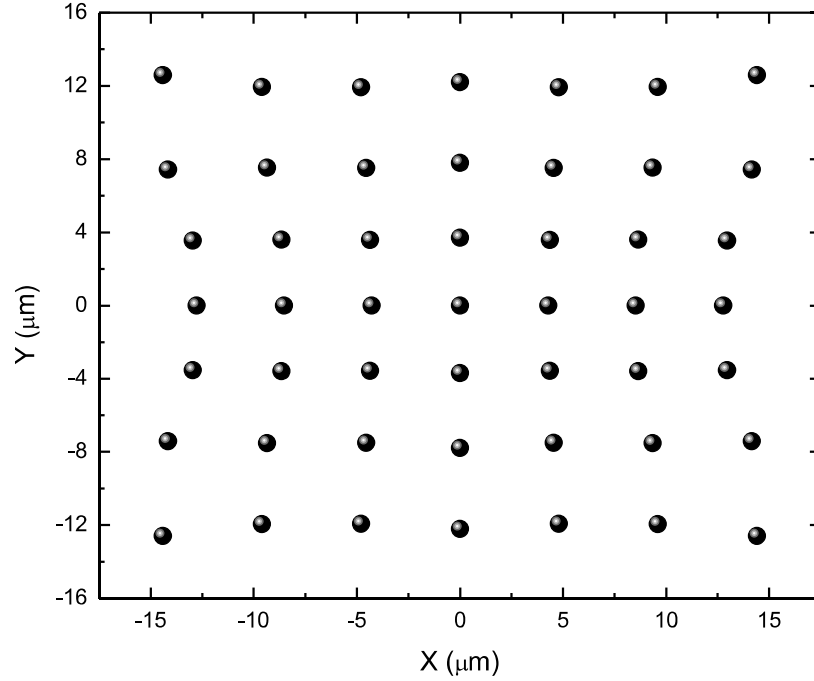
Figure 4-54: The stable 7x7 array of PS particles in water medium (n_m=1.33) after applying optical force. The Illumination wavelength: 980nm. Initial a: 2µm.

In order to predict the position of the incoming particle position in such a 2D square array, three lines are drawn as marked in Figure 4-55. As particles position themselves following a symmetric manner with respect to X and Y axis, only particles of the first quadrant are marked as 1,2,3 etc. The three lines marked as A, B and C pass along X, the diagonal and Y direction. The all three trend lines are expressed using the following equations:

$$A: 4.25m+.03$$

$$B: 0.2707m^2 +5.4497m -0.1388$$

$$C: 0.2145m^2+3.3475m+0.02$$

where m is the particle index marked as 1,2,3 and so on.
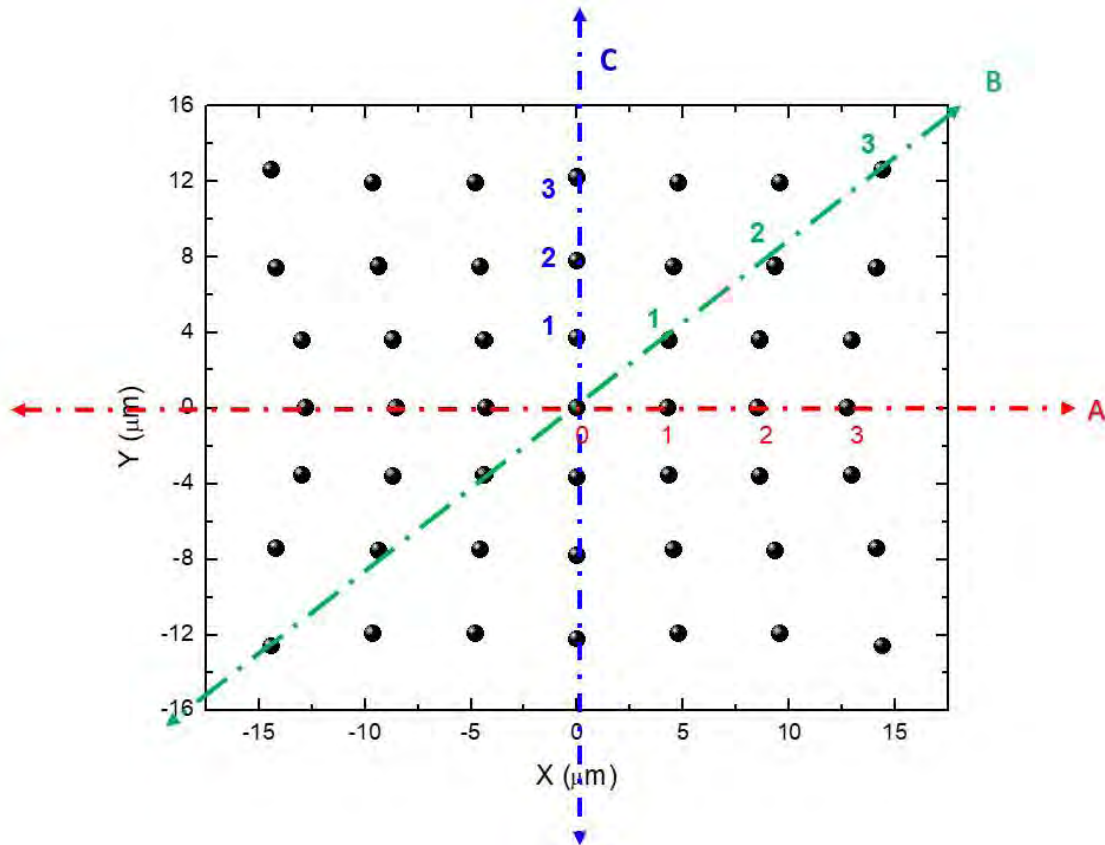
Figure 4-55: Prediction lines A, B and C. The red, green and blue dotted lines represent A, B and C along which the prediction is performed. Particles are marked as 1,2,3 for each case.

Line A depicts that the incoming particle will stay stable at a position that is linearly spaced along X axis, e.g., along A, the particle marked "1" will be at 4.25*1+0.03=4.28, "2" will be at 4.25*2+0.03=8.53 and so on. Line B and C represent that a slight nonlinearity is introduced along diagonal and Y direction. So the particles will not maintain the square structure as more particles are introduced along X and Y axis. The amount of deformation can also be predicted using these three lines. Although only one sided particle positions are predicted based on these three equations, the particles on the opposite side are assumed to occupy a mirror-symmetric position.

4.2.3 Resonant Characteristics of the 2D Reconfigured Photonic Crystal (PC)

As the reconfigured stable structure of an initially periodic 2D array is now available, the effect of optical force is discussed on their resonant behavior. According to the band structure of 2D square lattice changing "a" does not yield any band gap as well as any well-defined resonant wavelength for

2D PS PC in water medium. A 2D finite array of PS in water with interparticle spacing, a=2μm when illuminated by plane wave, displays no broadband reflectance region as well both in TM and TE mode. But between 2μm to 3μm, almost 94% reflectance is obtained at around 2.76μm from such a finite 7x7 PS array at for TM polarization and 83% at 2.73μm for TE [Figure 4-56]. As the application of photo-induced force causes displacement of particles, their transmission characteristics are affected as well. Figure 4-56 shows that before applying optical force using dual Gaussian beam system, the periodic array exhibits a dip for both TM and TE polarized plane wave. But force induced reconfigured 2D array shows a completely different picture. For TM mode, at around 2.48μm, ≈33% reflectance occurs while for TE mode no such pronounced dip is observed. In fact, the 2D array becomes almost transparent to all incident wavelengths for plane polarized TE illumination.
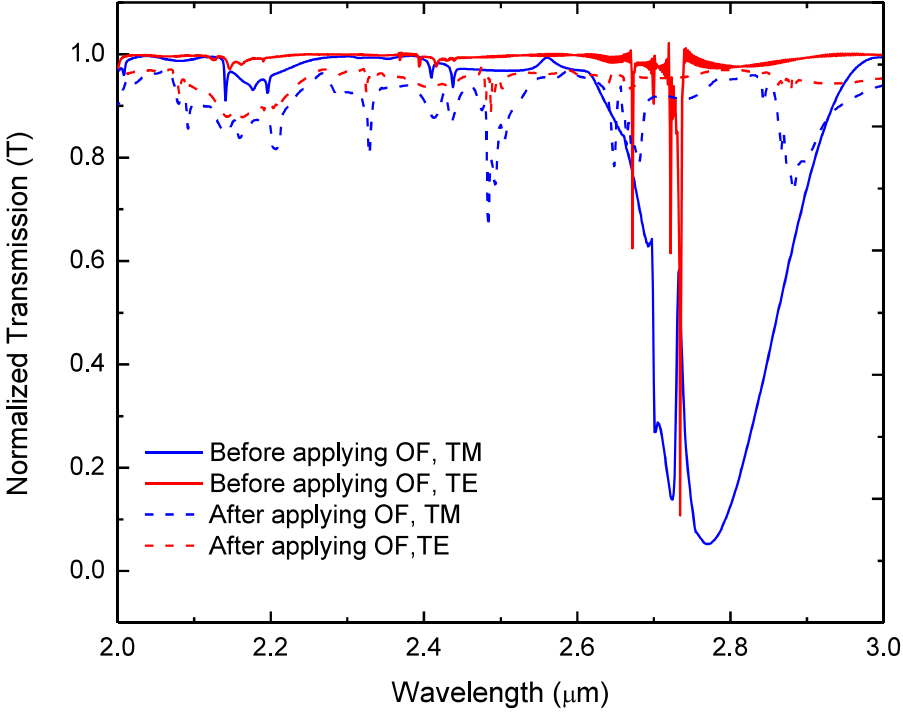
Figure 4-56: Transmission Characteristics of 2D PS array, before and after illumination. A 7x7 array is considered submerged in water medium. The red and Blue solid and dashed lines represent TE and TM polarization before and after applying optical force(OF) respectively. Before applying optical force (OF), a=2μm.

To further illustrate the resonant behavior of this 2D array before and after going through change in their spatial configuration, the Q factor is computed and a comparative picture of the quality factor corresponding each resonant wavelength is presented in Figure 4-57. Since narrower bandwidth yields better Q, TE polarized light results in Q≈4470 which is almost 6.5 times higher than that obtained from TM mode. The stable configuration does not provide any resonant mode for TM polarized plane wave illumination but for TE mode, it shows a Q≈ 2021 at around 2.48μm. This resonant mode corresponds to the small dip observed in the transmittance curve in Figure 4-56 marked by the dotted blue line.
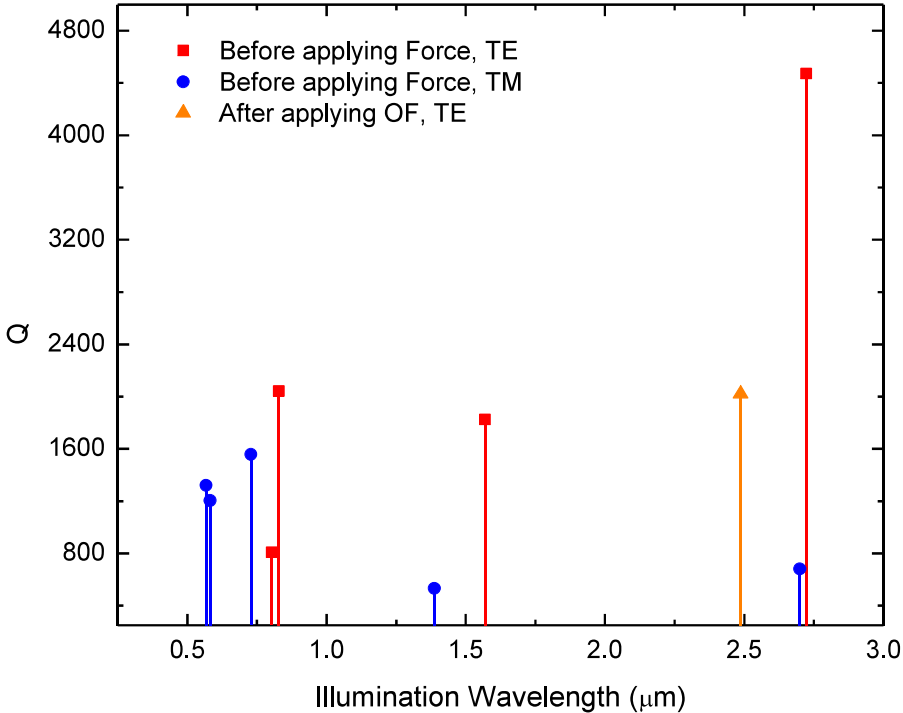
Figure 4-57: Quality Factor (Q) of a 2D square PS 7x7 array submerged in water medium. The red & blue droplines represent Q before applying Optical force(OF) for TE and TM polarized cases. The orange marked dropline is for Q factor after applying OF. Before applying optical force (OF), a=2μm.

4.3 Polystyrene Whispering Gallery Mode (WGM) Micro-Resonator and Optical Force Tuned Reconfiguration

After the discussion on the design and optical force tuned reconfiguration of 1D and 2D square lattice PS PC, this section focuses on the design of Whispering Gallery Mode Resonator based on rotationally symmetric PS microspheres and their optical force tuned reconfiguration process.

4.3.1 2D Hexagonal Lattice Polystyrene (PS) Photonic Crystal (PC)

Before discussing the rotationally symmetric PS microstructure and formation of WGM resonators, the band structure of PS hexagonal PC is briefly studied in this sub-section. Hexagonal close-packed monolayers of monodispersed PS microparticles were fabricated for practical experiments exploiting the self-assembly of colloidal PS [6][9]. The configuration of such 2D PC and its unit cell are presented in Chapter 3.
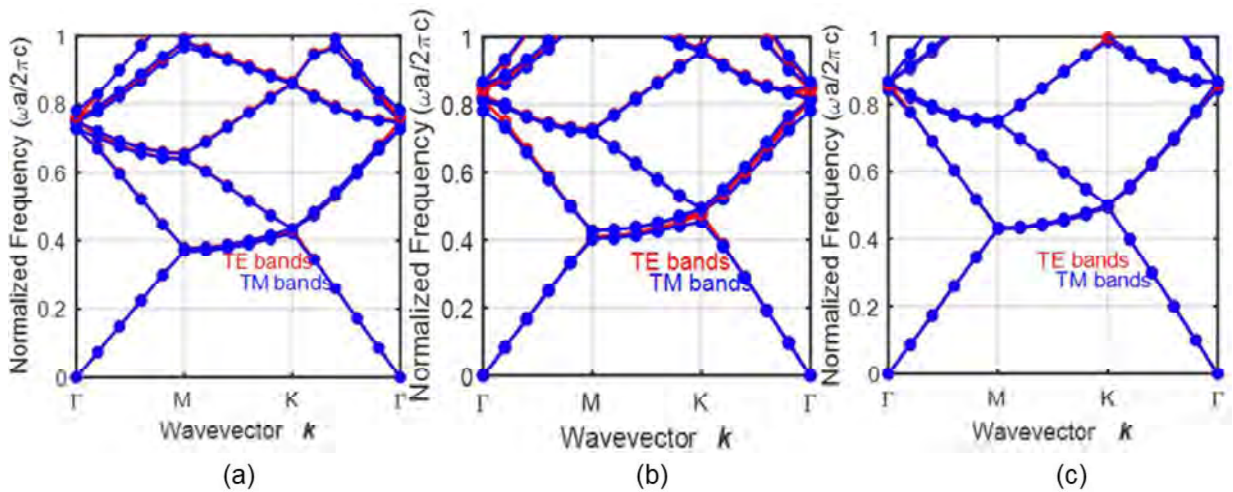
Figure 4-58: Band structure of 2D Hexagonal PS PC (a) a= 1.05 μm (b) a= 2μm (c) a=6μm. The red lines are for TE bands and blue curves are TM bands.

For an infinite 2D array of PS microparticles with a hexagonal lattice, band structures for three different interparticle spacing, "a" are showed in Figure 4-58. Same as the square 2D PC, there is no complete bandgap within M to K in its Brillouin zone for the variation of r/a ratio. Although the Brillouin zone of such hexagonal 2D PC is more circularly symmetric than the square one, PS-water configuration does not yield any pronounced gap. But if the background refractive index is changed from 1.33 to 2.25, a bandgap for TE polarized light is obtained for PS 2D hexagonal PC as shown in

Figure 4-59. But for TM mode, changing the background medium refractive index from 1 to 3.5, does not yield any such gap.

For three different background medium the band structures of hexagonal 2D lattice are showed in Figure 4-60. For $n_m=1$, there is a very narrow TM band gap which is almost invisible whereas for $n_m=2.3$, a narrow TE gap is observed. From the previous graph in Figure 4-59 it is seen that above $n_m=2.25$, TE gap gradually appears but TM gap vanishes. For $n_m=3.4$, a much larger band gap for TE mode is displayed in the right panel of Figure 4-60.
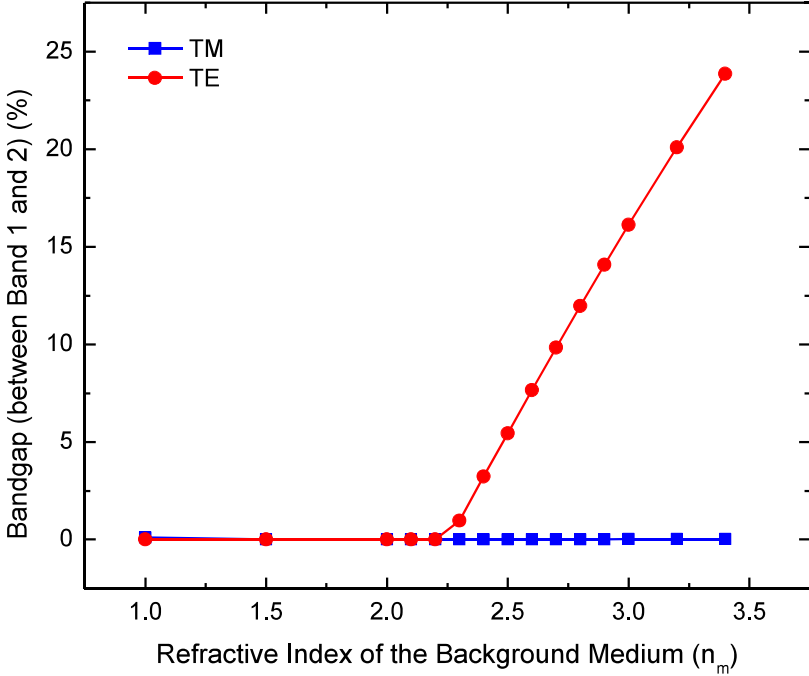
Figure 4-59: Percentage of Bandgap as a function of the refractive index of the background medium of 2D hexagonal PC consisting PS spheres. Lattice constant, a = 1.2μm and particle radius, r=0.5μm. Here the bandgap between the first two bands are computed. Red and blue curves represent TE and TM polarization respectively.
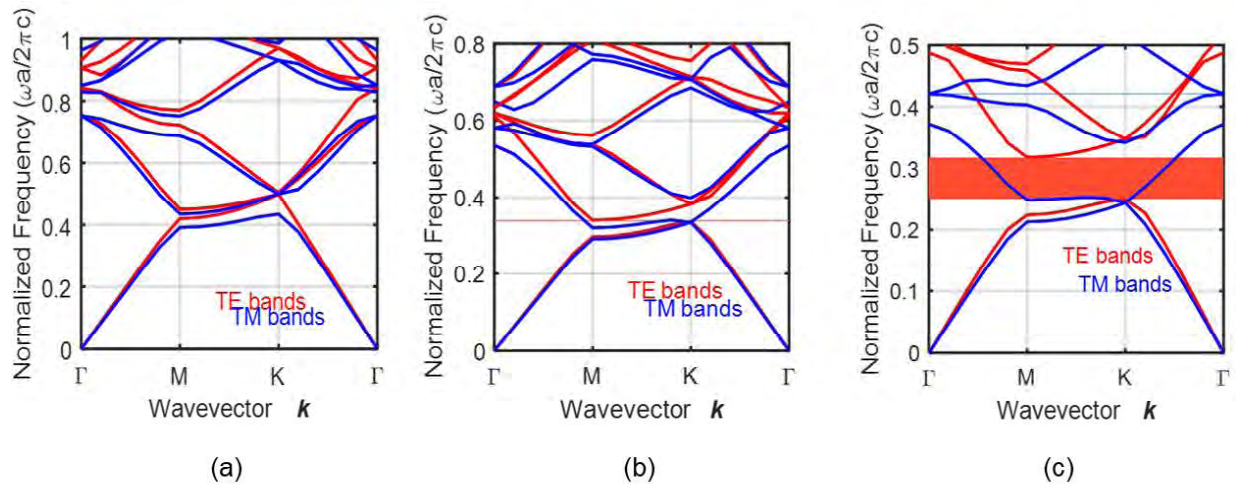
Figure 4-60: Band structures of 2D PS hexagonal lattice with three different background index (a) n_m=1 (b) n_m=2.3 (c) n_m=3.4. The blue and red lines represent TM and TE bands respectively. The area filled with light blue and red color present the bandgap from TM and TE polarization. Here, lattice constant, a= 1.2μm.

4.3.2   Polystyrene Monosphere and Multisphere WGM Resonator

To begin discussion on self-assembled PS microsphere based WGM resonators, first of all the formation of WGM resonance is studied in a solid microsphere of PS in water medium [Figure 4-61].
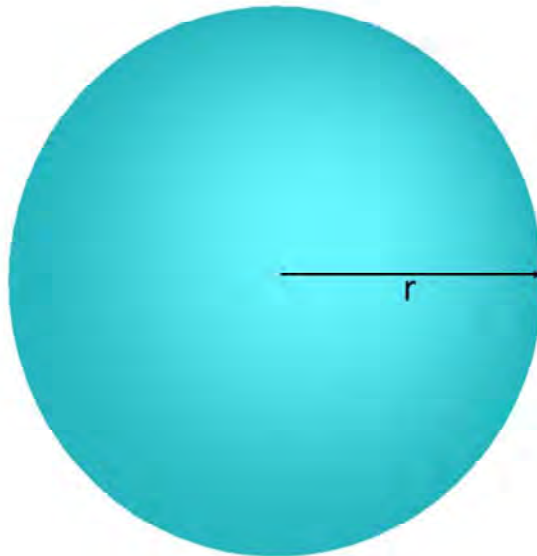
Figure 4-61: A solid PS microsphere with radius r. Particle refractive index, n_p=1.574.

A solid PS microsphere when illuminated using a point dipole source exhibits WGM mode within optical wavelength. At around 415.633nm, the single sphere shows a high-Q WGM resonance with an m (azimuthal mode number) of 114 when fully submerged in water medium. As already mentioned in Chapter 2, for a microsphere with $n_p > n_m$ resonance condition is fulfilled when: $2\pi R'n_p = m\lambda$, where n_P is the particle refractive index, R' is the effective radius of the particle which measures the distance from center to the point where the WGM modes appear and m is the azimuthal mode number. According to Figure 4-62, For the PS particle with radius 5µm, R' around 4.75µm and m=114, the approximated resonant wavelength is 412.07 nm which almost matches the resonant wavelength 415.633nm obtained from FDTD simulation. The mismatch between these two wavelengths arise due to the effect of refractive index in the vicinity of the resonator which is water in this case [56].
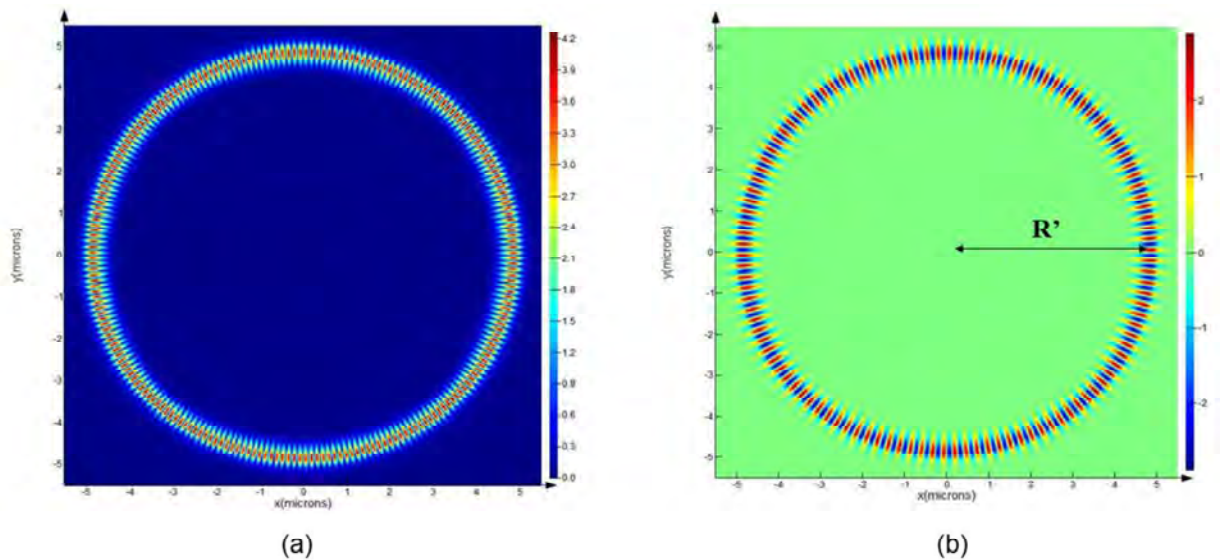
Figure 4-62: (a) Electric Field magnitude and (b) Ez profile of PS monosphere submerged in water (1.33). Particle radius, r=5µm. Resonant Wavelength: 415.633nm. Polarization type: TM. R' is the effective radius: the distance from center to the point of formation of WGM.

For closely spaced resonant peaks at 415.633nm, 419.126nm and 433.748nm, all three Electric field profile exhibiting WGM resonances are plotted in Figure 4-63. So, for PS-water combination TM polarized electric dipole source can excite high-Q WGM resonance along the circular periphery of the solid microparticle. However, TE polarized point source, i.e., magnetic dipole source is not good enough to induce such WGM in a solid PS microparticle with water as background medium.
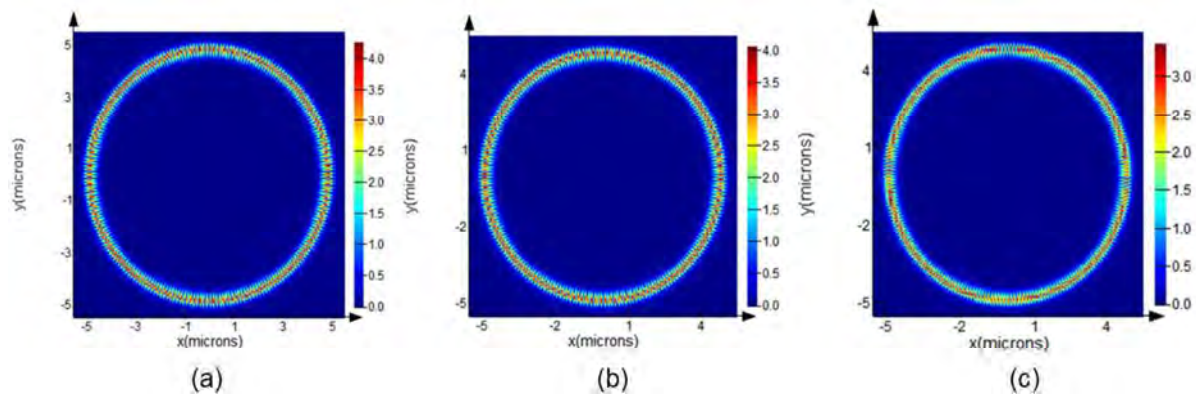
Figure 4-63: Electric Field Magnitude of a single PS microsphere in water medium. Particle diameter: 10μm. Illumination wavelength: (a) 415.633nm (b) 433.748nm (c) 419.126nm. Polarization type: TM.

A layer of uniform PS microparticles if self-assemble into a circular shape, looks like the one shown in Figure 4-64. To compare multisphere based structures with single solid microparticle a circular array of PS microspheres is considered to be in touching condition so that the diameter of the whole rotationally symmetric structure is also 10μm, same as the solid monosphere considered above.
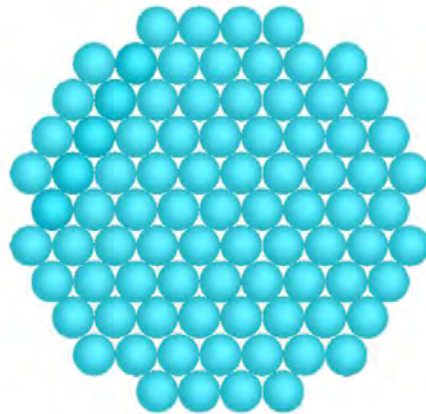
Figure 4-64: Rotationally symmetric structure of PS microspheres. Particle diameter: 1μm. The diameter of the whole circular structure ≈10μm.

The morphology dependence of WGMs inhibits the formation of such resonant modes in multispherical rotationally symmetric structures. The 10μm multi-sphere structure fails to show strong WGMs when illuminated either by electric or magnetic dipole source. The results are displayed in Figure 4-65 where it is observed that the WGMs leak out into the surrounding region when illuminated

by the same resonant wavelength that yields well-structured WGMs for a solid microsphere. The field magnitude also goes much lower even by fourth order for this multisphere model as evident from Figure 4-65.

Next WGM resonance is checked in a much larger solid microsphere with diameter 20μm. Under the same coupling method at around 403.638nm, a single PS sphere displays WGM when excited by the same electric point dipole (TM mode) placed at the center of the PS microparticle. Figure 4-66 displays the WGM resonance profile for such a monosphere. This large solid sphere yields a Q factor of around 91224.23 which is comparatively much higher than the ones reported in literature for such smaller resonators (below 20μm in diameter) in liquids [56].
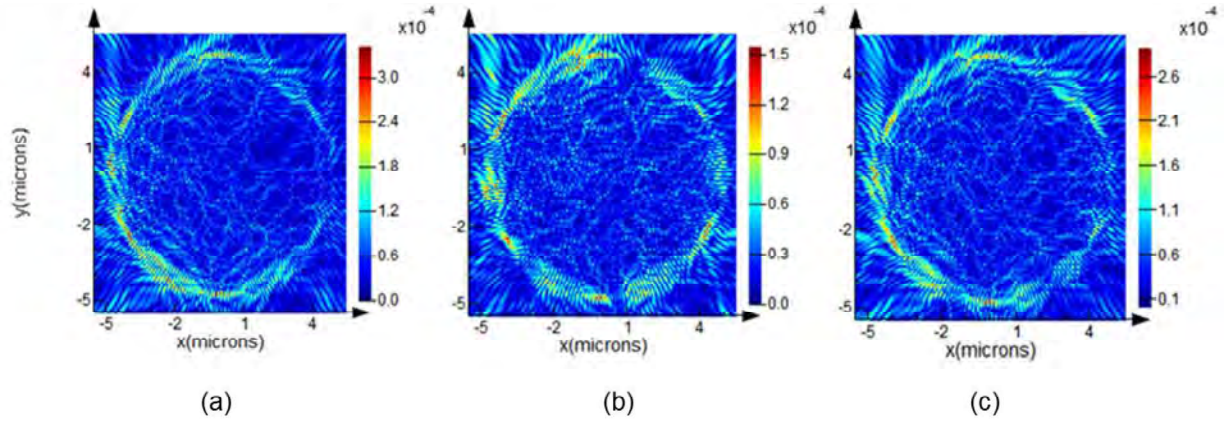
Figure 4-65: Electric Field Magnitude of microsphere based rotationally symmetric structure. Particle diameter: 1μm. The diameter of the whole circular structure≈10μm. Illumination wavelength: (a) 415.633nm (b) 433.748nm (c) 419.126nm. Polarization type TM.
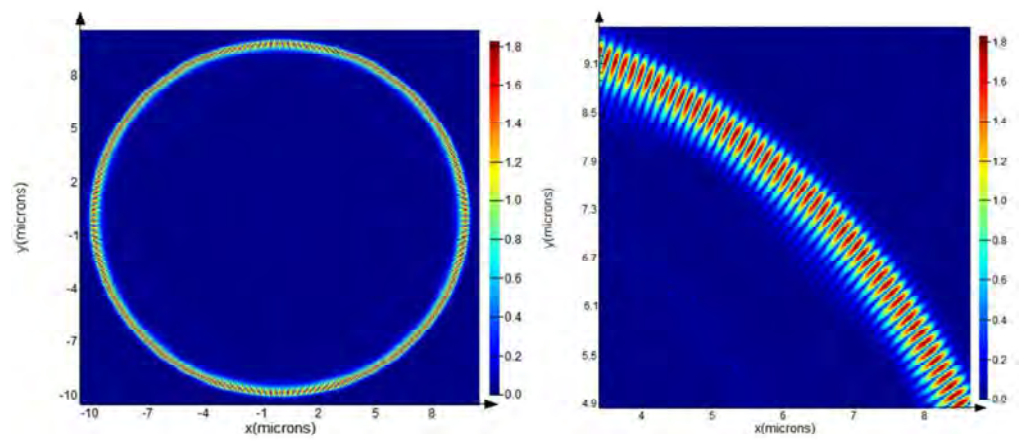
Figure 4-66: Electric Field profile of PS microsphere submerged in water (1.33). Particle radius, r=10μm. Resonant Wavelength: 403.638nm. Polarization type: TM.

In a similar manner another 20μm multisphere structure is investigated where the 1μm PS microspheres are assembled with a=1μm. Both of these PS models are displayed in Figure 4-67.

Like the 10μm multisphere structure, this 20μm multiparticle circular model also fails to show any strong confinement of EM waves along its periphery. In Figure 4-68 for TM polarized case the electric field profile is presented for 403.638nm illumination, where no WGM resonance is observed.

(a)   (b)
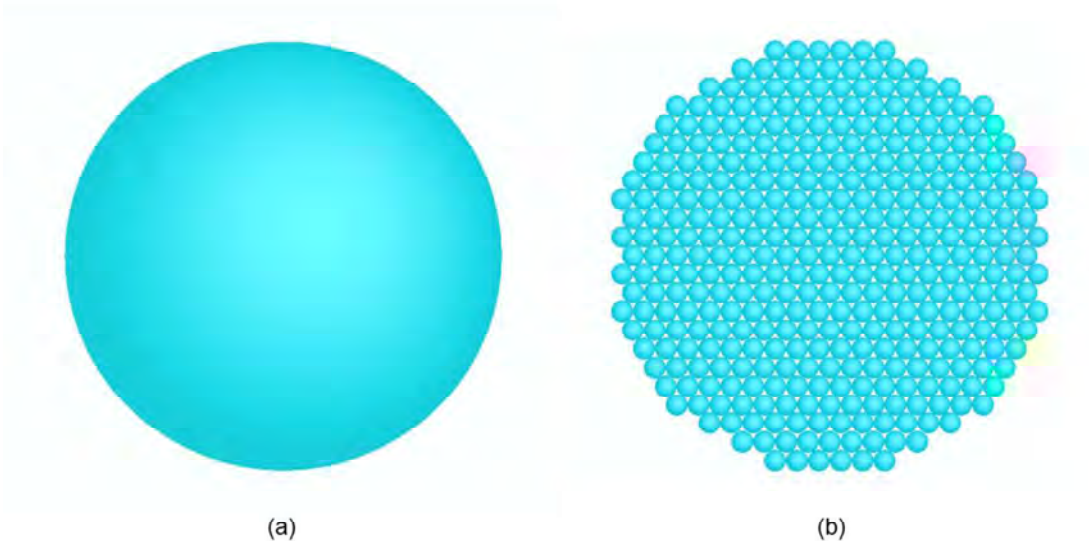
Figure 4-67: (a) A solid PS microsphere with diameter = 20μm (b) Rotationally symmetric structure of PS microspheres; Particle diameter: 1μm; The diameter of the whole circular structure ≈20μm.
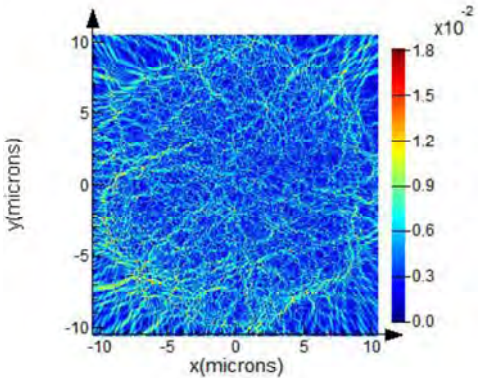
Figure 4-68: Electric Field Magnitude of multiple microsphere based rotationally symmetric structure submerged in water medium(n_m=1.33). Illumination Wavelength: 403.638nm. Particle diameter: 1μm. The diameter of the whole circular structure ≈20μm. Polarization type: TM. Interparticle spacing, a: 1μm.

The resonant characteristics of this 20μm multi-sphere PS structure shows very weak WGM at higher wavelengths as shown in Figure 4-71. The Quality factor, Q also degrades because of their low

confinement capability and leaky nature. Figure 4-69 displays the field profiles corresponding to its three different resonant modes: (a) 604.345nm (b) 1.14637μm (c) 2.45643μm when coupled by electric dipole point source.

Figure 4-69:Electric Field Magnitude of microsphere based rotationally symmetric structure submerged in water medium. Particle diameter: 1μm. The diameter of the whole circular structure ≈20μm. Illumination wavelength: (a) 604.345nm (b) 1.14637μm (c) 2.45643μm. Polarization type: TM. Interparticle spacing, a=1μm.

Changing the coupling source from electric to magnetic dipole (TE), no significant improvement is obtained in the resonant characteristics for this PS-water combination. Figure 4-70 shows weak WGM profiles with low Q at three different resonant modes of this 20μm multisphere structure under TE polarized condition.

Figure 4-70: Electric Field Magnitude of microsphere based rotationally symmetric structure submerged in water medium(n_m=1.33). Particle diameter: 1μm. The diameter of the whole circular structure ≈20μm. Illumination wavelength: (a)629.928nm (b)994.603nm (c)1268.23nm. Polarization type: TE. Interparticle spacing, a=1μm.

Figure 4-71: Quality Factor as a function of Resonant Wavelength. The blue and red symbols represent TM and TE modes respectively. Here, n_p=1.574, n_m=1.33 and a=1μm.

A comparative picture of the Q-factors of the all four structures discussed in this regard is presented Figure 4-71. In this plot all the Q factors corresponding to the resonant modes displayed in the previous pictures are recorded for both solid and multi-sphere based PS models submerged in water medium. So in water medium for solid single PS microspheres, WGM resonances yield a Q-factor which is higher than the ones obtained from multisphere structure by a factor of 3.
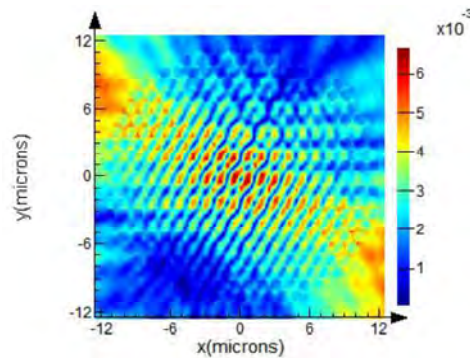
Figure 4-72: Electric Field Magnitude of microsphere based rotationally symmetric structure submerged in water medium(n_m=1.33). Particle diameter: 1μm. The diameter of the whole circular structure ≈24μm. Illumination wavelength: 2.96121 μm. Polarization type: TE. Interparticle spacing, a=1.2μm.

So water is not a good background medium to obtain high-Q WGMs from PS multisphere model. Even for increasing the interparticle spacing from 1μm to 1.2μm does not show any improvement in this case. Figure 4-72 shows the Electric field profile of the PS multisphere structure with a=1.2μm. This is a resonant mode for this structure when submerged in water medium but this mode doesn't result in WGM resonance.

4.3.3   Different Background Medium and WGM Resonance
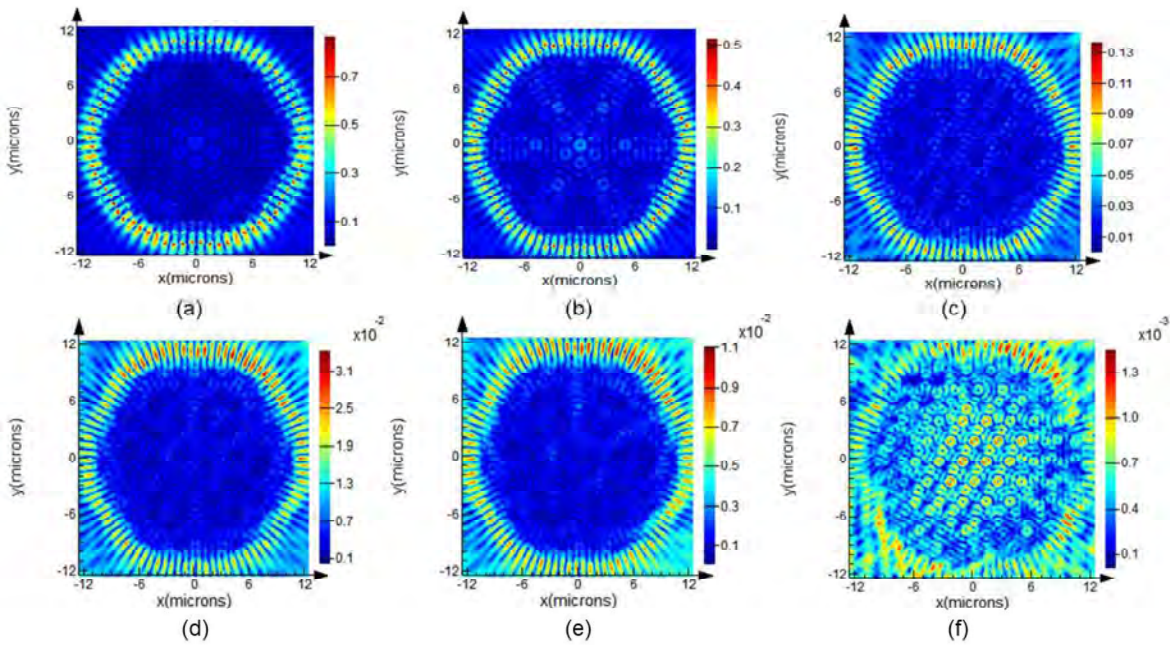
Figure 4-73: Electric Field Profile of multisphere rotationally symmetric structure for different background Medium. The diameter of the whole circular structure ≈24μm. n_p=1.574. Polarization type: TE. Illumination wavelength(λ_R) and background medium refractive index (n_m): (a) 2.42396μm for n_m=1 (b) 2.20999μm for n_m=1.1 (c)2.207704 for n_m=1.2 (d)2.11956μm for n_m=1.25 (e) 2.1432μm for n_m=1.28 (f)2.961μm for n_m=1.33.

In this section the WGM profiles are investigated for different background medium. According to this investigation, it is observed that when n_m >1.28, no WGM resonance can be obtained for a multisphere PS structure. Figure 4-73 illustrates this fact where WGM profiles are plotted for different background medium. It is evident from these figure that for decreasing the contrast between n_m and n_p, i.e., Δn, at resonance mode the magnitude of the Electric field as well as the strength of WGM becomes weaker. In Figure 4-73(a), for air medium (n_m=1) the electric field magnitude is the highest and also the

confinement is better. As the value of n_m is gradually increased from 1, the magnitude goes lower and in Figure 4-73(f) for $n_m=1.33$, the WGM profile vanishes completely.
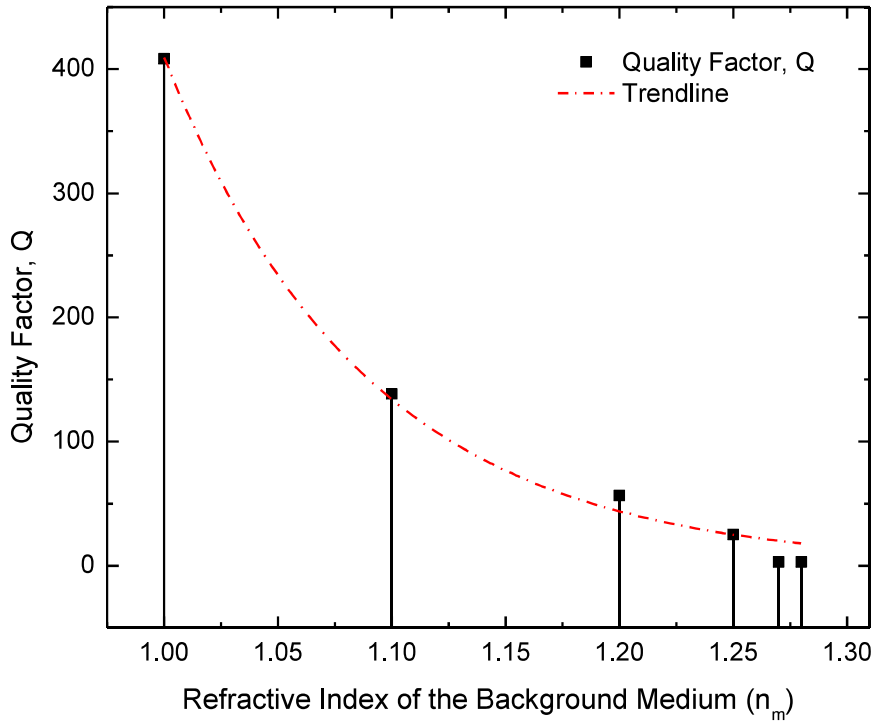
Figure 4-74: Quality Factor as a Function of the refractive index of the background medium. Interparticle Spacing, a=1.2μm. Particle refractive index, n_p=1.574. The Black symbols denote the Q factor and the red dotted curve shows the exponential trend.

The Quality factor corresponding to the resonant wavelengths mentioned in Figure 4-73 are computed and from Figure 4-74 it is observed that for increasing n_m, the downward trend is also applicable for "Q". The red trend line shows an exponential decay of the Quality factor for increasing n_m for this multisphere 24μm PS circular model. So to obtain WGM with the minimum "Q" Δn needs to be at least $\approx$0.241. And the highest Q is obtained when $n_m=1$.

4.3.4   Polystyrene WGM microresonator in Air Medium

Rarefied media like air offers better confinement of whispering gallery modes due to less damping and the high optical index contrast between the microsphere and the background medium [43]. In this section the multisphere PS WGM resonators placed in air medium are analyzed.

(a)   (b)   (c)
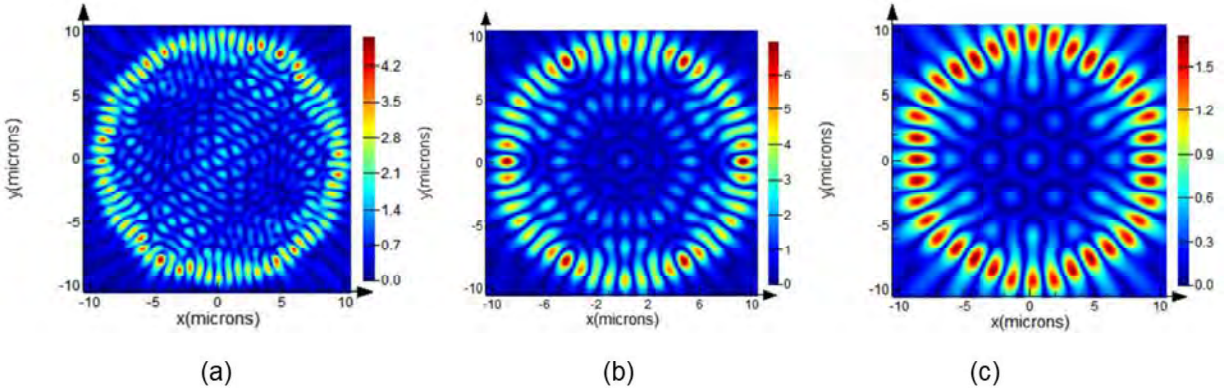
Figure 4-75:Electric Field Magnitude of microsphere based rotationally symmetric structure in air (n_m=1). Particle diameter: 1μm. Structure diameter ≈20μm. Illumination wavelength: (a)2.27903μm (b) 3.41752μm (c) 4.42102μm. Polarization type: TM. Interparticle spacing, a=1μm.

Figure 4-75 accumulates the Electric Field profile of ≈20μm circular structure for TM polarized point source when the microparticles are in touching condition. At around 3.41752μm, the electric field profile shows higher magnitude than the other two plotted in Figure 4-75. A similar comparison is presented in Figure 4-76 for TE polarized light source.

(a)   (b)   (c)
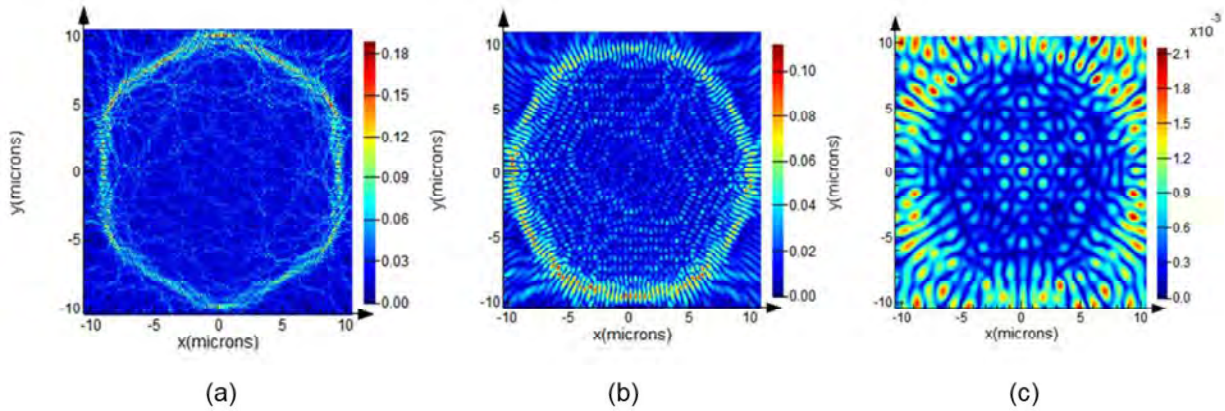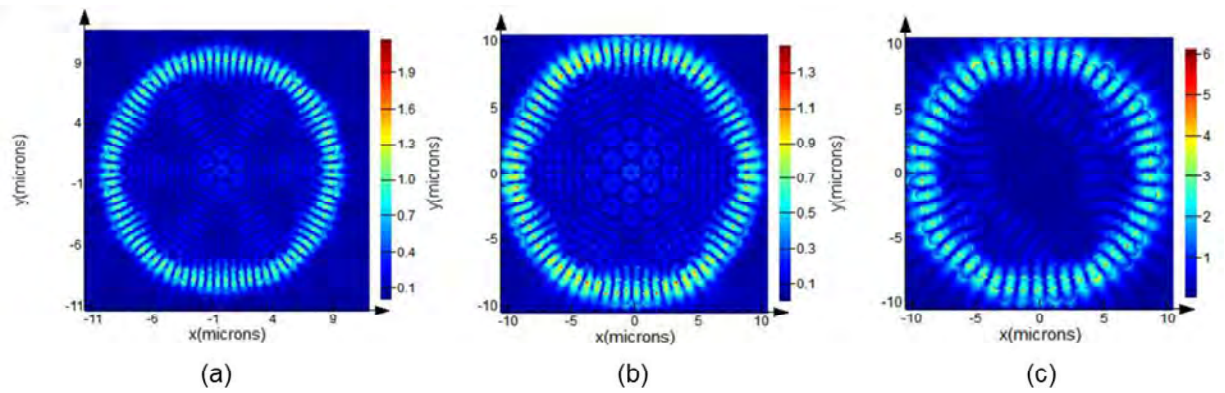
Figure 4-76: Electric Field Magnitude of microsphere based rotationally symmetric structure in air (n_m=1). Particle diameter: 1μm. Structure diameter ≈20μm. Illumination wavelength: (a)1.97509μm (b) 2.27338μm (c) 4.29221μm. Polarization type: TE. Interparticle spacing, a=1μm.
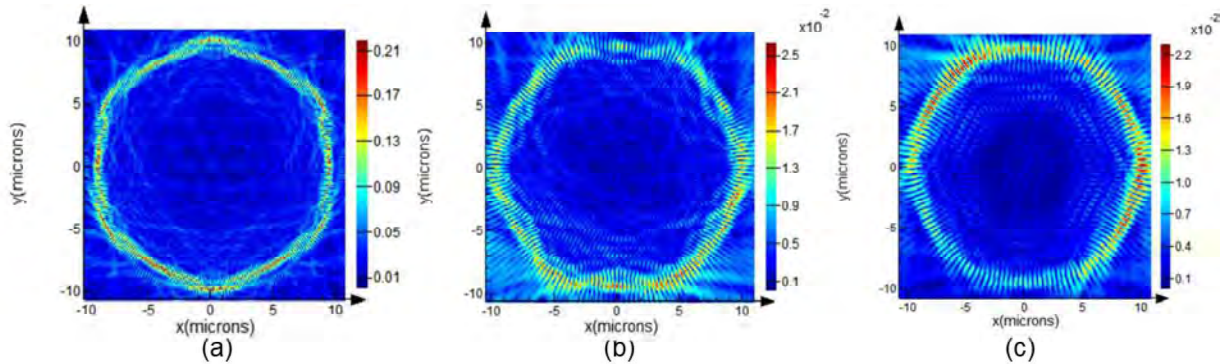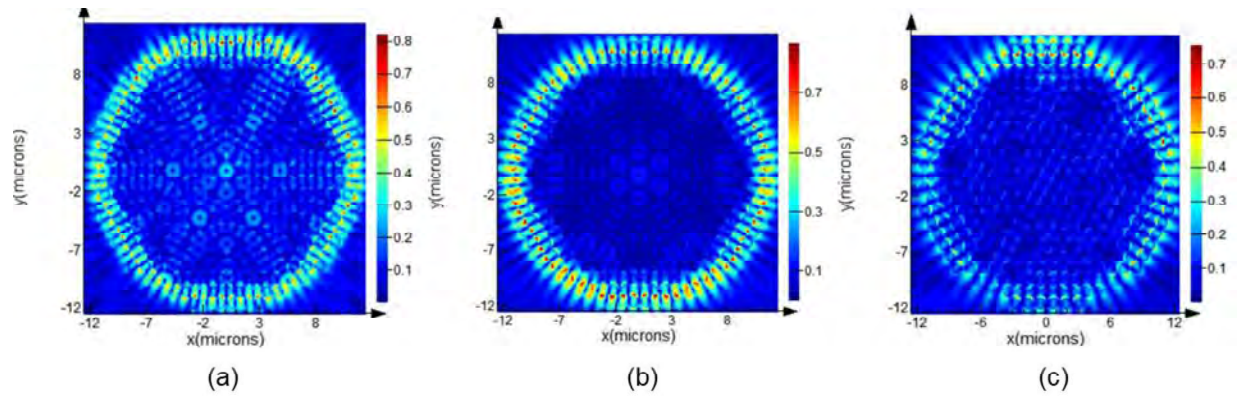
Figure 4-77:Electric Field Magnitude of microsphere based rotationally symmetric structure in air (n_m=1). Particle diameter: 1μm. Structure diameter ≈24μm. Illumination wavelength: (a)2.11938μm (b) 2.42396μm (c) 2.88629μm. Polarization type: TE. a=1.2μm.
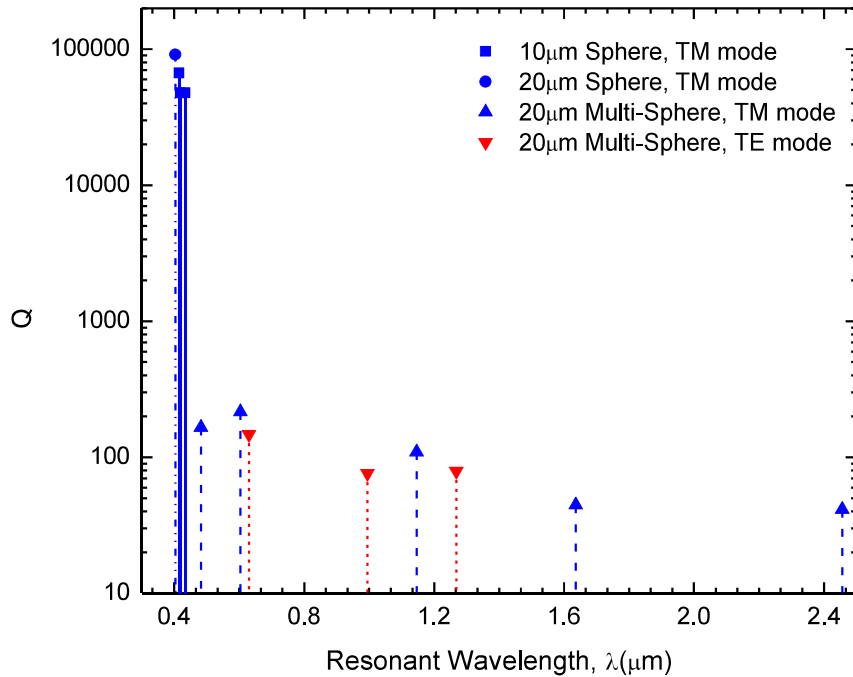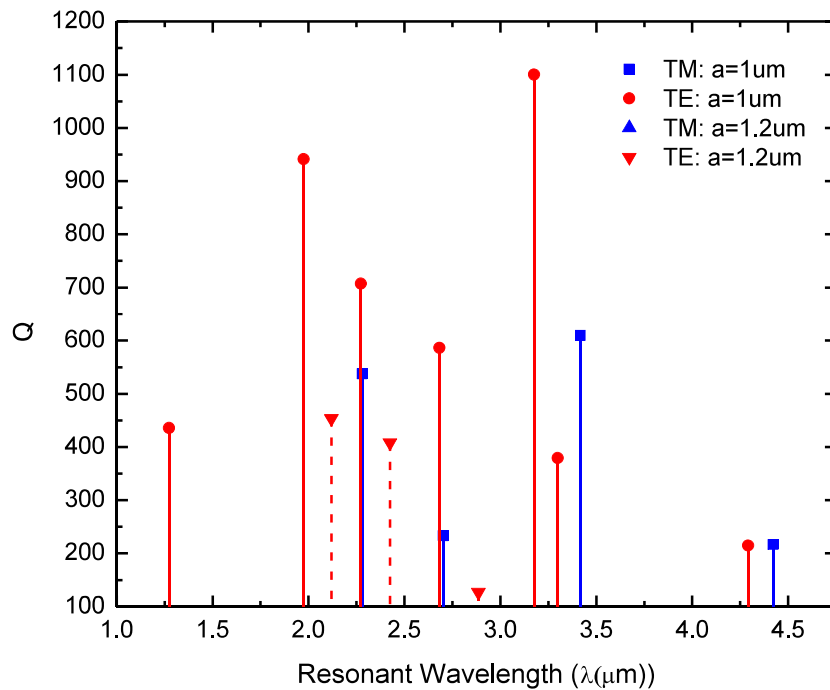

Figure 4-78: Quality Factor as a function of Resonant Wavelength. The blue and red symbols represent TM and TE modes respectively. Here, n_p=1.574, n_m=1 and a=1μm. The Q factors are plotted for multisphere model.

Figure 4-77 shows the field profile when the microparticles in the rotationally symmetric structure are maintaining an interparticle gap of 1.2μm and excited by a magnetic dipole (TE) source. For TM mode this value of a does not yield any WGM resonance condition. For PS-air combination the highest Q

factor ≈1100 is obtained for a=1μm, i.e., when the fill factor is the highest for this multisphere structure. For increasing "a" to 1.2μm the computed Q factors are comparatively lower. So in order to excite a WGM mode in air medium with Q factor on the order of 10^3, the particles need to form a close packed structure with minimum interparticle gap and must be coupled with magnetic dipole (TE polarized) point source.

4.3.5 Optical Force Tuned Rotationally Symmetric Structure

In order to analyze the optical forces acting on systems of rotationally symmetric dielectric microparticles like PS, the hexagonal lattice is illuminated by 980nm wavelength of light exerted by the dual Gaussian Beam. In water medium, this rotationally symmetric dielectric structure can assume different stable structures in presence of optical force.
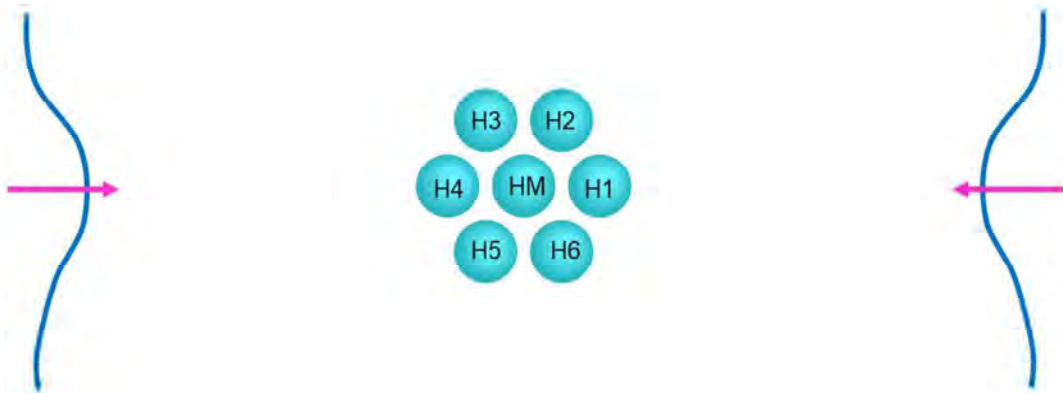
Figure 4-79: Hexagonal Lattice Placed in dual Gaussian Beam. The center particle is marked as HM, The other 6 particles are marked in a counterclockwise manner: H1, H2, H3, H4, H5and H6. Here, n_m:1.33. Illumination Wavelength: 980nm.

The interparticle separation, i.e., the hexagonal unit cell lattice constant, a is varied from 1.2 to 4.8μm. The resulted curves of optical force containing the Fx and Fy components are presented in Figure 4-80 and 4-81. Based on the zero crossing points of Fx and Fy, the stable x coordinates are approximated as a_x for H1 and H4, as $a_x/2$ H2, H3, H5, H6 and the y positions are estimated as $\sqrt{3}/2a_y$, where a_x is where Fx=0 and a_y is where Fy=0. In both cases the negative slopes are used to approximate the stable positions. To further illustrate their force dynamics, the direction of particles due to the presence of light force are plotted in Figure 4-82.
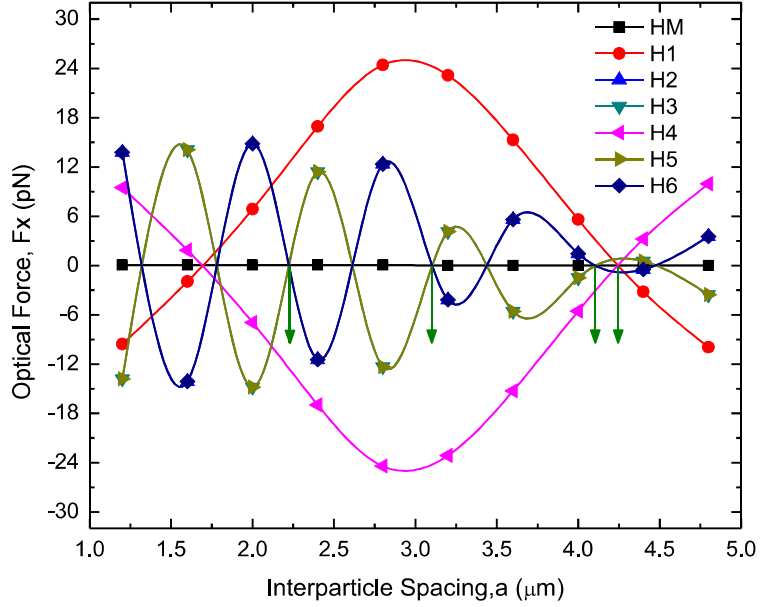
Figure 4-80: X component of Optical Force, Fx on the particles (HM, H1,.......,H6) in a hexagonal lattice in water medium. Illumination wavelength: 980nm. The green arrows represent the stable a_x coordinates.
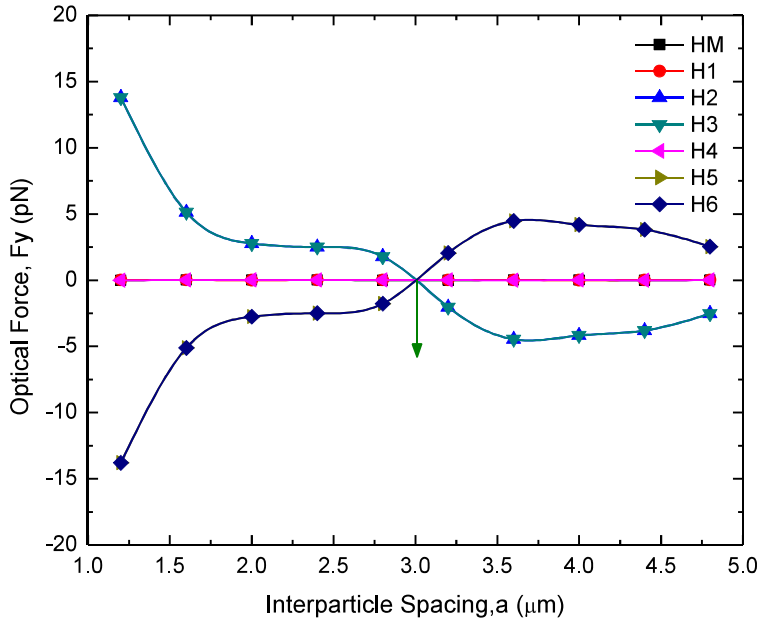
Figure 4-81: Y component of Optical Force, Fy on the particles (HM, H1,.......,H6) in a hexagonal lattice in water medium. Illumination wavelength: 980nm. The green arrows represent the stable a_y coordinates.
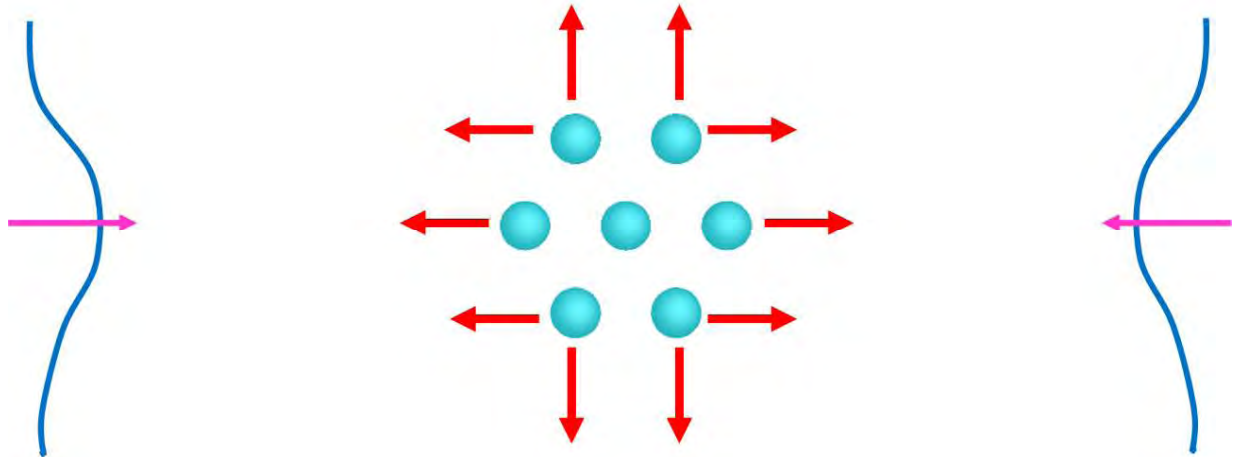
Figure 4-82: The direction of Particle Movement in Dual Gaussian Beam System. The red arrows point to the direction of particles in presence of light force.

For the hexagonal array, from dual Gaussian beam illumination, three different possible stable configurations are obtained as shown in Figure 4-83. Among these three, the one in (c) resembles the hexagonal structure more than the other two.
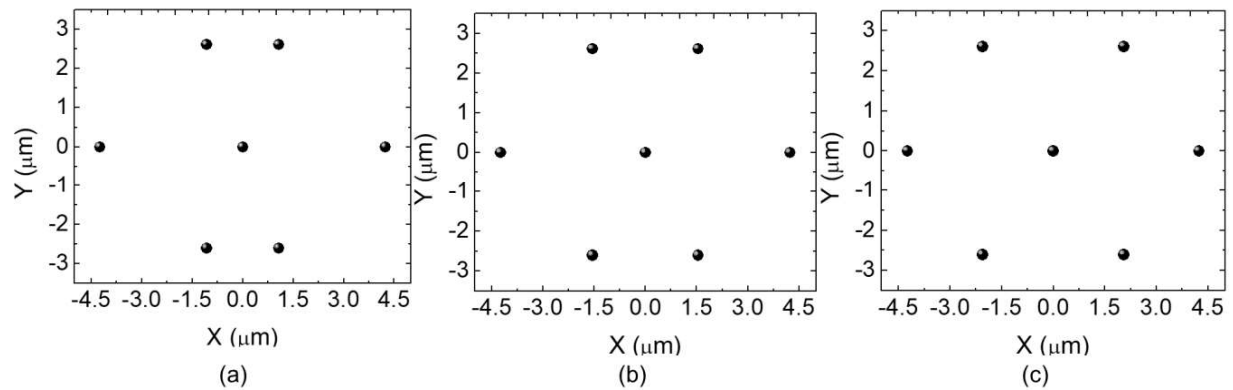
Figure 4-83: Three possible stable configurations of hexagonal lattice after applying optical force. Here, n_m =1.33.

Since the force computation is performed on the hexagonal unit cell, when optical force is applied to the multi-sphere model due to their rotational symmetry it should look somewhat like the one in Figure 4-84.
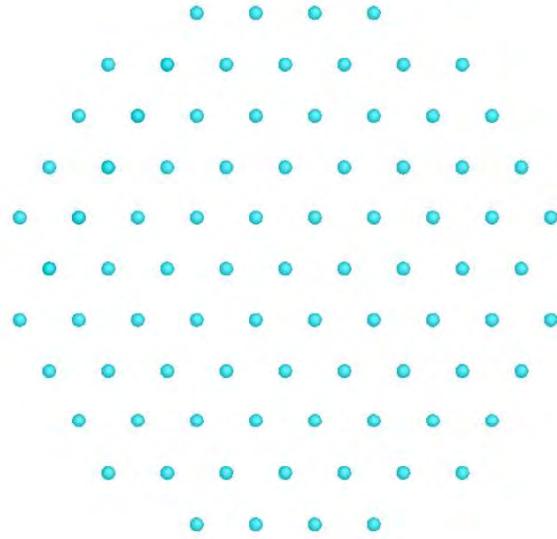
Figure 4-84: Extended Version of the force tuned stable configuration of Figure 4-83(c). Here, n_m=1.33.

When excited either by a point electric dipole or a magnetic dipole source, no Whispering Gallery resonance mode is obtained from this extended model. Two resonant modes of this force tuned stable extended structure are shown in Figure 4-85.

(a)

(b)
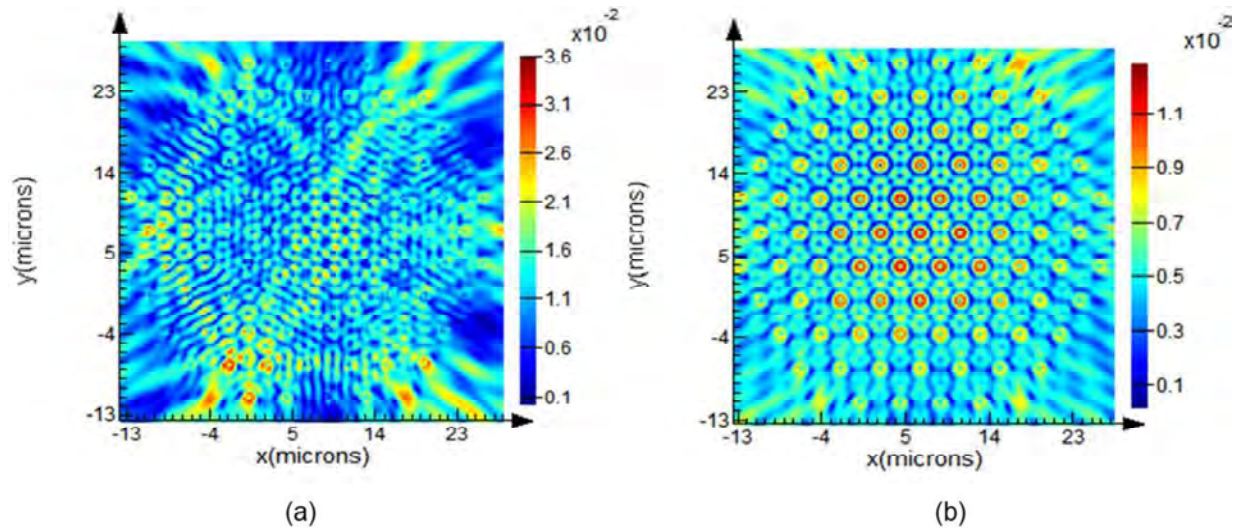
Figure 4-85: The resonant mode of the optical force tuned extended stable configuration submerged in water medium. The resonant wavelength λ_R: (a)2.147μm (b) 2.293μm. Polarization type: TE.

nce air medium yields the highest Q factor for WGM profile with a=1μm, the effect of force on the hexagonal lattice is also analyzed when placed in air medium. But the microparticles cannot be stabilized in air medium. So they are suspended on water with air as its background and optical force is exerted using dual Gaussian beam system. The configuration used for this case is shown in Figure 4-86.
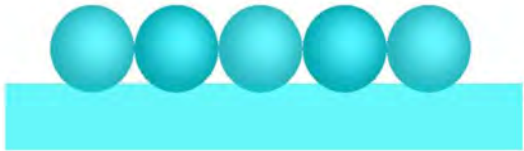
Figure 4-86: PS hexagonal lattice suspended on water and trapped in air (side view). Particle radius: 0.5μm.

For illuminating with 980nm wavelength, the computed force acting along x and y direction are plotted in Figure 4-87 and 4-88.
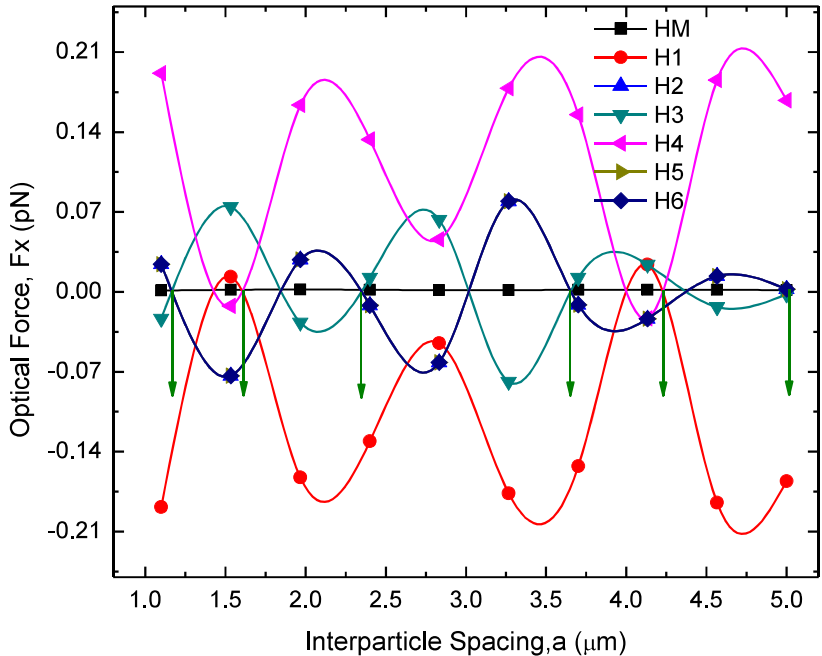
Figure 4-87: X component of Optical Force, F_x on the particles (HM, H1,......,H6) in a hexagonal lattice in water medium. Illumination wavelength: 980nm. The green arrows represent the stable a_x coordinates.

The stable configurations are estimated following the same procedure stated for water submerged PS microspheres. Within the range of "a" between 1 to 5µm, several possible stable structures can result from the exertion of optical force, among all possible configurations three cases are displayed in Figure 4-89.
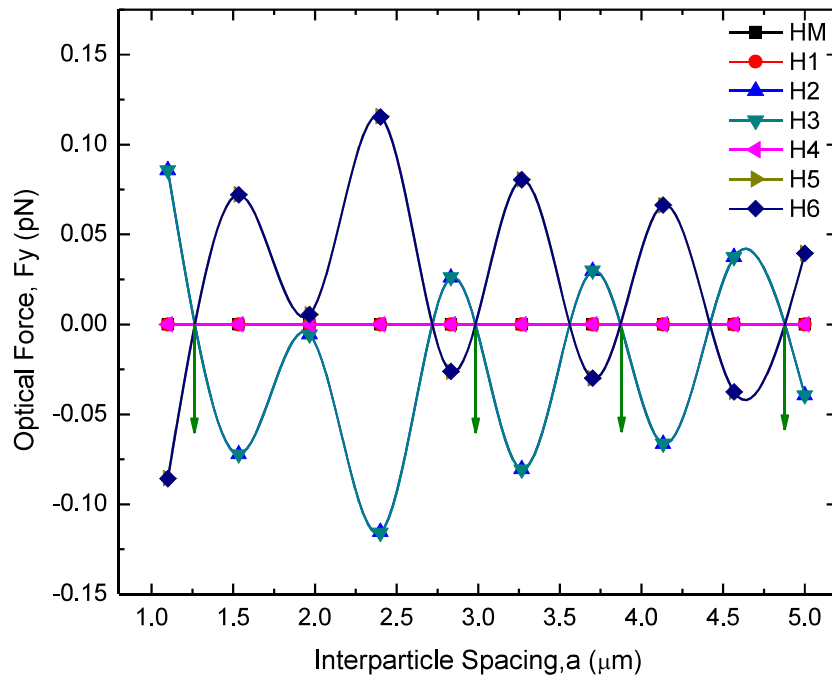
Figure 4-88: Y component of Optical Force, Fy on the particles (HM, H1,......,H6) in a hexagonal lattice in water medium. Illumination wavelength: 980nm. The green arrows represent the stable a_y coordinates.

(a)   (b)   (c)
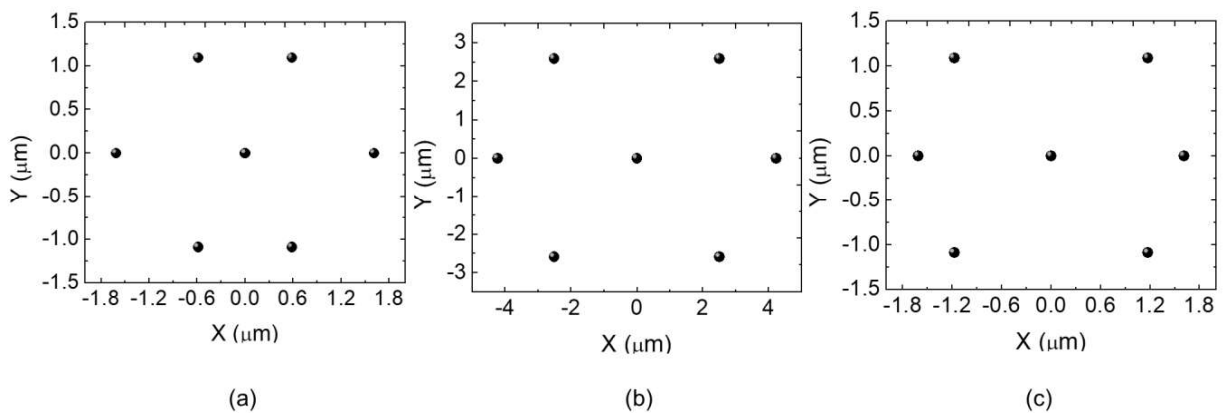
Figure 4-89: Three possible stable configurations of hexagonal lattice after applying optical force. Here, $n_m = 1$ and particles are suspended on water.

The reason behind choosing these three possible reconfigured structures is their similarity with hexagonal lattice. In a similar manner the WGM mode is searched for within the extended version of these structures. Among all three, the expansion of the stable configuration of Figure 4-89(b) results in a similar formation as in Figure 4-84.
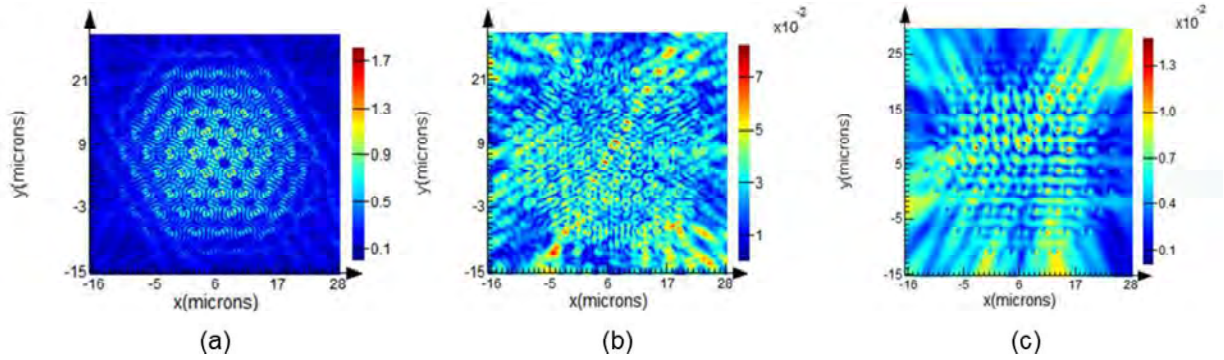
Figure 4-90: Electric Field Profile of the resonant modes of the extended stable structure after applying optical force. Particles are suspended on water. Here, $a \approx 4.23 \mu m$ and $n_m=1$. The resonant wavelength, λ_R:(a)1.449μm, (b) 2.141μm, (c) 3.1958μm. Polarization type: TE.

Now the resonant characteristics of this expanded structure is investigated and no WGM mode is obtained. For TE polarized case, three different resonant modes are plotted in Figure 4-90. But any of these resonant modes denotes WGM resonance. Similar phenomenon occurs for TM polarized point source.

A comparative picture of the resonant characteristics before and after illumination using dual Gaussian beam is presented in terms of Q factor in Figure 4-91. According to this representation, Q factor becomes very low for the optical force induced multi-sphere structure. Before illumination, the self-assembled rotationally symmetric multisphere structure provides a Q factor around 1100 for the highest percentage of fill factor but as an outcome of the photoinduced reconfiguration Q becomes lower than 100. The larger interparticle spacing, i.e., decrease in the percentage of fill factor due to the effect of optical force results in such low Q. Since no WGM modes also result from the resonant modes of the force induced stable structure, the quality factor degrades too.
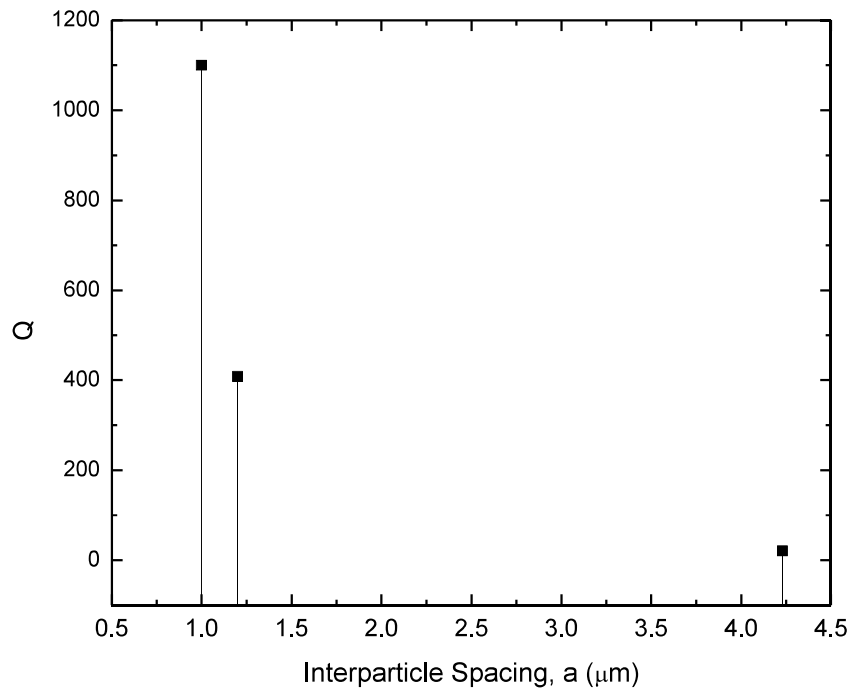
Figure 4-91: Q factor as a function of interparticle Spacing. In all three cases the multisphere structure is in air medium and suspended on water. The rightmost value is obtained from the optical force tuned reconfiguration.

Analyzing all these results for both water and air medium, it can be concluded that photoinduced force is capable of changing the configuration of a hexagonal close-packed structure consisting of dielectric PS microspheres. To change the interparticle gap of a rotationally symmetric multisphere structure, illumination of a certain wavelength can result in different possible stable configuration depending on the medium where it is placed. At the same time, the application of force reconfigures the resonant behavior of such structures as well as reconfigures their periodicity.

CHAPTER 5

SUMMARY, CONCLUSION AND SUGGESTIONS FOR FUTURE WORKS

5.1   Summary of Present Work

In this work one and two dimensional periodic polystyrene photonic crystals (PC) and whispering gallery mode (WGM) resonators are designed and counter propagating light field induced reconfiguration process is investigated for all these configurations. Three dimensional optical force exerted by the dual Gaussian beam system of monochromatic illumination is computed using Maxwell stress Tensor computed from the FDTD modeling of Maxwell's Equations. The effect of optical force on the periodicity of 1D, 2D and rotationally symmetric hexagonal structures is studied along with a comparative analysis of their resonant characteristics before and after the application of photo induced force.

Starting with a single microsphere, the possible displacement of water submerged 1μm Polystyrene(PS) particles of a 1D N particle array is estimated from the analysis of resulting forces exerted by the monochromatic counter propagating beams. Monochromatic illumination of 980nm wavelength with an intensity of 127.6mW/μm^2 yields inhomogeneous equilibrium spacing of particles and this inhomogeneity arises from the interplay of incident light beam and the dielectric particles. For an optically bound 1D structure, there is no unique stable configuration obtained rather multiple possible equilibrium arrays can result into for any number of microspheres present in the system. For left and right handed PS microspheres, the optical force patterns are mirror symmetric with respect to the particle at the center. Irrespective of the total number of particles in a 1D array, all possible stable positions remain same for a particular constituent but change for the others depending on their position from the center and also from the source. The inhomogeneous spacing of particles remain identical even after varying the illumination intensity from 1 to 10^{4}mW/μm^2. Under 980nm dual beam illumination, Increase of intensity only alters the magnitude of the exerted optical force in a linear manner while replacement of water with a different background medium results in different stable but still aperiodic configurations. Another important parameter that can contribute to the reconfiguration process as well as variation in interparticle separation is the incident wavelength from the dual

Gaussian beam. For changing the incident wavelength as a multiple of 980nm, an almost sinusoidal modulation is observed both in the mean stable spacing and the standard deviation of the microspheres from their mean equilibrium position. To further exploit this parameter for periodic reconfiguration, a relationship between the resonant wavelength of a periodic 1D PS array and the illumination wavelength required to maintain that periodic spatial configuration is established. Following this particular relation, the periodicity along with the resonant behavior of a 1D array can be periodically tuned by tuning the illumination wavelength while maintaining periodic interparticle spacing. To illustrate the resonant nature of 1D PS microarrays before and after illumination, their band structures are explored as well as corresponding transmission characteristics are studied to compare. These investigations are repeated for 2D square lattice periodic configurations. Unlike 1D array of water surrounded PS microparticles, no complete band gap is found in 2D structures but a dip in transmittance curve is observed between 2 to 3μm plane wave illumination. The application of optical force weakens and shifts the dip as well as decreases their quality factor. Besides this, the frequency domain analysis of optical force on three different square array: 3x3, 5x5 and 7x7 shows a predictable deformation pattern of their square shape and formation of a slightly rectangular configuration. In the last section the rotationally symmetric hexagonal lattice structures of PS microspheres are studied. A single polystyrene microsphere displays high-Q WGM resonance in water medium but this mode weakens and even vanishes for multisphere PS circularly symmetric configuration as an outcome of the decrease in the percentage of fill factor. In a water submerged 20μm solid single PS microsphere, WGM resonance yields a Q-factor of 91224.23 which is higher than the ones obtained from multisphere structure by 3 orders in magnitude. The quality factor improves for replacing the background medium with much lower refractive index than water and for increasing the refractive index contrast an exponential rise is obtained. The highest Q is obtained for placing multisphere PS structure in air with an interparticle spacing of 1μm. Next the effect of dual beam induced optical force on a hexagonal PS lattice is studied for cases when submerged in and suspended on water medium. Among the resulted multiple stable forms the ones resembling more with the hexagonal lattice are checked for whispering gallery resonant modes. For larger separation of microspheres in the rotationally symmetric optically bound multisphere structures, the quality factor goes down along with absence of WGM modes.

5.2 Conclusion

In conclusion, for reorganizing polymer microparticle based photonic structures in a tunable optical force bound environment, our design and analysis of optical force tuned photonic crystal and whispering gallery mode resonators can play a significant role. The possibility of reversibly change and recover the resonant characteristics of these photonic structures and the ease and versatility of the practical implementation of such systems are reflected in this research.

5.3   Suggestions for Future Work

There are numerous scopes of future work on the areas of this study. In fact, the convenience of such optical force tuned reconfiguration method can remove the long standing challenge in the design of PC and WGM resonators and also can pave the way for research in the following sectors:

- Because of limited resource and opportunity to validate this optical forcr based reconfiguration technique, practical implementation of this method was not possible in this research. So, in future optical manipulation of the resonance behavior of a photonic crystal can be investigated and verified via practical experiment provided that there are enough available resources. Practical implementation of this method can contribute to reconfigure large photonic structures avoiding the hassles of re-fabricating the whole structure.

- The Relationship between the resonant condition and optical binding force in reconfigurable PC and WGM resonators can be checked for other dielectrics and also for plasmonic particles of different shapes and sizes. The effect of temperature can also be studied for such reconfiguration method.

- The dual beam Gaussian trap can be practically investigated to study the efficiency of optically trapping large number of microparticles. Depending on such experiments, the reconfiguration of microsphere based large PCs and WGMs can be implemented. The beam parameters can be explored too to tune the reconfiguration process.

- The reconfiguration method described in this work can be extended to explore three dimensional (3D) PC and WGM resonators. For efficient trapping in three dimension research on required beam shape and surrounding environment can be carried on.

- Based on the study of the effect of background medium in photoinduced reconfiguration as well as in resonant characteristics of two different photonic structures, different liquid and gaseous medium can be experimented on to obtain desired reconfigurations.

- Since optical force is capable of tuning the resonant behavior as well as the Quality factor of the microparticle based photonic structures, it can be implemented to design gain medium which can be further extended for lasing applications. The aperiodic reconfiguration via optical force can be further explored to apply it in design of random lasers.

- The dependence of quality factor as well the resonant behavior on the interparticle gap of the microspheres and the medium surrounding them can be exploited in detection and novel sensing schemes. The relationship between quality factor and the refractive index contrast can be implemented to design refractive index sensor consisting rotationally symmetric dielectric microspheres.

Apart from developing a comprehensive understanding of the optical force induced tunability of PS microparticle based PC and WGMs, our work can contribute to shed light on the necessity of the practical implementation of optical force tuned reconfiguration process as well as its further application in novel sensing, detection and lasing.

LIST OF REFERENCES

[1]   Joannopoulos, John D., Steven G. Johnson, Joshua N. Winn, and Robert D. Meade. "Molding the flow of light." *Princeton Univ. Press, Princeton, NJ [ua]* (2008).

[2]   Wait, James R. "Electromagnetic whispering gallery modes in a dielectric rod." *Radio science* 2, no. 9 (1967): 1005-1017.

[3]   Fan, Huibo, Xiaodong Gu, Dawei Zhou, Huili Fan, Li Fan, and Changquan Xia. "Confined whispering-gallery mode in silica double-toroid microcavities for optical sensing and trapping." *Optics Communications* 434 (2019): 97-103.

[4]   Wu, Darran KC, Boris T. Kuhlmey, and Benjamin J. Eggleton. "Ultrasensitive photonic crystal fiber refractive index sensor." *Optics letters* 34, no. 3 (2009): 322-324.

[5]   Vollmer, Frank, and Stephen Arnold. "Whispering-gallery-mode biosensing: label-free detection down to single molecules." *Nature methods* 5, no. 7 (2008): 591.

[6]   Ioppolo, Tindaro, Michael Kozhevnikov, Vadim Stepaniuk, M. Volkan Ötügen, and Valery Sheverev. "Micro-optical force sensor concept based on whispering gallery mode resonators." *Applied optics* 47, no. 16 (2008): 3009-3014.

[7]   Tao, Yi Chen, Xue Dong Wang, and Liang Sheng Liao. "Active whispering-gallery-mode optical microcavity based on self-assembled organic microspheres." *Journal of Materials Chemistry C* 7, no. 12 (2019): 3443-3446

[8]   Sukhoivanov, Igor A., and Igor V. Guryev. *Photonic crystals: physics and practical modeling*. Vol. 152. Springer, 2009.

[9]   Ellis, Bryan, Marie A. Mayer, Gary Shambat, Tomas Sarmiento, James Harris, Eugene E. Haller, and Jelena Vučković. "Ultralow-threshold electrically pumped quantum-dot photonic-crystal nanocavity laser." *Nature photonics* 5, no. 5 (2011): 297.

[10]   Sandoghdar, Vea, F. Treussart, J. Hare, V. Lefevre-Seguin, J-M. Raimond, and S. Haroche. "Very low threshold whispering-gallery-mode microsphere laser." *Physical review A* 54, no. 3 (1996): R1777.

[11]   Bayn, Igal, Boris Meyler, Alex Lahav, Joseph Salzman, Rafi Kalish, Barbara A. Fairchild, Steven Prawer et al. "Processing of photonic crystal nanocavity for quantum information in diamond." *Diamond and related materials* 20, no. 7 (2011): 937-943.

[12]   Li, Peng-Bo, Shao-Yan Gao, and Fu-Li Li. "Quantum-information transfer with nitrogen-vacancy centers coupled to a whispering-gallery microresonator." *Physical Review A* 83, no. 5 (2011): 054306.

[13]   Ghenuche, Petru, Hervé Rigneault, and Jérôme Wenger. "Hollow-core photonic crystal fiber probe for remote fluorescence sensing with single molecule sensitivity." *Optics express* 20, no. 27 (2012): 28379-28387.

[14]   Kotsina, Nikoleta, Federico Belli, Shou-fei Gao, Ying-ying Wang, Pu Wang, John C. Travers, and Dave Townsend. "Ultrafast molecular spectroscopy using a hollow-core photonic crystal fiber light source." *The journal of physical chemistry letters* 10, no. 4 (2019): 715-720.

[15]   Huckabay, Heath A., and Robert C. Dunn. "Whispering gallery mode imaging for the multiplexed detection of biomarkers." *Sensors and Actuators B: Chemical* 160, no. 1 (2011): 1262-1267.

[16]   Demésy, Guillaume, and Sajeev John. "Solar energy trapping with modulated silicon nanowire photonic crystals." *Journal of Applied Physics* 112, no. 7 (2012): 074326.

[17]   Cho, Hyunmin, Seungyong Han, Jinhyeong Kwon, Jinwook Jung, Hyun-Jong Kim, Hyunseok Kim, Hyeonjin Eom, Sukjoon Hong, and Seung Hwan Ko. "Self-assembled stretchable photonic crystal for a tunable color filter." *Optics letters* 43, no. 15 (2018): 3501-3504.

[18]   Erickson, David, Troy Rockwood, Teresa Emery, Axel Scherer, and Demetri Psaltis. "Nanofluidic tuning of photonic crystal circuits." *Optics letters* 31, no. 1 (2006): 59-61.

[19]   Soref, Richard. "Reconfigurable integrated optoelectronics." *advances in optoelectronics* 2011 (2011).

[20]   Wang, Benjamin, J. A. Rodríguez, and Mark A. Cappelli. "3D woodpile structure tunable plasma photonic crystal." *Plasma Sources Science and Technology* 28, no. 2 (2019): 02LT01

[21]   Deotare, Parag B., Irfan Bulu, Ian W. Frank, Qimin Quan, Yinan Zhang, Rob Ilic, and Marko Loncar. "All optical reconfiguration of optomechanical filters." *Nature Communications* 3 (2012): 846.

[22]   Fang, Yin, Yongliang Ni, Sin-Yen Leo, Curtis Taylor, Vito Basile, and Peng Jiang. "Reconfigurable photonic crystals enabled by pressure-responsive shape-memory polymers." *Nature communications* 6 (2015): 7416.

[23]   Schuller, Ch, F. Klopf, J. P. Reithmaier, M. Kamp, and A. Forchel. "Tunable photonic crystals fabricated in III-V semiconductor slab waveguides using infiltrated liquid crystals." *Applied Physics Letters* 82, no. 17 (2003): 2767-2769.

[24]   Ashkin, Arthur, James M. Dziedzic, J. E. Bjorkholm, and Steven Chu. "Observation of a single-beam gradient force optical trap for dielectric particles." *Optics letters* 11, no. 5 (1986): 288-290.

[25]   Tumkur, T. U., M. A. Hurier, M. D. Pichois, M. Vomir, B. Donnio, J. L. Gallani, and M. V. Rastei. "Photoinduced Atomic Force Spectroscopy and Imaging of Two-Dimensional Materials." *Physical Review Applied* 11, no. 4 (2019): 044066

[26]   Nowak, Derek, William Morrison, H. Kumar Wickramasinghe, Junghoon Jahng, Eric Potma, Lei Wan, Ricardo Ruiz et al. "Nanoscale chemical imaging by photoinduced force microscopy." *Science advances* 2, no. 3 (2016): e1501571.

[27]   Peirs, Jan, Joeri Clijnen, Dominiek Reynaerts, Hendrik Van Brussel, Paul Herijgers, Brecht Corteville, and Sarah Boone. "A micro optical force sensor for force feedback during minimally invasive robotic surgery." *Sensors and Actuators A: Physical* 115, no. 2-3 (2004): 447-455

[28]   Vasudevan, K., M. C. Divyasree, and K. Chandrasekharan. "Enhanced nonlinear optical properties of ZnS nanoparticles in 1D polymer photonic crystal cavity." *Optics & Laser Technology* 114 (2019): 35-39

[29]   Huang, Dali, Minxiang Zeng, Ling Wang, Lecheng Zhang, and Zhengdong Cheng. "Biomimetic colloidal photonic crystals by coassembly of polystyrene nanoparticles and graphene quantum dots." *RSC advances* 8, no. 61 (2018): 34839-34847.

[30]   Qiao, Pengfei, Weijian Yang, and Connie J. Chang-Hasnain. "Recent advances in high-contrast metastructures, metasurfaces, and photonic crystals." *Advances in Optics and Photonics* 10, no. 1 (2018): 180-245.

[31]   Yablonovitch, Eli. "Inhibited spontaneous emission in solid-state physics and electronics." *Physical review letters* 58, no. 20 (1987): 2059.

[32]   John, Sajeev. "Strong localization of photons in certain disordered dielectric superlattices." *Physical review letters* 58, no. 23 (1987): 2486.

[33]   Gorodetsky, Michael L., and Vladimir S. Ilchenko. "Optical microsphere resonators: optimal coupling to high-Q whispering-gallery modes." *JOSA B* 16, no. 1 (1999): 147-154.

[34]   Collot, Lefevreseguin, V. Lefevre-Seguin, M. Brune, J. M. Raimond, and S. Haroche. "Very high-Q whispering-gallery mode resonances observed on fused silica microspheres." *EPL (Europhysics Letters)* 23, no. 5 (1993): 327.

[35]   Kobayashi, Yumeki, Masaki Michihata, Zheng Zhao, Bohuai Chu, Kiyoshi Takamasu, and Satoru Takahashi. "Radial mode number identification on whispering gallery mode resonances for diameter measurement of microsphere." *Measurement Science and Technology* 30, no. 6 (2019): 065201.

[36]   Akahane, Yoshihiro, Takashi Asano, Bong-Shik Song, and Susumu Noda. "High-Q photonic nanocavity in a two-dimensional photonic crystal." *nature* 425, no. 6961 (2003): 944.

[37]   Srinivasan, Kartik, and Oskar Painter. "Momentum space design of high-Q photonic crystal optical cavities." *Optics Express* 10, no. 15 (2002): 670-684.

[38]   Sun, Lin, Haixin Lin, Kevin L. Kohlstedt, George C. Schatz, and Chad A. Mirkin. "Design principles for photonic crystals based on plasmonic nanoparticle superlattices." *Proceedings of the National Academy of Sciences* 115, no. 28 (2018): 7242-7247.

[39]   Xie, Bi-Ye, Guang-Xu Su, Hong-Fei Wang, Hai Su, Xiao-Peng Shen, Peng Zhan, Ming-Hui Lu, Zhen-Lin Wang, and Yan-Feng Chen. "Visualization of higher-order topological insulating phases in two-dimensional dielectric photonic crystals." *Physical Review Letters* 122, no. 23 (2019): 233903.

[40]   Ashkin, Arthur. "Acceleration and trapping of particles by radiation pressure." *Physical review letters* 24, no. 4 (1970): 156.

[41]   Singer, Wolfgang, Manfred Frick, Stefan Bernet, and Monika Ritsch-Marte. "Self-organized array of regularly spaced microbeads in a fiber-optical trap." *JOSA B* 20, no. 7 (2003): 1568-1574.

[42]   Metzger, N. K., K. Dholakia, and Ewan M. Wright. "Observation of bistability and hysteresis in optical binding of two dielectric spheres." *Physical review letters* 96, no. 6 (2006): 068102.

[43]   Guillon, Marc, Olivier Moine, and Brian Stout. "Longitudinal optical binding of high optical contrast microdroplets in air." *Physical review letters* 96, no. 14 (2006): 143902.

[44]   Kawano, M., J. T. Blakely, R. Gordon, and D. Sinton. "Theory of dielectric micro-sphere dynamics in a dual-beam optical trap." *Optics express* 16, no. 13 (2008): 9306-9317.

[45]   Renaut, C., J. Dellinger, Benoit Cluzel, T. Honegger, D. Peyrade, E. Picard, Frederique De Fornel, and E. Hadji. "Assembly of microparticles by optical trapping with a photonic crystal nanocavity." *Applied Physics Letters* 100, no. 10 (2012): 101103.

[46]   Cui, Liyong, Xiao Li, Jun Chen, Yongyin Cao, Guiqiang Du, and Jack Ng. "One-dimensional photonic crystals bound by light." *Physical Review A* 96, no. 2 (2017): 023833.

[47]   Shimada, Ryoko, Aya Imada, Takao Koda, Toru Fujimura, Keiichi Edamatsu, Tadashi Itoh, Kazuo Ohtaka, and Kenji Takeda. "Self-assembled polystyrene microparticle layers as two-dimensional photonic crystals." *Molecular Crystals and Liquid Crystals Science and Technology. Section A. Molecular Crystals and Liquid Crystals* 327, no. 1 (1999): 95-98.

[48]   Hu, Xiaoyong, Qi Zhang, Yuanhao Liu, Bingying Cheng, and Daozhong Zhang. "Ultrafast three-dimensional tunable photonic crystal." *Applied physics letters* 83, no. 13 (2003): 2518-2520.

[49]   Oh, Jeong Rok, Jung Ho Moon, Sungho Yoon, Chan Ryang Park, and Young Rag Do. "Fabrication of wafer-scale polystyrene photonic crystal multilayers via the layer-by-layer scooping transfer technique." *Journal of Materials Chemistry* 21, no. 37 (2011): 14167-14172.

[50]   Yadav, A., R. De Angelis, M. Casalboni, F. De Matteis, P. Prosposito, F. Nanni, and I. Cacciotti. "Spectral properties of self-assembled polystyrene nanospheres photonic crystals doped with luminescent dyes." *Optical Materials* 35, no. 8 (2013): 1538-1543.

[51]   Smith, Natasha L., Zhenmin Hong, and Sanford A. Asher. "Responsive ionic liquid–polymer 2D photonic crystal gas sensors." *Analyst* 139, no. 24 (2014): 6379-6386.

[52]   Burratti, L., F. De Matteis, M. Casalboni, R. Francini, R. Pizzoferrato, and P. Prosposito. "Polystyrene photonic crystals as optical sensors for volatile organic compounds." *Materials Chemistry and Physics* 212 (2018): 274-281.

[53]   Liu, Ye, Fei Qin, Zhi-Yi Wei, Qing-Bo Meng, Dao-Zhong Zhang, and Zhi-Yuan Li. "10 fs ultrafast all-optical switching in polystyrene nonlinear photonic crystals." *Applied Physics Letters* 95, no. 13 (2009): 131116.

[54]   Lutti, Julie, Wolfgang Langbein, and Paola Borri. "A monolithic optical sensor based on whispering-gallery modes in polystyrene microspheres." *Applied Physics Letters* 93, no. 15 (2008): 151103.

[55]   Kosma, Kyriaki, Gianluigi Zito, Kay Schuster, and Stavros Pissadakis. "Whispering gallery mode microsphere resonator integrated inside a microstructured optical fiber." *Optics letters* 38, no. 8 (2013): 1301-1303.

[56]   François, Alexandre, Kristopher J. Rowland, V. Shahraam Afshar, Matthew R. Henderson, and Tanya M. Monro. "Enhancing the radiation efficiency of dye doped whispering gallery mode microresonators." *Optics express* 21, no. 19 (2013): 22566-22577.

[57]   Dholakia, Kishan, and Pavel Zemánek. "Colloquium: Gripped by light: Optical binding." *Reviews of modern physics* 82, no. 2 (2010): 1767.

[58]   Zhao, Yang, Amr AE Saleh, and Jennifer A. Dionne. "Enantioselective optical trapping of chiral nanoparticles with plasmonic tweezers." *ACS Photonics* 3.3 (2016): 304-309.

[59]   Nieto-Vesperinas, M., J. J. Sáenz, R. Gómez-Medina, and L. Chantada. "Optical forces on small magnetodielectric particles." *Optics express* 18, no. 11 (2010): 11428-11443.

[60]   Novotny, Lukas, and Bert Hecht. *Principles of nano-optics*. Cambridge university press, 2012.

[61]   Bekshaev, A. Ya. "Subwavelength particles in an inhomogeneous light field: optical forces associated with the spin and orbital energy flows." *Journal of Optics* 15, no. 4 (2013): 044004.

[62]   Chaumet, Patrick C., and Manuel Nieto-Vesperinas. "Time-averaged total force on a dipolar sphere in an electromagnetic field." *Optics letters* 25, no. 15 (2000): 1065-1067.

[63]   Gordon, James P. "Radiation forces and momenta in dielectric media." *Physical Review A* 8, no. 1 (1973): 14.

[64]   Nieto-Vesperinas, M., P. C. Chaumet, and Adel Rahmani. "Near-field photonic forces." *Philosophical Transactions of the Royal Society of London. Series A: Mathematical, Physical and Engineering Sciences* 362, no. 1817 (2004): 719-737.

[65]   Arias-González, J. Ricardo, and Manuel Nieto-Vesperinas. "Optical forces on small particles: attractive and repulsive nature and plasmon-resonance conditions." *JOSA A* 20, no. 7 (2003): 1201-1209

[66]   Hulst, Hendrik Christoffel, and Hendrik C. van de Hulst. *Light scattering by small particles*. Courier Corporation, 1981.

[67]   Yang, Honghua U., and Markus B. Raschke. "Resonant optical gradient force interaction for nano-imaging and-spectroscopy." *New Journal of Physics* 18, no. 5 (2016): 053042.

[68]   Sukhoivanov, Igor A., and Igor V. Guryev. "Physics and Practical Modeling: Photonic Crystals." (2009).

[69]   Seminar on Whispering gallery modes by University of Ljubljana, Author: Matjaž Gomilšek, Mentor: asist. dr. Miha Ravnik

[70]   Oraevsky, Anatolii N. "Whispering-gallery waves." *Quantum electronics* 32, no. 5 (2002): 377

[71]   Bunyaev, Sergey A., Alexander A. Barannik, and Nickolay T. Cherpak. "Microstrip Whispering-Gallery-Mode Resonator." *IEEE Transactions on Microwave Theory and Techniques* 63, no. 9 (2015): 2776-2781.

[72]   Franchimon, Ellen. "Modelling circular optical microresonators using whispering gallery modes." Master's thesis, University of Twente, 2010.

[73]   Schunk, Gerhard, Josef U. Fürst, Michael Förtsch, Dmitry V. Strekalov, Ulrich Vogl, Florian Sedlmeir, Harald GL Schwefel, Gerd Leuchs, and Christoph Marquardt. "Identifying modes of large whispering-gallery mode resonators from the spectrum and emission pattern." *Optics express* 22, no. 25 (2014): 30795-30806.

[74]   Kippenberg, Tobias Jan August. "Nonlinear optics in ultra-high Q whispering-gallery optical microcavities." PhD diss., California Institute of Technology, 2004.

[75]   Tobing, Landobasa YM, and Pieter Dumon. "Fundamental principles of operation and notes on fabrication of photonic microresonators." In *Photonic Microresonator Research and Applications*, pp. 1-27. Springer, Boston, MA, 2010.

[76]   Ye, Qian, and Haoze Lin. "On deriving the maxwell stress tensor method for calculating the optical force and torque on an object in harmonic electromagnetic fields." *European Journal of Physics* 38, no. 4 (2017): 045202

[77]   Neves, Antonio Alvaro Ranha, and Carlos Lenz Cesar. "Analytical calculation of optical forces on spherical particles in optical tweezers: tutorial." *JOSA B* 36, no. 6 (2019): 1525-1537.

[78]   Griffiths, David J. "Introduction to electrodynamics." (2005): 574-574.

[79]   Taflove, Allen, and Susan C. Hagness. *Computational electrodynamics: the finite-difference time-domain method*. Artech house, 2005.

[80]   Boundy, Ray H., and Raymond F. Boyer, eds. *Styrene: its polymers, copolymers, and derivatives*. No. 115. Reinhold, 1952.

[81]   Gedney, Stephen D. "Introduction to the finite-difference time-domain (FDTD) method for electromagnetics." *Synthesis Lectures on Computational Electromagnetics* 6, no. 1 (2011): 1-250.

[82]   Sullivan, Dennis, Jun Liu, and Mark Kuzyk. "Three-dimensional optical pulse simulation using the FDTD method." *IEEE transactions on microwave theory and techniques* 48, no. 7 (2000): 1127-1133.

[83]   Ng, Jack, Z. F. Lin, C. T. Chan, and Ping Sheng. "Photonic clusters formed by dielectric microspheres: Numerical simulations." *Physical Review B* 72, no. 8 (2005): 085130.

[84]   Karásek, V., K. Dholakia, and P. Zemánek. "Analysis of optical binding in one dimension." *Applied Physics B* 84, no. 1-2 (2006): 149-156.

[85]   Dapasse, F., and J-M. Vigoureux. "Optical binding force between two Rayleigh particles." *Journal of Physics D: Applied Physics* 27, no. 5 (1994): 914.

[86]   Burns, Michael M., Jean-Marc Fournier, and Jene A. Golovchenko. "Optical matter: crystallization and binding in intense optical fields." *Science* 249, no. 4970 (1990): 749-754.

[87]   Chen, Huajin, Yikun Jiang, Neng Wang, Wanli Lu, Shiyang Liu, and Zhifang Lin. "Lateral optical force on paired chiral nanoparticles in linearly polarized plane waves." *Optics letters* 40, no. 23 (2015): 5530-5533.

[88]   Karásek, V., Čižmár, T., Brzobohatý, O., Zemánek, P., Garcés-Chávez, V. and Dholakia, K., 2008. Long-range one-dimensional longitudinal optical binding. *Physical review letters*, *101*(14), p.143601.